MULTI-TEMPORAL STUDY OF EARTHQUAKE INDUCED LANDSLIDES: A COMPARATIVE CASE STUDY OF BEICHUAN, CHINA AND CENTRAL ITALY
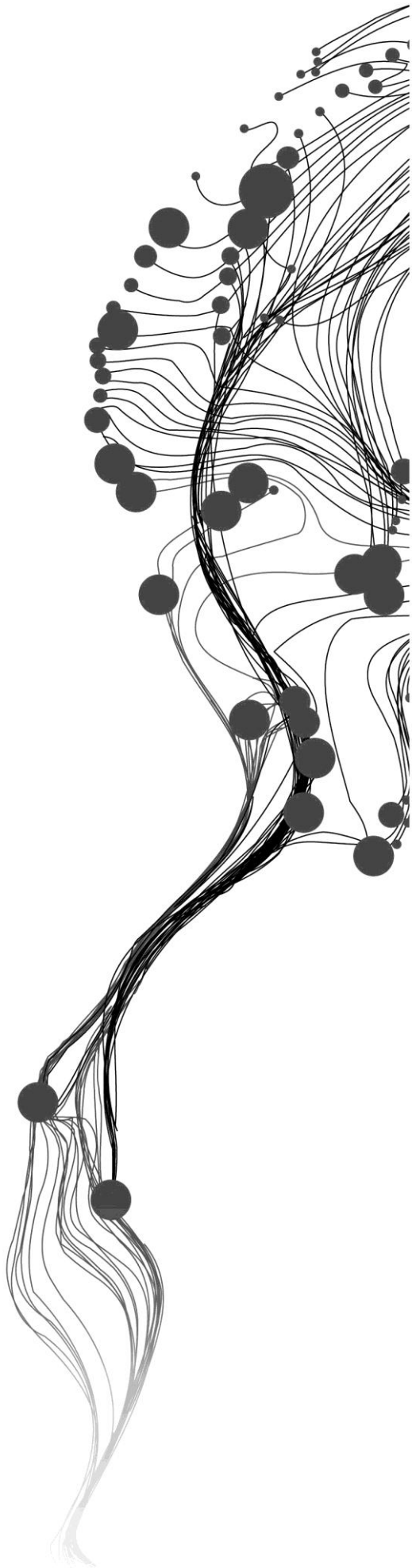
DARWIN EDMUND L. RIGUER
February, 2011

SUPERVISORS:
Dr., C.J., van Westen
Drs., R.P.G.A, Voskuil

MULTI-TEMPORAL STUDY OF EARTHQUAKE INDUCED LANDSLIDES: A COMPARATIVE CASE STUDY OF BEICHUAN, CHINA AND CENTRAL ITALY

DARWIN EDMUND L. RIGER
Enschede, The Netherlands, February, 2011

SUPERVISORS:
Dr., C.J., van Westen
Drs., R.P.G.A, Voskuil

THESIS ASSESSMENT BOARD:
Prof. Dr., V.G., Jetten (Chair)
Dr., E.A., Addink (External Examiner, Utrecht University)
MSc., T., Gorum (PhD Observer)
Drs., T.M., Loran (Observer)

ABSTRACT

Spatial relations and distribution on how landslides behave in response to a triggering factor have been analyzed by many researchers in which they have stated out that earthquake induced landslide (EIL) are related to geo-environmental precursors and seismic parameters such as fault type, displacement, earthquake depth and magnitude. However, most studies that relate the landslides caused by earthquakes to certain parameters were determined through comparing inventories from different study areas and therefore an area where different earthquakes occurred with such occasions are relatively rare. That is why Beichuan area offers opportunity to map a recent very large EIL event (2008, Mw=7.9) and a sub-recent lesser event (1958, Mw=6.2). Therefore, an investigation of different EIL inventories from the same area is useful because such investigation presents an opportunity for determining event-based landslide distributions triggered by two earthquakes of different magnitudes at different points in time within the same study region. The Beichuan area in China and Central Italy prove to be the suitable areas for such investigation. For the Beichuan area, the two events were the devastating earthquake that occurred with moment magnitude (Mw) 7.9 at Wenchuan adjacent to the Sichuan basin on 12 May 2008 (Zhang et al., 2008) and the earthquake of magnitude (Mw) 6.2 occurring in 1958. In Central Italy along the Apennine chains, the two seismic events that occurred in the same area were the Umbria-Marche earthquake that occurred on September 1997 (Mw 5.8) and the L'Aquila earthquake that happened on April 2009 (Mw 6.3). It can be concluded that, although earthquakes of different magnitudes may happen in the same area, they may create quite different landslide inventories, which are not clearly related to the same geo-environmental factors. Earthquakes that happen in different geo-environmental settings, such as Central Italy and the Sichuan mountains in China, may also produce EILs with entirely different characteristics. Different earthquakes may not have the same effect on the geo-environment such as in the maximum spatial relation to slope, slope aspect, and lithology. This study has shown that as far as the two study areas and four EILs that were studied are concerned, it is not possible to draw general conclusions that can be used for designed an improved method for earthquake induced landslide susceptibility assessment

ACKNOWLEDGEMENTS

TABLE OF CONTENTS

1. INTRODUCTION

1.1. Background

Due to their prevalent nature and socio-economic impacts such as deaths, injuries, industrial disruptions and income losses, and destruction of the built and natural environment, landslides have long been known to constitute a major hazard. From 1909 to 2011, more than 60,000 people were killed, 13 million people affected, and about 8 million US dollars in revenues lost due to landslides (EM-DAT, 2011) (table 1. 1.) These figures, however, are modest estimates because damages out of landslides are more attributed to main events such as floods, typhoons, and earthquakes. The result therefore is a great underestimation of the impact of landslides worldwide. For instance about a third of the fatalities caused by the Wenchuan earthquake in 2008 were not by the earthquake itself but due to the landslides that it induced. Therefore, there is a need to study the relation between main triggering events and the landslides they induced to distinguish and examine more accurately the impacts of landslides.

The occurrence of earthquake induced landslides (EIL) is a particularly striking area of research. Documentation of EILs traces back to as early as 372 BC in Greece by Seeds (1968)and 1789 BC in China by Hansen and Franks (1991) and. Over the past few decades, however, knowledge about landslides has increased with improved resources and technologies such as aerial photography, remotes sensing, and geographic information systems as exemplified in the works done by Guzzetti et al. (1999), van Westen, (2000), Dai and Lee (2002), Chung and Fabbri (2008), Lee et al. (2008), Gorum et al. (2010), Dai et al. (2011).

	No. of events	People killed	People affected	Damage (000's US$)
Africa	35	1,401	55,889	No data
Americas	170	21,916	5,514,078	2,721,727
Asia	328	23,173	8,073,646	2,540,916
Europe	76	16,809	48,805	3,108,889
Oceania	19	572	21,315	2,466
TOTAL	628	63,871	13,713,733	8,373,998

Table 1.1. Worldwide statistics of landslides from November 1909 to October 2010 (EM-DAT, 2011).

1.2. Problem statement

The risk assessment of EIL should be based on good hazard maps capable of generating models of potential landslide distribution incorporating all possible earthquake locations based on seismological studies. Each earthquake produces its own event-based inventory, with associated scenarios pertaining to temporal probability, size probability and spatial probability. An ideal hazard map integrates all these scenarios. However, current methods for EIL hazard assessment are not effective in predicting the variable pattern of landsides in association with all earthquakes, each with a given location, magnitude, depth and fault type. Most of the current methods only arrive at data on susceptibility for shallow landslides. The Newmark method is an example of these methods (Jibson et al., 2000). Further, new methods try to model only seismic acceleration for a given earthquake and associated landslide pattern. It is therefore important to generate more event-based EIL maps because there is a need to establish relationships between landslide occurrence and seismic and geo-environmental factors.

Many researchers such as Keefer (1984), Chigira et al. (2003), Wang et al., (2003), Khazai and Sitar (2004), Yin et al. (2009), Yun-Jie et al. (2009), Chigira et al. (2010), and Dai et al.(2011) have analyzed the spatial distribution of landslides in response to a seismic triggering event. Their findings point out that EILs are related to geo-environmental factors and to seismic parameters such as rupture type, displacement, earthquake depth and magnitude. Thus, it is crucial to evaluate and study in detail the relationship of an EIL to topography, geology, geomorphology, and seismic parameters. Areas where different earthquakes occurred will enable a better evaluation of the relationship between landslides, geo-environmental factors and seismic factors, as the effect of two earthquakes in the same environment can be studied. This allows to better separate the effect from the geo-environmental factors and the seismic factors. However, such areas are relatively rare.

A good analysis of the relationship between the landslide distribution and the sets of geo-environmental and seismic factors requires the availability of earthquake induced landslide inventories over extensive areas. However, mapping landslides is a tedious work, depending on the availability of suitable post earthquake images, experience of the mapper, and time involved. As a consequence, individual landslides are often identified as points, which might make the resulting statistical analysis with the casual factors less accurate. The low reliability and accuracy of landslide analysis, in turn, may result in insufficient understanding of landslide distribution such as in a pre- and post-earthquake scenario. Therefore, there is a need to map landslides with a complete classification of landslide types, subtypes, and materials involved if possible.

Most studies that relate the landslides caused by earthquakes to certain parameters were carried out by comparing inventories from different study areas. Although a relation can be studied between fault mechanisms, magnitude, depth of earthquake, and the distance of landslides from fault rupture, the geo-environmental factors (lithology, geomorphology, and topography) are also crucial. However, geo-environmental factors vary between different areas. Therefore, an investigation of different EIL inventories from the same area is useful because such investigation presents an opportunity for determining event-based landslide distributions triggered by two earthquakes of different magnitudes at different points in time within the same study region. The Beichuan area in China and Central Italy prove to be the suitable areas for such investigation. For the Beichuan area, the two events were the devastating earthquake that occurred with moment magnitude (Mw) 7.9 at Wenchuan adjacent to the Sichuan basin on 12 May 2008 (Zhang et al., 2008) and the earthquake of magnitude (Mw) 6.2 occurring in 1958. In Central Italy along the Apennine chains, the two seismic events that occurred in the same area were the Umbria-Marche earthquake that occurred on September 1997 (Mw 5.8) and the L'Aquila earthquake that happened on April 2009 (Mw 6.3) (Guzzetti, 2009).

1.3.   Objectives

The main objective of this MSc research is to improve knowledge on earthquake induced landslide susceptibility assessment by studying the relation between event-based landslide distribution patterns and controlling factors, both geo-environmental factors as well as seismic parameters for two earthquakes happening in the same area.

1.4.   Specific objectives

Specifically, the study will have the following objectives:

1. To generate detailed earthquake induced landslides inventories from multi-temporal, high resolution pre- and post-earthquake satellite imagery for 2 earthquake events in Beichuan County (China) and Central Italy;
2. To analyze for each event the spatial distribution of landslides and their characterization in terms of landslide type, activity, and size distribution;
3. To analyze the relationships of landslides with the geo-environmental factors, such as lithology, slope, distance to ridges and valleys;
4. To analyze the relationships of landslides with seismic factors such as distance to epicenter, magnitude, distance to fault rupture, hanging wall effects etc.

1.5. Research questions

1. What are the landslide types, subtypes, and materials observed in each earthquake event and how are these distributed?
2. Which geological, structural, topographic, and seismic parameters relate to the EIL distribution in the two earthquakes with different magnitudes?
3. What is the smallest landslide size that can be recognized in both Beichuan and Central Italy?
4. How do the landslides vary in terms of size and typology throughout the multi-temporal inventory?
5. How are the parameters spatially associated with the landslides?
6. Are there any differences between landslide distribution and density on the foot wall and hanging wall areas of the fault rupture?

1.6. Thesis structure

The thesis structure is outlined by the following chapters:

1. Introduction – Contains the general idea and the rationale of the research. Particularly, a background about landslides pictured on a global scale is stated. This is then linked to the importance of EIL followed by the objectives and statement of the problems.
2. Literature review – This chapter looks into landslide on a general view, that is the landslide definition and classifications, and to more extent, susceptibility and hazard assessment. Further, methods and techniques used in landslides mapping-interpretation and its theoretical considerations are elaborated. Landslide distributions are also dealt with and how are they analyzed.
3. Study area – The discussion is separated into the earthquake event that triggered the occurrences of EIL in Beichuan and in Central Italy. The geo-environmental setting such as the geology and active tectonics of each area are presented. The mechanism for the EIL occurrences is also expounded here.
4. Landslide inventory – This part begins with detailing the available data that is used for generating the EIL inventory. The approach to the EIL interpretation is further discussed at the middle part of the chapter. At the end of the chapter, the EIL inventory made here is compared with existing inventories done by interpreters.
5. Spatial distributions – In this chapter, the areas covered by the landslide were discussed. The landslide area density, and number density is also presented here. Landslide distributions an analysis of the EIL activity is addressed at the last part.
6. Spatial associations – This chapter quantifies spatial associations of EILs to causal factors. The causal factors include the surface rupture.

2. LITERATURE REVIEW

This chapter recapitulates the concepts and methods that relates to landslide susceptibility and hazard assessment. The first part discusses an overview on landslide definitions and classifications followed by landslide inventories. Further, the general trends on landslide characterization are discussed as exemplified by landslide activity, landslide density, and size frequency estimation. Finally, a discussion on landslide susceptibility and hazard with examples of researches that dealt with EIL.

2.1. Landslide definition and classification

A landslide is defined as "the movement of a mass or rock, debris or earth, down a slope" (Cruden, 1991), which implies that any movement of material under the direct influence of gravity is considered as a landslide.

Landslides includes events such as rock falls, topples, slides, spreads, and flows, such as debris flows commonly referred to as mudflows or mudslides (Cruden and Varnes, 1996). Table 2-1 summarizes these events. Landslides are classified according to the type of material and type of movement. Thus, the names of landslides are denoted by the type of material, which forms the first half of its name, and by the type of its movement, which forms the second half of the name (e.g., rock [type of material] fall [type of movement]).

Landslide in a strict sense is also a specific type of slope movement of particular material type, configuration, and speed along a clearly defined failure surface. However, the term landslide has been widely used as a generic term. Thus, in this research landslide is synonymous to mass movement, slope movement, mass wasting, mass failure, and slope.

Type movement	Type of material Bedrock	Engineering soils Predominantly coarse	Predominantly fine
Fall	Rock fall	Debris fall	Earth fall
Topple	Rock topple	Debris topple	Earth topple
Slide	Rock slump	Debris slump	Earth slump
	Rock slide/block slide	Debris slide	Earth slide
Spread	Rock spread	Debris spread	Earth spread
Flow	Rock flow	Debris flow	Earth flow
Complex	Combination of two or more principal types of movement		

Table 2-1. Landslide classification according to type of movement and type of material adopted from Cruden and Varnes (1996).

2.2. Landslide inventories

A landslide inventory is the simplest and the most fundamental form of a landslide susceptibility map (Pašek, 1975; Hansen, 1984; Wieczorek, 1984). Landslide inventory maps can be prepared through different techniques, depending on their purpose, the extent of the study area, the scales of base maps and aerial photographs, and the resources available to carry out the work (Guzzetti et al., 2000). For convenience, landslide inventory maps can be classified based on their scale or the type of mapping used, that is geomorphological inventory map (all landslides and geomorphological units observed at the present), multi-temporal landslide inventory (all landslides in a given period of time), and event inventories (all landslide caused by a single triggering event):

1. Geomorphologic inventory – Geomorphologic maps take into account hillslope and other landscape forming processes. The method developed by Verstappen and Van Zuidam (1968) is used to determine geomorphological units. A geomorphological inventory map shows the sum of a number of landslide events over a period of many years. Geomorphological inventories are typically prepared through a systematic interpretation of a series of aerial photographs or satellite imageries, combined with extensive fieldwork. Geomorphological inventory maps cover areas ranging from a few tens to a few thousand square kilometres, at mapping scales ranging from 1:10,000 to 1:100,000 depending on the extent of the study area, the availability, scale and number of the aerial photographs, the complexity of the study area, and the time and resources available to complete the project (Guzzetti et al., 1999).

2. Multi-temporal inventory – A multi-temporal inventory shows the location and types of mass movement, and portrays the spatial and temporal transformations of these movements. A multi-temporal inventory requires systematic interpretations of satellite imageries and aerial photographs, of data gathered from fieldworks, of archive and bibliographical data, and of information from other remote sensing techniques (e.g., laser scans, geodetic surveys, synthetic aperture radars). Since the inventory constitutes comprehensive data, its preparation requires expertise and ample amount of time. Moreover, due to the complexity of acquiring the data, multi-temporal inventories are rare and when available only cover a limited scope (Guzzetti et al., 2005).

3. Event based inventories – An event landslide inventory map shows all the slope failures triggered by a single event, which can be earthquake, a heavy rainfall and could also be a volcanic eruption. It was coined as "multiple occurrence regional landslides' or MORE by Crozier (2005). High-resolution satellite imageries are used to produce pre- and post-earthquake inventories. These landslide inventories account for the most important steps in this research.

The final product represents the distributions of landslide either as a polygon or as a point. With polygon, landslide can be delineated as a whole feature. It is also possible to use the polygons in differentiating the source area, accumulation zone, transporting parts, etc. Landslides can also be represented by points but precision is severely affected since they occur with dimensions in reality. For example, the accumulation part is not really a point but rather an area in a two-dimensional space and a volume in three-dimensional space. So is true is the whole landslides is represented as a point. Polygon based landslide inventory will tell which area is potentially affected by the landslides and therefore can also be a proxy for landslide susceptibility assessment if expressed as a density within a certain mapping unit. The approach is also used to determine the spatial association of the landslides in connection with the factors since it tells where landslides are located. However, landslide distribution assessment is only valid for an inventory immediately after the event; thus, no temporal variability can be deduced from the distributions of the slope failures.

2.4.   Theoretical considerations and framework

Any attempt to map landslides needs to have a firm basis. Assumptions on landslides are helpful in establishing the way in which to conduct a landslide inventory. The following are the widely accepted assumptions on landslides (Varnes et al., 1984; Carrara et al., 1991; van Westen, 1993; Hutchinson, 1995; Guzzetti, et al., 1999; Guzzetti, 2005):

1. Landslides leave discernible signs that can be recognized, classified, and mapped through various methods: (1) field survey, (2) stereoscopic aerial photos and (3) satellite imagery (Rib and Liang, 1978; Varnes, 1978; Crozier, 1984; Hansen, 1984; Hutchinson, 1988; Turner and Schuster, 1996). Most landslides leave morphological signatures on the surface, such as scarps and accumulational bodies that can be recognized later. Surface or sub-surface changes including lithological changes,

geological changes, and land use changes also indicate the occurrence of a landslide. Landslides otherwise could not be recognized and mapped in the field or by using satellite imagery without the observable and measurable surface and sub-surface changes that they cause (Guzzetti, 2005).

2. Mechanical laws govern landslides and therefore they do not occur randomly or by chance. As a consequence, landslides can be analyzed empirically, statistically or in a deterministic way (Hutchinson, 1988; Crozier, 1986; Dietrich et al., 1995). It follows therefore that knowledge on landslides can be generalized (Aleotti and Chowdhury, 1999; Guzzetti et al., 1999).

3. The morphological signature of a landslide (Pike, 1988) depends on the type (i.e., fall, flow, slide, complex, translational, rotational, etc.) and the rate of movement of the slope failure (Pašek, 1975; Varnes, 1978; Hansen, 1984; Hutchinson, 1988; Cruden and Varnes, 1996; Dikau et al., 1996). In general, the same type of landslide will result in a similar signature. The morphological signature left by a landslide can be interpreted to determine the extent of the slope failure and to infer the type of movement. From the appearance of a landslide, an expert can also infer qualitative information on the degree of activity, age, and depth of the slope failure. However, care must be exercised when inferring the characteristics and properties of landslides because morphological convergence is possible. For example, slides may combine into other slides forming a suite of landslides or a rockfall merging with an earth slide making it look altogether like a debris slide. Therefore, delineating the extent for an individual slide is difficult since there is a merge of boundary. In effect, the same morphological signs may result from different processes.

4. The principle of uniformitarianism holds that the present is the key to the past, thus the present is a key to the future (Varnes et al., 1984; Carrara et al., 1991; Hutchinson, 1995; Aleotti and Chowdhury, 1999; Guzzetti et al., 1999). Applied on landslides, this principle implies that slope failures in the future will be more likely to occur under the conditions that led to past and present instability. Mapping recent slope failures therefore is integral to understanding the geographical distribution and arrangement of past landslides, and landslide inventory maps are fundamental information to help forecast the future occurrence of landslides (Guzzetti, 2006). However, one has to keep in mind that the triggering factors might change dramatically, and was evidenced in Wenchuan China where an Mw 7.9 earthquake triggered landslides on May 12 2008 and four months later, a heavy rainfall activated EIL and created new landslides (rainfall induced landslides).

5. The identification of landslides, including the type of data and the techniques that make data collection feasible, is dependent on scale-related input data (van Westen, 1993; Mantovani, et al., 1996; Soeters and van Westen, 1996). For example, seismic peak ground acceleration collected through catalogues from earthquake observatories has low importance for regional scale, moderate importance for medium scale, and high importance for large scale (van Westen, et al., 2009).

In the process of identifying a landslide either through field survey or through airborne-spaceborne imagery, the basic assumptions cited previously should ideally be satisfied. Assumptions not met indicate limitations of all the derivatives of the landslide inventory. However, the application of these assumptions can be conceptually or operationally complex and tedious because not all processes are readily observed such as when landslides leave faint traces, or the landslides occurred in a dense forest, or the landslide were immediately mitigated by the affected community (e.g., ploughing) (Guzzetti, et al., 1999). van Westen (2009) enumerated seven groups of techniques or tools that are widely used in mapping and identifying landslides. The list includes:

1. Image interpretation – interpretation from stereo aerial photographs, high resolution satellite images, and Light detection and ranging (LiDAR) shaded relief maps. Images may either be in analog or digital format with single or multi-temporal dataset facilitated through monoscopic or stereoscopic view (Rib and Liang, 1978; Crozier, 1984; Turner and Schuster, 1996).

2. Semi automated classification: spectral characteristics – interpretation from aerial photographs, medium resolution multi-spectral images, and combinations of optical and radar imagery. This can be performed via simple calculations like image ratioing and thresholding to more complex pixel based image classification and segmentation. Dataset may be single data image or multi-temporal.

3. Semi-automated classification: altitude characteristics – interpreted from Interferometric synthetic aperture radar (InSAR) by way of radar interferometry on extensive areas and permanent scatters for pointwise displacement data. LiDAR can used by superimposing DEMs of different period. Lastly, photogrammetry by overlaying DEMs derived from aerial photographs and high resolution satellite images.

4. Field investigations methods – can be performed by field mapping, ground truth survey from image interpretations, and interviews. Field survey can be done by conventional methods and utilizing mobile GIS and GPS for attribute data collection. Interviews are done by questionnaires and workshops.

5. Archive studies – is done by historical analysis of archives, chronicles, and newspapers to identify landslide events, to compile landslide catalogues, and to prepare landslide maps. This is also possible through extracting information from road maintenance organizations that keeps logbooks (e.g., oberseved linear features along a roadcut).

6. Dating methods for landslides – can be direct or indirect. Direct dating includes dendochronology, radiocarbon dating while indirect includes pollen analysis, and lichenometry.

7. Monitoring networks – performed through various devices such as extensometer that measures speed, networks of electronic distance measurement (EDM), differential global positioning systems (DGPS), total stations as networks of theodolite measurements, groundbased InSAR through radars with slide rail, and terrestrial LiDAR for repeated laser scanning.

Traditionally, landslide inventories are carried out and adopted via the visual interpretation of stereoscopic aerial photographs (Rib and Liang, 1978; Crozier, 1984; Turner and Schuster, 1996). However, interpretation via high resolution satellite imagery is catching up because of recent advances in technology. Guzzeti (2006) identified two advantages of aerial photograph interpretation that are applicable to interpreting satellite images:

1. Aided by vertical exaggeration introduced via stereoscopic vision, a trained investigator can readily recognize and map a landslide through aerial photographs or satellite images . The vertical exaggeration amplifies the morphological appearance of the terrain, reveals subtle morphological (topographical) changes, and facilitates the recognition and the interpretation of the topographic signature typical of a landslide (Rib and Liang, 1978; Pike, 1988).

2. For a trained geomorphologist, interpretation of the aerial photography is an intuitive process that does not require sophisticated technological skills. The technology and tools needed to interpret aerial photographs are simple (e.g., a stereoscope) and inexpensive, compared to other monitoring or landslide detection methods. Information obtained from the aerial photographs can also be readily transferred to paper maps or stored in computer systems.

2.5.   Landslide activity

Landslide activity or sometimes called landslide persistence is the degree to which new slope failures occur in the same place as existing landslides (Guzzetti 2005). The activity of landslides can be determined and quantified by comparing geomorphological, multi-temporal, and event-based inventory maps in a GIS setting. For example, in the work done by Cardinalli et al. (2007), the landslide persistence of landslides were calculated through statistical and geographical comparisons cumulative area extent to older slope failures of multi-temporal landslides inventory maps of the Appenine chains in Italy. Van Westen (1993) developed a three-step approach to an analysis of landslide activity. The steps include the digitization of recent landslides as guide for previous landslides, image interpretation of the differences in activity between two different dates, and calculation of all landslides that were initiated and reactivated in the period between the landslide events. Landslide activity maps are unique because they can account for undetectable landslides present before imageries were collected. They are indispensable tools in landslide assessments as they indicate which landslides had been reactivated by the event. However, several factors should be noted when interpreting landslide activity analysis like the type of environment, type and size of landslide, size of landslide, the triggering mechanism, and the availability of imagery after an event. The type of environment may affect the activity of the landslides such as when landslides occurred and was immediately mitigated by the community. Infrastructures or a community may also be build up and cover large proportions of the landslides. The type of landslide will also be a factor. For example, shallow mass movements may easily be re-vegetated, hence would be difficult to observe in (e.g.) aerial photos. This in turn is related to the size of the landslide. Often, small landslides are easily re-vegetated while bigger one tends to persist longer than the small ones. This is now related to the coverage of the imagery for a certain event. The imagery may have been taken long after the event that triggered the landslides or that the imagery only covers a portion of the whole area affected by the slides. This can now be related back to the environment or geography whether the area is prone to triggers like intense precipitation in the tropical areas, whether landslides occurs in seismically active regions like those in the Pacific ring of fire, whether the area is a mountainous terrain or flat areas, etc.

2.6.   Landslide density

Landslide density maps are also essential in examining landslide distributions since it can be an indirect approach to predict and quantify possible future slope failures (Guzzetti, 1999). The density can be quantified by calculating the ratio of the landslide area to a mapping unit. Examples of mapping units are DEM derived slope units where the area is divided into hydrological drainage and divides (Carrara, 1988), terrain mapping units (Verstappen, 1983), or even administrative units. Density can also be represented through percent area coverage on a regional scale using counting filters exemplified by Wright et al. (2004) where they presented a method for calculating landslide deposits isopleths based on intersecting circles on landslide polygon based maps. Another way is to present density is through counting the number of landslide occurrences such as the work done by Gorum et al. (2010). In this method, a kernel is selected over the study area counting the number of landslides. Values can be stated as number of landslides per area but is usually presented as number of landslides per square kilometer. Apart from being a potential proxy for landslide susceptibility assessment, landslide density mapping can show the general picture of the landslide distribution, the abundance of landslides, the magnitude of landslides from the earthquake, and the spatial distribution of the short term frequency of landslides (Guzzetti, 2006).

2.7.   Size-frequency distribution

Landslide geometry as indicated by area and volume of individual landslides varies widely from a couple of meters to several hundreds. Exceptionally large landslides are easily mapped in satellite imageries and aerial photos but the small ones are typically undersampled. For this reason, characterizing the size-

frequency, particularly the area of the landslides is relevant. Examining literatures reveals that much of researches characterize landslide size-frequency via cumulative distribution statistics such as what was done by Dai et al. (2011) in the case of the Wenchuan earthquake in China (figure 2-1a). However, as pointed out by Stark and Hovius (2001), fitting the area cumulative known functions is not advisable since "the residuals in estimated of the probability function are strictly one-sided and asymmetrically distributed, biasing any regression fit which assumes normally distributed error and any crossover from a non-power to a power law is hidden intergration smoothing". As such, Dai et al. (2011) in figure 2-1a were unable to model the occurrences of smaller landslide from their log-linear fit. A more robust function was proposed by (Stark and Hovius, 2001) using what they call as "double-pareto" distribution function and "inverse-Gamma" distribution function by (Malamud et al., 2004) (figure 2-1b). Through their proposed equations, one can estimate the total area or volume of landslides and the area of the most frequent landslides even when inventory is incomplete.

| (a) | (b) |
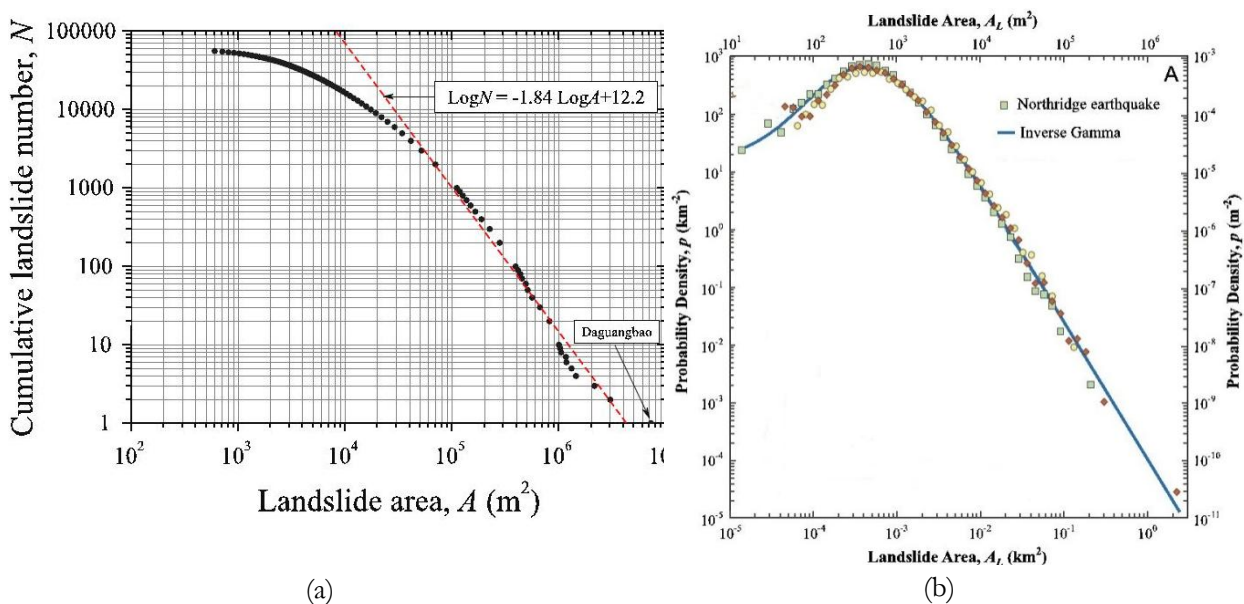
Figure 2-1a-b. Probability density of size-frequency cumulative distribution of the Wenchuan earthquake (a) by Dai et al. (2011) and the probability density distribution of the Northridge EIL (b) plotted by Malamud et al. (2004).

2.8.   Landslide susceptibility and hazard assessment

A wide variety of definitions for susceptibility, hazard and even risk are available in literature and as a consequence, there are no consistent definitions and landslide susceptibility, hazard, and even risk are exchangeably used (Fell et al., 2008). Landslide susceptibility is defined as "a quantitative or qualitative assessment of the classification, volume (or area) and spatial distribution of landslides, which exist or potentially may occur in an area" (Fell et al., 2008). On the other hand, landslide hazard is a condition with the potential of causing an undesirable consequence and is described by the location, volume (or area), classification and velocity of the potential landslides and any resultant detached material. Landslide hazard also refers to the probability of its "occurrence within a given period of time" (Fell et al., 2008). In summary, susceptibility accounts for the relative spatial likelihood of landslide occurrence while hazard accounts for the likelihood of landslide occurrence in a specified area at a specified time. As emphasized by van Westen et al. (2005, 2008), landslide assessment on susceptibility or hazard should start by securing the required data. The schematics of data needed for landslide analysis are divided into three categories as enumerated below and as illustrated in figure 2-1:

1. Landslide inventory - The landslide inventory is by far the most important data set in all the categories as they provide understanding of location, size, typology, activity, materials involved, frequency of occurrences, and to some extent, volume, causal factors, and damage.

2. Environmental factors - Environmental factors pertain to what influence or affect the occurrence of landslides, and thus are also referred to as part of the causal factors. Environmental factors are important because they are relevant for the prediction of the occurrence of future landslides. The factors can also be grouped as digital elevation models, geology, soils, hydrology, geomorphology, and land use. Data layers and types of these groups are detailed in table 2-2. For consistency purpose, the environmental factors is treated the same as "geo-environmental" factors.

3. Triggering factors - Triggering factors initiate landslide events (van Westen et al., 2008) and dependent on the scale of analysis, landslide type, study area, and failure mechanisms (Glade and Crozier, 2005). This can be in a variety of form or event such as seismic event, intense precipitation, snow melts, volcanic eruptions, various anthropogenic activities, etc. Particularly in this research, seismic event or the earthquake played the main role in causing the landslides. Although earthquake is usually associated with its magnitude, peak ground velocity, peak ground acceleration, Arias intensity (Lee et al., 2008) as the triggering factor, in reality, it is a complex interplay between the energy released by the earthquake propagating into and affecting the environmental factors. For example, the 12 May 2008 Wenchuan earthquake event had a Mw = 7.9 (energy released) created a 240 km surface rupture, propagated unilaterally, and at some point coincided in the active faults in the Longmenshan region in China (Shen et al., 2009). Therefore in this research, the term "seismic factor" that includes magnitude and surface rupture is favored.
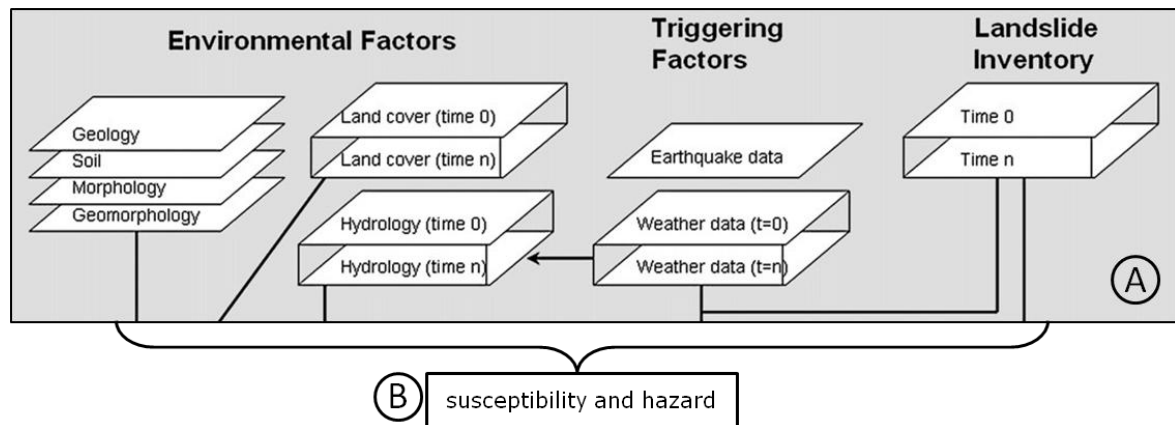
Figure 2-2. Spatial data for landslide risk assessment modified after van Westen (2005). Any assessment should begin by preparing the basic data (a) before any susceptibility-hazard (b) analysis.

Group	Data layers and types	Group	Data layers and types
Digital elevation models	Slope gradient	**Geology**	Rock types
	Slope direction		Weathering
	Slope length/shape		Discontinuities
	Flow direction		Structural aspects
	Internal relief		Faults
	Drainage density		
Group	**Data layers and types**	**Group**	**Data layers and types**
Soils	Soil types	**Hydrology**	Water table
	Soil depth		Soil moisture
	Geotechnical properties		Hydrologic components
	Hydrological properties		Stream network

Group	Data layers and types	Group	Data layers and types
Geomorphology	Physiographic units	**Landuse**	Land use map
	Terrain mapping units		Land use changes
	Geomorphology		Vegetation
	Slope facets		Roads/buildings

Table 2-2. Summary of environmental factors (modified from van Westen et al, 2008).

2.9.   Earthquake induced landslides and causal factors

The schematic illustrated in figure 2-1 provides an insight to a landslide hazard assessment. This scheme, however, only provides a general view and is usually difficult to implement. In the case of EIL hazard assessments, most approaches tend to probe into causal factors and their complex interplay with geo-environmental factors and the seismic factors. Seismic factors cover such aspects as earthquake magnitude, intensity, depth, focal mechanism, fault plane geometry, co-seismic slip, intensity, ground motion, deformation rates, and distance to epicenter (Gorum et al., 2010). Geo-environmental factors cover geological parameters that are crucial in EIL assessments because of their extreme sensitivity to exogenetic processes, which create variable types of landslides. The most common geological parameters are lithology, bedding, and discontinuities, information on which can be derived from geologic maps and reports. Finally, geomorphic (landforms) and topographic (topography) parameters are widely acknowledged to have influence on landslides. A few of the most significant landforms and topographic attributes are elevation, slope angle, slope aspect (Yin et al.., 2009; Yun-Jie, et al., 2009; Dai et al., 2011), slope length, slope curvature (Moore et al., 1991)., wetness index, distance from ridge (Meunier et al., 2007; Meunier et al., 2008), distance from fault (Keefer, 2000; Keefer, 2002), distance from a river head, distance from a river bend, and the normalized differential vegetation index (Lee et al., 2008) Inferences from the relationship of EILs and their causal factors have resulted in improved prediction of landslides due to earthquake events.

Most of the parameters previously referred to had been analyzed either separately or collectively. Keefer (1984, 1993, 1994, 1998, 2000, 2002), Esposito et al. (2000) and Rodriguez et al (1999) correlated EIL distribution to distance to epicentre, earthquake magnitude, and distance to co-seismic fault rupture (CSFR) (figure 2-3). These studies led to the inference that EIL and its distance to CSFR have a direct relationship. However, this is in contrast with case in Wenchuan when about 100 km from the epicenter, a huge mass failure in Daguanbao occurred (Huang and Li (2009). Sato el al (2007) later had a similar finding. He argued that rather than the distance to the epicenter, it is the projection of the fault plane to the surface that affects EIL distribution. On the other hand, studies that consider the parameters on modified mercalli intensity (MMI) and peak ground acceleration (PGA) found a higher correlation of these parameters with the landslide distribution pattern (Meunier et al., 2006; Meunier et al., 2007; Meunier, et al., 2008; Lee et al., 2008). For example, Meunier et al. (2008) studied the patterns of EIL near Northridge, California, Chi-Chi, Tawain, and the Finisterre Mountains and reported a close relation to combined peak ground accelerations and topographic site effects. In a separate work, Meunier et al. (2007) examined linear correlations to both vertical and horizontal PGA. Other studies found a strong relation between geologic and morphological parameters and EIL distribution (Jibson and Keefer, 1989; Densmore and Hovius, 2000; Khazai and Sitar, 2003; Wang et al., 2003; Chigira and Yagi, 2006; Wang et al., 2007; Owen et al., 2008; Guzzeti et al., 2009; Dai et al., 2011; Ghosh and Carranza, 2010; Gorum et al., 2010). Still in others, findings point to higher EIL densities in weakly-cemented lithologies, in unconsolidated to semi-consolidated lithologies, and in highly fractured and weakened rocks. Apart from analyzing the causal factors, other studies calculated the magnitude-frequency relations of EIL in relation to area frequency (Stark and Hovius, 2001), and earthquake magnitude in relation to EIL area and volume (Malamud et al., 2004a, Malamud et al., 2004b).
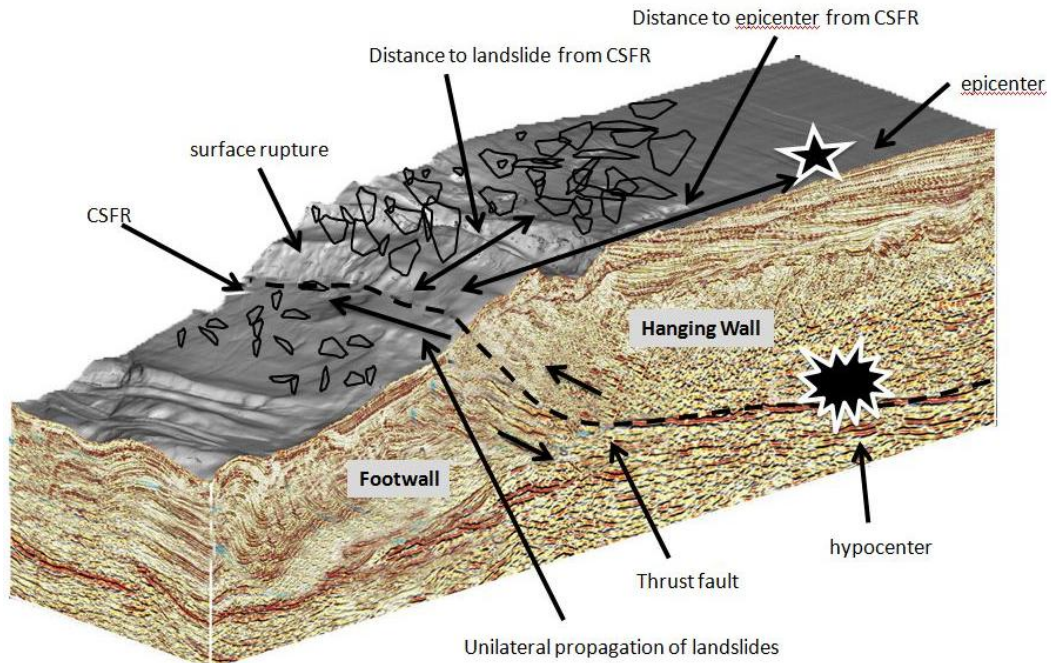
Figure 2-3. Schematic illustration of different factors in EIL scenario.

Therefore, a detailed analysis of the causal relations of the seismic, geologic, geomorphological, and topographic parameters is important for a comprehensive understanding of an EIL distribution. The following sections review some of the most common techniques applied to EIL researches

2.9.1. Earthquake induced landslide susceptibility

The three methods most widely utilized for EIL susceptibility validation and testing are the Newmark method developed by Jibson et al. (2000), the statistical approach developed by Lee et al. (2008). Using the permanent-deformation analysis of Newmark (1965), Jibson et al (2000) incorporated into the assessment of the dynamic performance of slopes from the 1994 Mw = 6.7 Northridge earthquake in California comprehensive inventory of landslides, strong motion records of main shocks, a medium scale (1:24,000) geologic mapping, extensive data on engineering properties of the geological units mapped, and high resolution digital models elevation (figure 2-1a). The resulting displacements were then compared with the EIL inventory to create a probability curve of displacement against probability of failure (figure 2-1b) and then estimated by a Weibull distribution.

(a)

$$P(f) = 0.335[1-\exp(-0.048D_n^{1.565})]$$

(b)

(c)
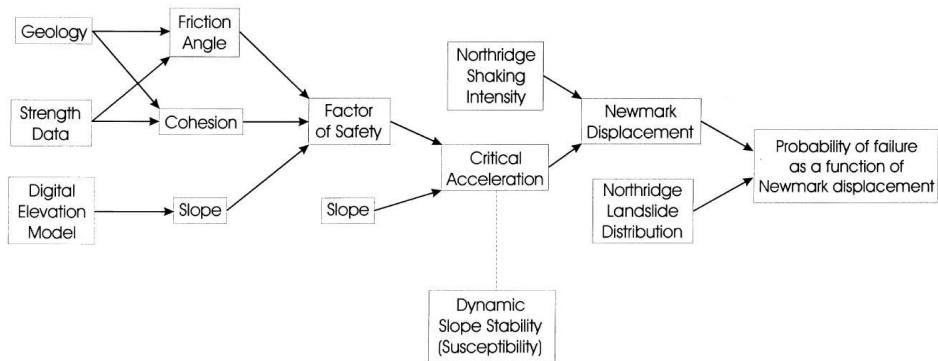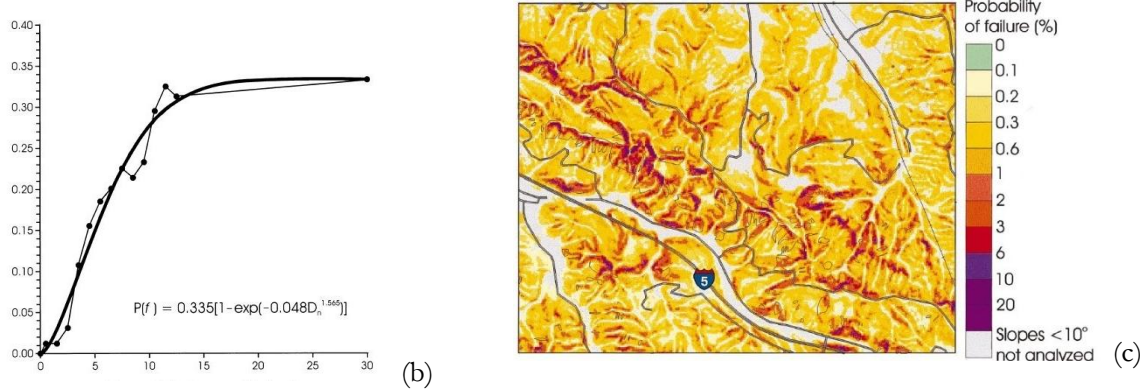
Figure 2-4a-c. The utilization of the newmark method by Jibson et al. (2000) where the steps are outlined in the a flowchart (a). Probability distribution of slope failure as a function of Newmark displacement modelled by a Weibull function (b) and the probability map of EIL (c). Images taken from Jibson et al. (2000).

(a)

(b)
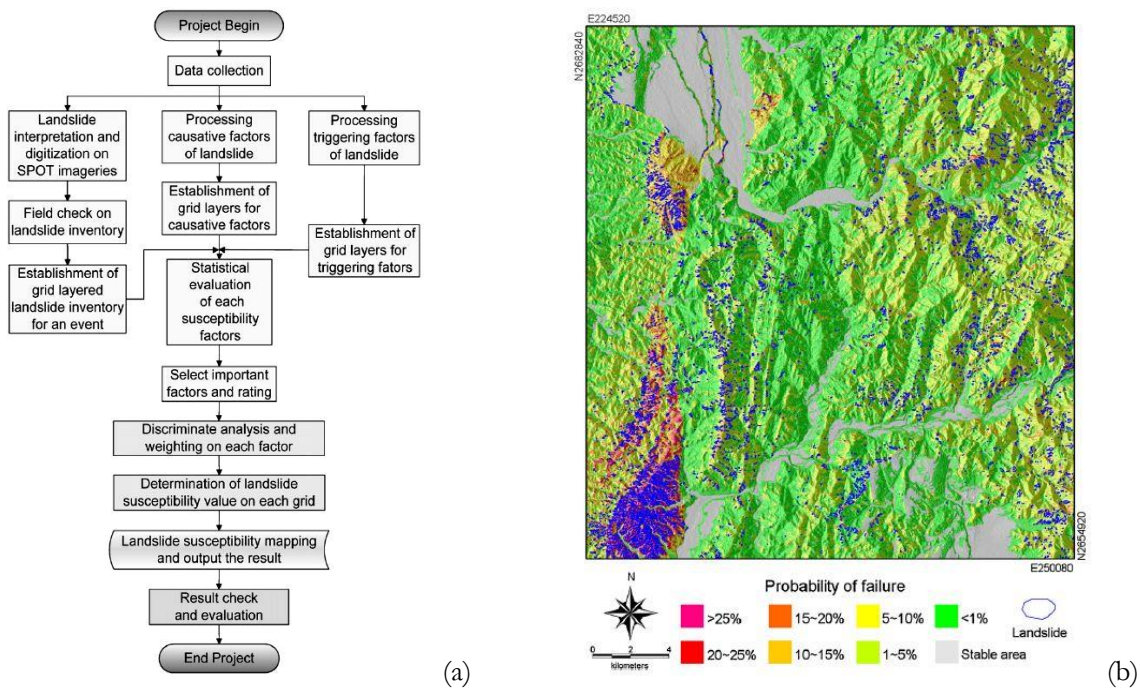
Figure 2-5a-b. The steps used by Lee et al (2008) in determining landslide susceptibility (a) using multivariate-discriminant analysis and the resulting hazard map (b).

2.10.   Chapter summary

In this chapter, the most utilized methods for characterizing landslides were discussed. But before any analysis is done, a good preparation of landslide identification and inventory should first be secured. Afterwards, analysis such as landslides distributions, landslides activity or persistence, and size-frequency can be performed. At the later part of the chapter, focus is given to EIL susceptibility and hazard assessment. A brief discussion was discussed about the spatial data essential to susceptibility and hazard. It was further elaborated by giving examples of pertinent researches made by studying relationships of EIL and causal factors such as geology, geomorphology, and event the seismic factors. At the last part of the chapter, the two most prominent EIL susceptibility is tackled: the method using probality density distribution fit to Newmark displacement (Jibson et al., 2000) and the multivariate discriminant analysis of Lee et al. (2008).

3. STUDY AREA

This chapter discuss the two study areas: the Beichuan area in Sichuan province in China and the Central Italy study area. Each section begins with the earthquake scenario that triggered the landslides. The last part describes the available dataset for each respective study area.

3.1. Beichuan China

3.1.1. 12 May 2008 Wenchuan earthquake

On the 12th of May 2008, a devastating earthquake occurred with a moment magnitude (Mw) 7.9 at Wenchuan, a county adjacent to the Sichuan basin in China. The epicenter was located at 31.0° N and 103.4° E with a depth of ~14 km to 19 km (USGS, 2008; Zhang et al., 2008). The fault propagated unilaterally northeastward rupturing the surface to a total length of about 320 km (Shen et al., 2009). A total of 35,819 aftershocks were recorded up to 04 November 2008 by the China Earthquake Data Center. Official estimates from the Government of China reported 69,197 deaths, 18,209 missing, and 374,176 injuries as a result of earthquake and earthquake triggered even (Wang et al., 2009). Immediately after the earthquake, the National Disaster Response Plan of China was executed and 27 hours later, more than 150,000 rescuers composed of military personnel and medical crews were dispatched in hard hit areas (Lee, 2008). The earthquake triggered widespread occurrence of landslides, rock avalanches and debris flows. Some of the landslides formed natural dams in the rivers and threatened secondary hazard of subsequent flooding. One third of the casualties of the earthquake were said to have been caused by landslides (Wang et al., 2009).

The Wenchuan earthquake occurred in the NE-trending Longmenshan thrust fault belt, the boundary between the Tibetan Plateau and the Sichuan Basin, representing one of the steepest mountain fronts along the margins of the Tibetan Plateau, and produced extensive surface rupturing over a distance of approximately 320 km along the preexisting Beichuan and Pengguan Faults (Fig. 1). The fault belt consists of a series of active parallel thrusts, among which the Wenchaun-Maowen fault, Yingxiu-Beichuan fault and Pengguan fault (See Fig.1) are considered to be seismogenic (Chen et al., 2007, Li et al., 2003; Densmore et al., 2007). Seismic source inversion of the Wenchuan earthquake shows that the rupture could be divided into two sub-events (Fig.1). One sub-event near Yingxiu Town underwent oblique right-lateral thrusting slip, while the northeast sub-event near Beichuan Town exhibited mainly right-lateral slip (Chen et al., 2008). In addition, the slip distribution (fault) models after the earthquake (Ji and Hayes, 2008; Zhang et al., 2008(a) and (b); Wang et al., 2008) and the dislocation models (Wang et al., 2009) established from these models using the geodetic and geophysical data (GPS displacement and gravimetric measurements) also show that the fault changes its character around Beichuan town.

Detailed mapping by Lin et al., 2009(a) and (b); Xu et al. 2009 and Zeng et al., 2009, Wu et al., 2009 shows that the Wenchuan earthquake ruptured both the Yingxiu-Beichuan fault and the Pengguan fault. The Yingxiu-Beichuan rupture surface is the main rupture with a length of about 240 km, which starts at (31.061°N, 103.333°E) in the west and separates to two branches around Yingxiu town. The other rupture zone, the Pengguan rupture surface, extends 70 km northeastward. The Yingxiu-Beichuan fault and the Pengguan fault are connected with each other by a 6 km long left-lateral fault, almost perpendicular to the thrust belt (Fig.1). The dextral strike-slip rate of Yingxiu-Beichuan fault since late Pleistocene is less than 1 mm/year, and the thrust rate is 0.3-6 mm/year (Li et al., 2003; Densmore et al., 2007). Such low slip rates are consistent with Global Positioning System (GPS) estimates of the shortening rate across the Longmenshen range of < 3 mm yr-1 (Shen, et al., 2009; Xu et al. 2009).

Different methods were used to obtain the rupture mechanism, geometry and slip distribution, such as field investigations, measurements of the co-seismic deformation using Global Positioning System (GPS), Interferometric Synthetic Aperture Rardar (InSAR) data, and seismologically derived models (e.g. moment tensor and seismic fault models).

Historic data since 638 AD show that the 66 earthquakes with surface wave magnitude (Ms) larger than 4.7 which occurred in the eastern margin of the Tibetan Plateau were mainly concentrated in the Minjiang fault and the southern part of the Longmenshan fault zone (Li et al., 2008). For instance, a strong earthquake (Ms 7.5) was induced by the tectonic activity along the Minjiang fault zone in 1933, while two earthquakes with magnitude Ms 7.2 occurred between Songpan and Pingwu on 16 and 23 August 1976. Further, three earthquakes were reported along the middle and southern part of the Longmenshan fault zone: in 1657 (Wenchuan, with Ms 6.5), 1958 (Beichuan, with Mw 6.2) (Chen, et al., 1994) (figure 3-1) and 1970 (Dayi, with Ms 6.2) (Kirby et al., 2000; Li et al., 2008; Xu et al., 2009).

There are rarely written articles about the 1958 event. The only sensible information can be gathered from the work of Chen et al (1994) but is then very limited and only discussed about the epicenter and magnitude of the earthquake (figure 3-1). Other data such as depth of the hypocenter, occurrence of CSFR, length of CSFR, ground motion measurement, mass movement reports are among the few data that would have been very helpful in understanding the nature of the earthquake and its relation to any possible EIL.
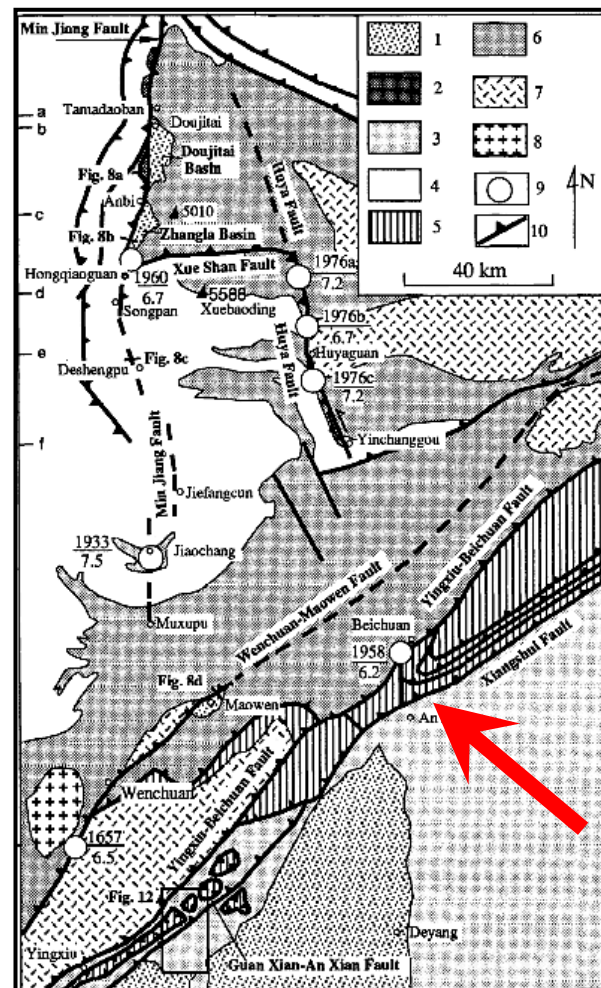
Figure 3-1. Simplified geologic map historical earthquake events in the Longmenshan mountain range in China (Chen et al., 1994) and the location of notable historical earthquake like in Beichuan (red arrow).

Figure 3-2. Fatal landslide examples from Beichuan town. a, General view of the Beichuan town after the earthquake. b-c Pre- and post-photos of Beichuan Middle-school rock avalanche. This landslide caused 700 deaths. d-e, Pre- and post-photos of Wang Jiayan landslide which caused almost 1700 deaths. (pre-earthquake photographs courtesy of Chengdu University of Technology).

3.1.2. Research findings on the Longmenshan fault zone and landslides

The large co-seismic slip offsets generated by the Wenchuan earthquake also resulted in the occurrence of around 56,000 (Dai et al.., 2011) to 60,000 (Gorum et al., 2011) individual landslides with different sizes and types, which makes this one of the most extreme events in terms of earthquake triggered landslides in the last century (Gorum et al., 2011). The landslide distribution shows a very distinct pattern, and the distribution of landslides is considerably wider around the middle and southwest parts of the surface rupture (between Yingxiu and Beichuan towns) and becomes narrower northeast of Beichuan town (figure

3-2). Other research on landslide distribution and characteristics was carried out by several authors. Huang and Li (2009) studied the distribution of what they called "geo-hazards" triggered by the earthquake. They identified a total of 11,300 landslide initiation points on the basis of rapid inventory using air photos and satellite images. Sato and Harp (2009) carried out a preliminary study on landslides interpretation by using pre- and post- earthquake FORMOSAT-2 imageries. Wang et al. (2009) presented preliminary investigation results of some large landslides triggered by the earthquake. Yin et al. (2009) analyzed the earthquake induced-landslides distribution and the characteristics and mechanism of some typical landslides, and assessed the hazards caused by some of the landslide dams. Tang et al. (2009) developed a numerical rating system, using five factors that contribute to slope instability to assess the landslide susceptibility in Qingchuan County, Sichuan. Studies on landslide dams induced by the earthquake were carried out by Cui et al., (2009) who listed more than 200 landslide dams in the earthquake-hit region and made a preliminary risk evaluation of some key landslide-dammed lakes. Xu et al. (2009) presented a statistical analysis of the distribution, classification, characteristics and hazard evaluation of 32 main landslide dams induced by the earthquake. Liu et al. (2009) studied the largest barrier lake, Tangjiashan, and presented a risk analysis, emergency planning and the effect of emergency measures.
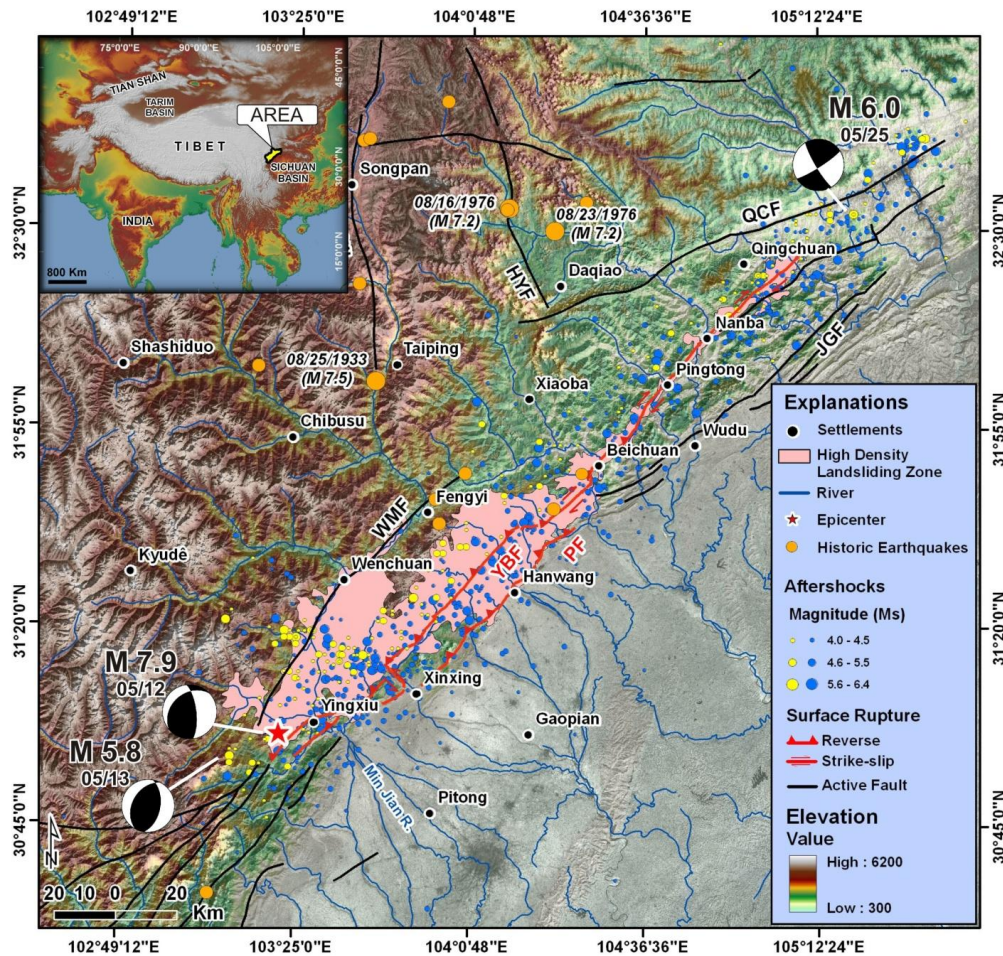
Figure 3-3. Wenchuan earthquake fault surface rupture map, and focal mechanisms (black and white) of the main earthquake (05/12/2008) and two of the major aftershocks (05/13 and 05/25). The following faults are indicated: WMF: Wenchuan-Maowen fault; YBF: Yingxiu-Beichuan fault; PF: Pengguan fault; JGF: Jiangyou-Guanxian fault; QCF: Qingchuan fault; HYF: Huya fault; MJF: Minjian fault. Based on the following sources: Surface rupture: Xu et al., 2009; Epicenter and aftershocks: USGS (yellow points) 2008 and CEA (blue points) 2008; Historic earthquakes: Kirby et al., 2000; Li et al., 2008; Xu et al., 2009.

Figure 3-4. Study area with the surface rupture, co-seismic sliprate of the 2008 Wenchuan earthquake. Also indicated is the 1958 earthquake epicenter.

3.2.   Central Italy

The central Italy study area is subdivided into two sub areas: The Umbira-Marche region and the L'Aquila - Abruzzo, which are both located in the Central appenines.

3.2.1.   1997 Umbria-Marche, Italy earthquake and associated landslides

Earthquake tremors began in the regions of Umbria and Marche, of the Central Apennines, Italy on the 3rd of September 1997, with an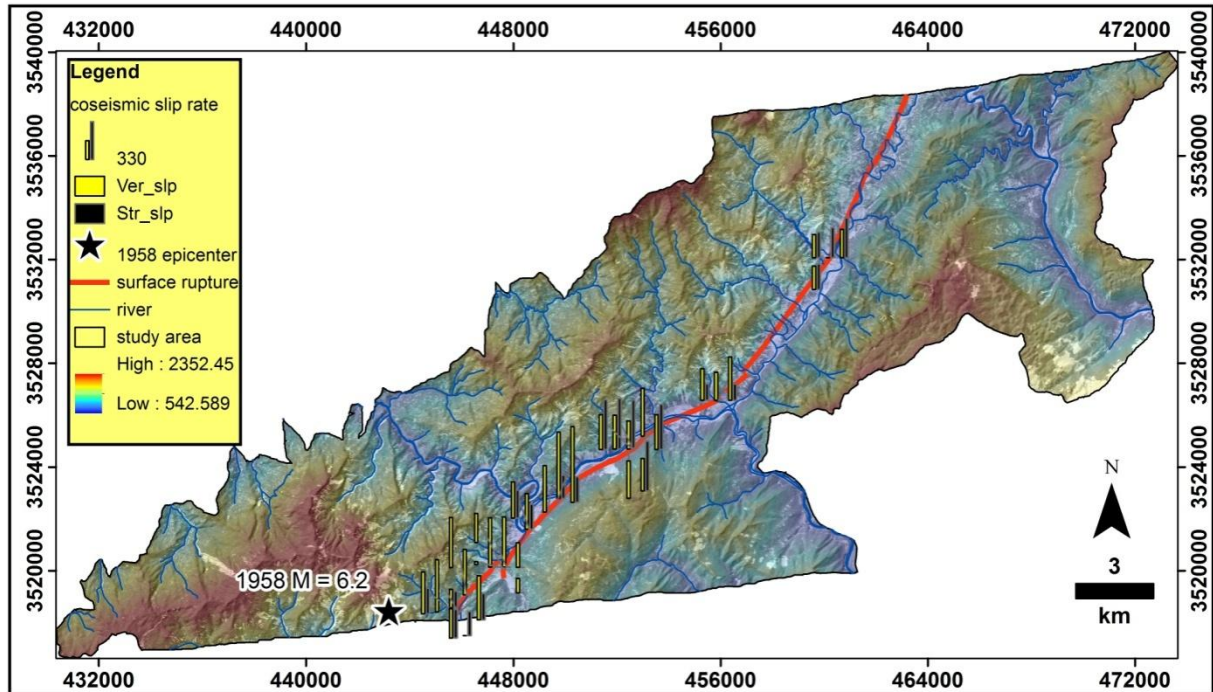 earthquake of Mw=4.5. On 26 September at 0.33 UTC, the area was shaken by a severe earthquake of magnitude Mw=5.7. The epicentre was located to the south of the village of Colfiorito (Esposito et al., 1998). A few hours later at 9:40 UTC, another earthquake of slightly larger magnitude (Mw=6.0) shook the same area. Vertical accelerations of more than 0.4 g were recorded. The hypocentres of both earthquakes were located at a depth of about 12 kilometres. On the 14th of October at 15:23 GMT, the Umbria-Marche Apennines were shaken by an earthquake of similar magnitude (Mw=5.6) with an epicentre located near the village of Forfi. The last earthquake happened on the 3rd of April 1998 an earthquake of magnitude Mw=5.3 with the epicenter recorded between Gualdo Tadino and Nocera Umbra (Amato et al., 1998; Ekstrom et al., 1998).

In the Umbria-Marche region, the sequence of earthquakes killed ten people, left thousands homeless, and caused extensive damage to the towns and villages of the area. Damage to the cultural heritage was extremely large: tens of churches and historical buildings, which include the upper basilica of San Francisco in Assisi were severely damaged. The main shocks and the several hundreds of perceptible aftershocks caused numerous ground fractures and landslides, most of which were rock falls and topples. Landslides triggered by seismic shaking in the Umbria-Marche region were mostly rock falls, minor rock slides and rock topples. Guzzetti et al., reported that this is in agreement with what is expected from the energy released by earthquakes of M_L < 6.0 (Keefer, 1984; Rodríguez et al., 1999; Papadopulos et al., 2000). The distribution of rock falls fitted the observed macroseismic intensity pattern as reported by Guzzetti et al. (2009) (figure 3-5). Of about 250 mapped rock falls (of all sizes), 50% occurred within a radius of 13 km from the 26 September 1997 epicentres, and within a radius of 17 km of the 14 October

1997 epicentre (Guzzetti et al., 2009). Ninety per cent of all rock falls occurred within 28 km of both epicenters and the majority of the largest failures were located within 25 km.

3.2.2. 2009 L'Aquila, Central Italy earthquake and associated landslides

Earthquake tremors began in the L'Aquila area, Abruzzo Region - central Italy on December 2008. On 6 April 2009, at 3:32 a.m. (1:32 UTC), the L'Aquila area was shaken by a severe earthquake of $M_W = 6.3$. The epicentre of the earthquake was located WSW of the city of L'Aquila, at a depth of about 8.8 km. On April 7 and April 9, two earthquakes of $M_W > 5$ occurred in the same general area: the first (was located 11 km SSE of L'Aquila, and the second ($M_L = 5.1$) 15 km NNW of L'Aquila. In the period April – June 2009, at least 90 earthquakes with $M_L > 3.5$ and several thousand events of lower magnitude were recorded in the Aterno Valley by the Istituto Nazionale di Geofisica e Vulcanologia.

The sequence of earthquakes caused 299 fatalities, injured more than 1500 people, and left more than 17,000 homeless (Guzzetti, 2009). Seismic shaking produced severe and widespread damage along the Aterno Valley. The Onna village suffered the highest damage, with a macoseismic intensity, I = X. Damage to the cultural heritage was large, with tens of churches and historical buildings severely damaged. The main shocks and some of the most severe aftershocks triggered landslides, chiefly rock falls and minor rock slides. Some of these landslides caused severe damage to towns (e.g., Fossa, AQ), individual houses (e.g., San Demetrio ne' Vestini, AQ), and the transportation network (e.g., the San Venanzo gorges) (Guzetti, et al. 2009).
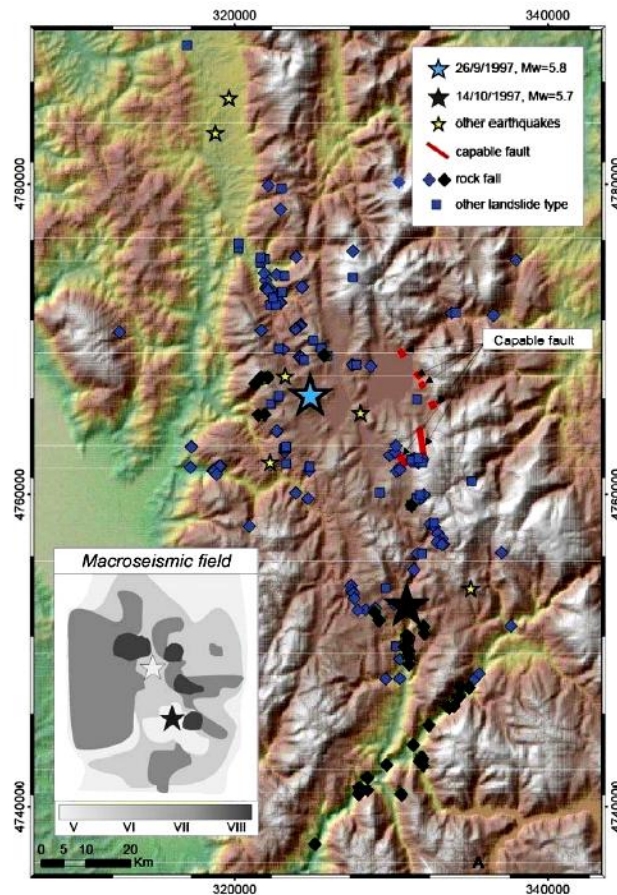

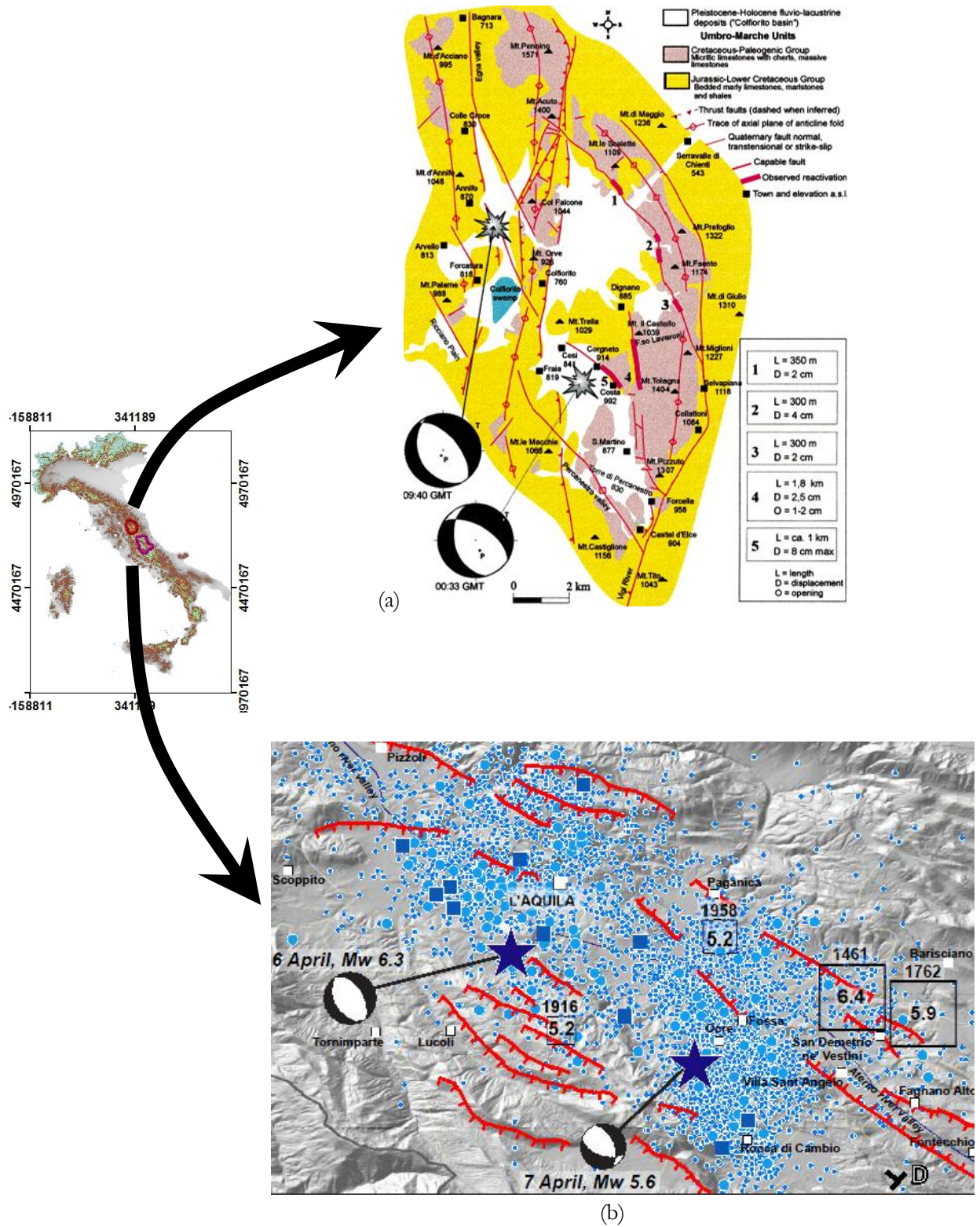Figure 3-5. Macroseismic field index with the associated EIL in L'Aquila (Guzzetti, 2009).

Figure 3-6a-b. The 1997 Umbria-Marche earthquake event after Esposito et al., (2008) (a) and the 2009 L'Aquila event (b) (Emergeo, 2009).

4.   GENERATING LANDSLIDE INVENTORIES

4.1.   Data preparation

Multiple satellite imageries are necessary to have a better mapping capability for landslide mapping. The images listed in table 4-1 were available data for the Beichuan area. Of the following images, ID's 1 to 6 were used in the EIL inventory. The spatial extent of the following data set is illustrated in figure 4-1. IDs 7 to 10 were used as cross-checks for EIL

ID	Pre/post EQ	Date of acquisition	Sensor	Resolution (m)	Spectral information	source
1	Pre-EQ	20 Dec 1968	Corona	2.75	Panchromatic	USGS Earth Explorer
2	Pre-EQ	31 Mar 07	ALOS	10	multispectral	JAXA
3	Pre-EQ	31 Mar 07	ALOS	10	multispectral	JAXA
4	Pre-EQ	19 Apr 07	CARTOSAT1	2.5	panchromatic	ISRO
5	Post-EQ	04 Jun 08	ALOS	10	multispectral	JAXA
6	Post-EQ	04 Jun 08	SPOT5	5	panchromatic	-
7	Post-EQ	24 Sep 08	SPOT5	2.5	panchromatic	-
8	Post-EQ	24 Jan 09	CARTOSAT1	2.5	panchromatic	ISRO
9	Post-EQ	31-Jul-09	Worldview	0.5	panchromatic	Digital Globe
10	Post-EQ	19 Jul 10	ASTER	15	multispectral	TERRA-ASTER

Table 4-1. Available satellite images for the Beichuan area.

Other dataset acquired for the Beichuan area are:

1. Aerial photographs – taken shortly after the earthquake event;
2. Pre-earthquake contour lines – derived from topographic contours with the scale of 1:10,000 and 1:5,000;
3. Lithology – lithologic units derived from a geologic map 1:250,000;
4. Fault lines - included all the active fault lines in the Wenchuan area; co-seismic surface rupture derived from Xu et al. (2009);
5. Location map of towns.
6. Other EIL inventory particulary the EIL inventory done by Gorum et al. (2010) and Dai et al. (2011).

The following are the available data set for the L' Aquila and Umbria-Marche earthquake event:

1. Landslide inventory – For the 1997 Umbria-Marche EIL, the data was gathered from field surveys done by Esposito et al. (2000) and image interpretation of aerial photographs as well as field check by Antonini et al. (2002). The 2009 L'Aquila inventory was taken from field surveys and high resolution satellite imagery and aerial photographs taken after the earthquake event conducted by the CNR-IRPI team. All data were represented as points.
2. CFSR – The co-seismic fault generated by the 1997 Umbria-Marche event was delineated from the work of Esposito et al. (2000); the CSFR for the 2009 L'Aquila event is from field surveys conducted by the CNR-IRPI team.

3. Epicentres – Data for the Umbria-Marche event was taken from Amato et al. (1998) and from the CNR-IRPI team for the 2009 L'Aquila event.
4. Digital elevation model – 90 meter resolution digital elevation model from SRTM (USGS, 2004).
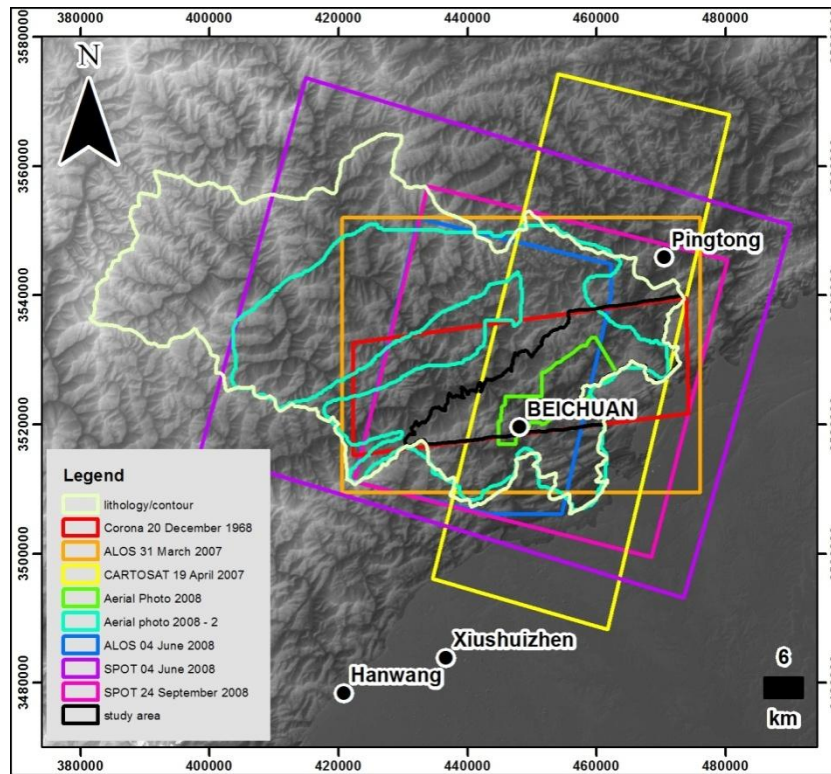

Figure 4-1. Extent of the available data used for the Beichuan area, particularly those that were used in the inventory.

4.2.   Existing EIL for the 2008 Earthquake in Wenchuan

It is a must to find existing inventory that accounted the whole EIL since the study area is just a portion of a bigger scenario of landslides triggered by the 2008 earthquake. Thorough searches among various literatures have found out that several authors have produced EIL inventories attributed to the 2008 Mw 7.9 Wenchuan Earthquake and these authors were Huang ang Li (2009), Sato and Harp (2009), Wang et al. (2009), Yin et al. (2009), Tang et al. (2009), Cui et al. (2009), Xu et al (2009), Liu et al. (2009), Gorum et al. (2011), Dai et al. (2011). Inspection among the mentioned literature lead to the conclusion that the work of Gorum et al. (2011) and Dai et al. (2011) accounted the most complete EIL inventory of the May 2008 Wenchuan earthquake. Gorum et al. (2011) identified 60, 107 active landslides through monoscopic visual interpretation of high resolution satellite imageries. The EIL were represented as points marking the source areas. Dai et al. (2011) accounted more than 56,000 individual landslides. The EIL were represented as polygons delineating each EIL. Although both inventories covered the whole EIL scenario, their inventories are to some extent less precise since: 1.) only the source area was represented in the Gorum et al (2011) inventory, 2.) the source areas were represented as points, also in the Gorum et al (2011) inventory, and 3) even when the EIL are identified as individual polygons, the type of landslide was not identified. These three circumstances can cause several imprecision such as area coverage and damage caused by the landslides cannot be assessed if landslides are represented as points or even when area is defined, the mechanism of failure cannot be justified since type is not identified. It is in these lines of reasons that the inventory made in this research accounts landslides as a polygon with identified type, subtype, and if possible, the materials involved. The data identified by Gorum et al. (2010) within the study area is 2,416 active landslides while 3, 487 individual landslides distinguished by Dai et al. (2011)
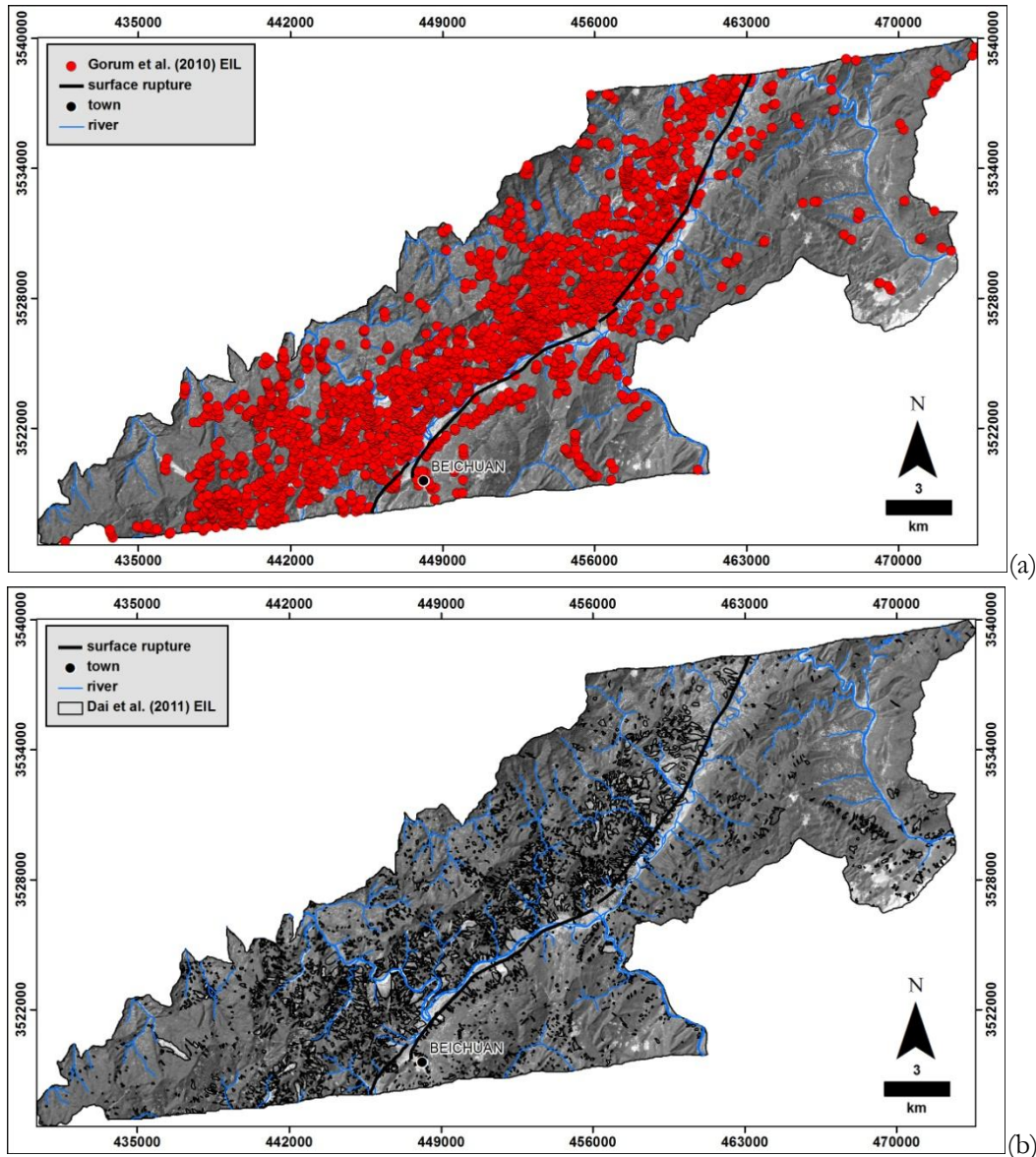
Figure 4-2a-b. EIL inventory made by Gorum et al. (2010) (a) and by Dai et al. (2011) (b) for the 2008 earthquake event bounded within the study area.

4.3. Landslide inventory

While landslide inventories may vary in terms of methods, they are mostly dependent on input data. The input data in turn depend on quality, the study area, scale, details of information, and other resources available according to the objective of the study. This section discusses the landslide inventory technique used for the dataset pertaining to China and Italy landslide events.

4.3.1. Geometric correction

For a proper landslide inventory analysis using different images, it is a prerequisite that the images are geometrically correct, are precisely fitting on a pixel basis and are on the same geographic reference and coordinate system. This will certify the integrity of landslide inventories especially when comparative analyses are carried out using the landslide and other spatial data (e.g., geology). The procedure is also necessary since landslide inventories are undertaken in different time intervals, and therefore have to be compared spatially . The images have to be geometrically corrected because they were taken by different

satellites with respective capabilities, platforms, sensors, radiometric resolution, spectral resolution, and spatial resolution.

The exact location of a pixel in an image can be determined through different techniques. For instance, using global positioning system (GPS) measurements in the field, ground control points (GCPs) can be taken and registered back so that the exact location of the pixel is identified. Another way would be to take feature locations from an absolutely determined georeference material such as topographic map produced by government geodetic survey offices. Taking locations of different features (e.g., road crossings, rooftop, and monuments) and inserting them to the image is called a tie-point procedure. However, taking GCPs and feature locations from an absolutely determined georeference material are not readily available for this study. To make up for this shortcoming, a relative georeferencing was instead used. Through relative georeferencing, the absolute location of the pixel values of the 2008 September event SPOT image was selected as the reference image. The reason for this choice is as follows: 1.) the image covers the entire study area, 2.) the cloud cover is minimal, and 3.) the image produced is almost nadir looking.

Aside from pixel location, geometric distortion of the images due to elevation differences is another consideration of the study. Since the study area has large elevation differences, the relief displacement may have affected the landslide inventory and thus might have resulted in inaccurate or wrong map coordinates. To correct this problem, all the images used were orthorectified. An optimal 15m (pixel size) digital elevation model (DEM) was derived from a combined 1:10,000 and 1:5,000 contour map following the procedure of Hengle (2005).

After all the images are properly georeferenced and orthorectified, the creation of stereoscopic imagery or anaglyph came next. A stereoscopic view of all imageries were created in Integrated Land and Water Information System (ILWIS) v3.7.1. The use of stereo image interpretation is crucial as it helps interpreter deduce, verify, and associate features in a three dimensional perspective rather than in a two dimensional perspective. The use of stereoscopic view helps illustrate the diagnostic features produced by landslides such as scars, changes in vegetation cover, and drainage disruptions. For example in, a barren landscape in an image may indicate a mass movement but can be further substantiated if located in a very steep slope or very near to a steep ridge.

4.4. Visual interpretation elements

Interpretation from stereoscopic optical images of any terrain features that include mass movements is a complex, largely empirical technique that requires a systematic method and well-defined interpretation criteria (Speight, 1977; Rib and Liang, 1978; van Zuidam, 1985).

The phases of interpretation include photo reading, analysis, classification, and deduction. The photo-interpreter will first take into consideration whether features can be detected, recognized, and identified. Then based on experience, analysis, combinations of image observations, sets of characteristics or signatures, the interpreter will deduce the features. Combinations of this set of characteristics are called interpretation elements which include tone/color, texture, pattern, shape, size, location or association (Ray, 1960; Miller, 1961; Allum, 1966; Rib and Liang, 1978; van Zuidam, 1985). This elements were used:

- Tone is defined as the relative brightness in a panchromatic image, or the color in the true-, or false-color composite. It is a fundamental, if not the most indispensable element, for distinguishing and differentiating vegetated and non-vegetated areas that are most indicative of recent landslides [number 1 in figure 4-1].
- Texture refers to the repetition of tonal variations. It is the result of the composite appearance presented by an aggregate of unit features too small to be recognized. By identifying the texture, the interpreter can infer, e.g., the materials composing the landslide. A landslide with smoother

texture can be interpreted as finer materials such as sand-sized particles as opposed to a coarser texture which may indicate presence of other debris (number 2 in figure 4-2).

- Pattern refers to the spatial arrangement of visibly discernible features and characterizes orderly repetition of certain forms, tones, textures, and relationships. For example, re
- Shape or form refers to the structure, outline and geometric aspects of individual objects in the image. It is the single most useful characteristic in combination with the stereoscopic vision for the classification of a feature such as landslide in satellite and aerial images.
- Size refers to the dimension of a feature. It is useful for interpretation purposes but is very useful in identifying properties such as extent of the target features.
- Association refers to the occurrence of features and its relation with other objects in proximity. This makes it possible to infer identification, meaning, and to some extent the meaning of the function of the features (van Zuidam, 1985). For example,
- The morphological elements that are related to the landslides (e.g., topographic site) constitute another set of elements that is crucial in interpretation. These elements determine the position of a place with reference to its surroundings (i.e., curvature, convexity, escarpment, slope steepness, drainage disruption, existence of lakes, etc.). Likewise, they are important as landslides are locally indicated by topographic anomalies.

Features are deduced by determining the relationship between interpretation elements and morphological elements (figure 4-5). For example, upper concavity and lower convexity on a slope typically indicates the presence of a landslide. Further, the combination of cone-shaped geometry (i.e., in plan) and upwardly convex slope profile is diagnostic of an alluvial fan, a debris cone, or a debris flow deposition zone. Great care must be taken when inferring the characteristics and properties of geological and geomorphological objects because morphological convergence is possible such as delineating the extent of an individual landslide may be tough when they coalesce along a hillslope or when a rock avalanche originating from the ridgecrest eating debris along its way may look like a debris flow but in fact started as rock avalanche. Then, the quality of the image is also important. Low resolution satellite imagery are not able to picture small landslide. Cloud cover is also a factor. Landslide may be undersampled if there is sufficient cloud cover. The coverage of the image is also important. A big landslide or series of landslides may not be entirely taken or seen on satellite tv ddw

All the previously described interpretation criteria are commonly used by the photo-interpreter in preparing a landslide inventory map. However, due to the large variability of landslide phenomenon, not all landslides are clearly and easily recognizable from aerial photographs or in the field. Immediately after a landslide event, individual landslides are "fresh" and usually clearly recognizable. The boundaries between the failure areas (depletion, transport and depositional areas) and the unaffected terrain are usually distinct, making identification and mapping of the landslide relatively easy for the geomorphologist, particularly for small, shallow landslides, such as soil slides or debris flows. On the other hand, for large, complex slope movements, the boundary between the stable terrain and the failed mass is transitional, particularly at the toe, while the limit is transitional along the sides.
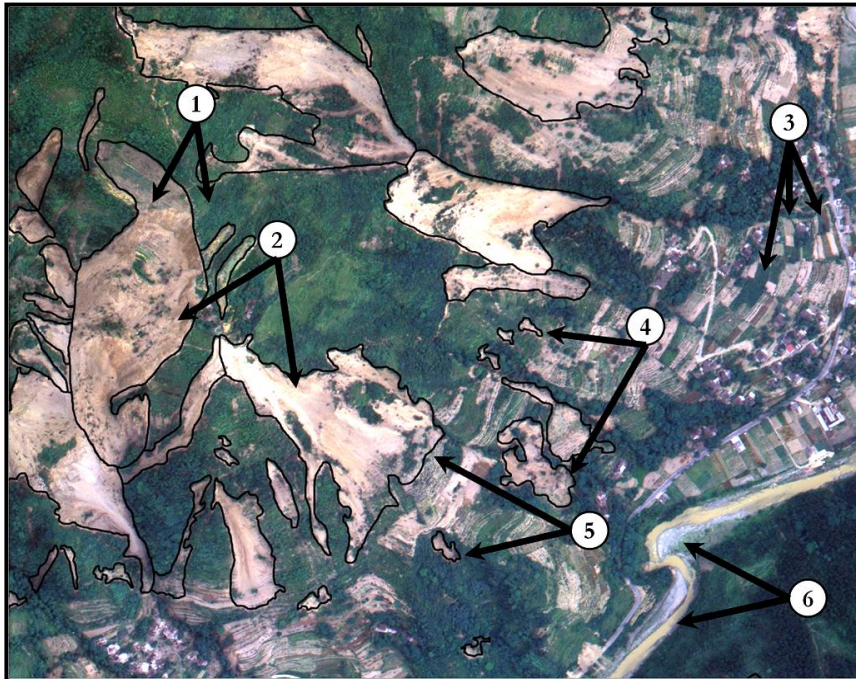
Figure 4-3. Visual interpretation element applied to image interpretation of landslides and other associated features. 1 – color difference between the landslide and its surrounding environment that is vegetation; 2 – texture difference between a coarser and smoother landslide; 3 – lath-like patterns of cropfields; 4 – shape difference of a lobular landslide compared to a very irregular outline; 5 – size difference between a relatively smaller landslide to a bigger one; 6 – association of river deposits in river bends.
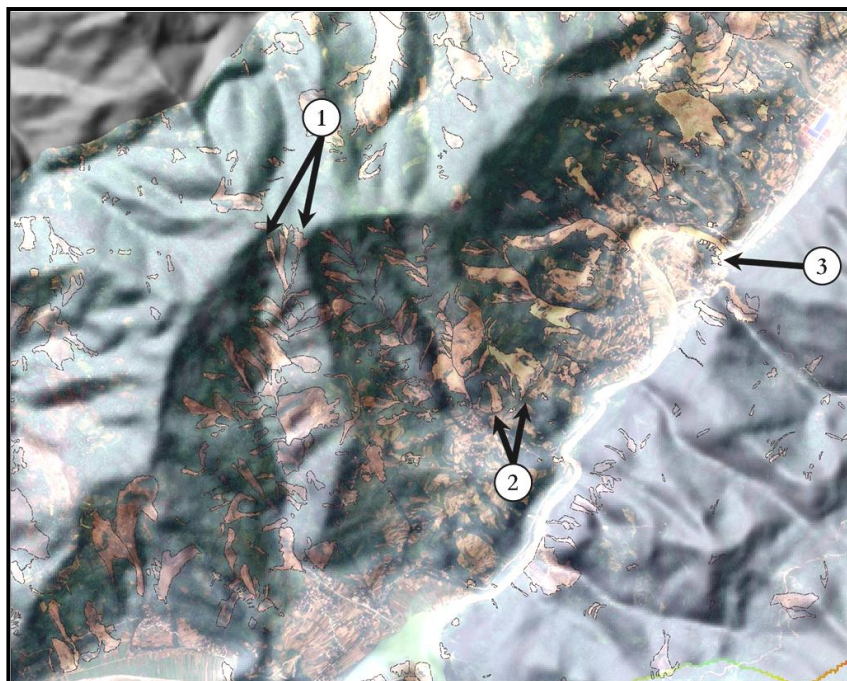

Figure 4-4. Morphological element aids in interpreting landslides. The use of stereoscopic views helps visualize the topography in three dimension therefore making landslides more apparent.1 – landslide triggered near ridges; 2 – landslides triggered at mid-slopes; 3 – landslides triggered very near the river.

For large deep-seated landslides, identifying the exact limit of the failed mass may not be easy even for fresh failures, particularly in urban or forest areas. Conversely, landslide boundaries become increasingly indistinct with the age of the landslide. This is caused by various factors, including local adjustments of the landslide to the new morphological setting, new landslides, and erosion, and vegetation re-growth (Malamud et al., 2004).

Brandinoni et al. (2003) and Korup (2005c) outlined the limitations of mapping landslides from aerial photographs in heavily forested mountain terrain, noting significant error bars and frequency underestimates resulting from the interpretation of aerial photographs when compared to detailed field studies. Nonetheless, interpretations and deductions should be maximized from the data at hand and should be justified in a scientific manner. This is treated in the following sections.

4.5. Approach to different landslide inventory

Given the limitations previously stated, a photo checklist is required. This study initially used the classification scheme of Varnes (1996). However, because the complexity of the classification could not be directly observed from the images, a modified and simplified checklist was consequently used (table 4-1).

	Type	Subtype	Materials
1	Slide	Translational	Rock
2	Flow	Rotational	Debris
3	Fall	Complex	Earth
4	Avalanche		Soil

Table 4-2. Simplified photo criteria for landslide interpretation.

The landslides were mapped as polygons delineating individual active landslides. The scarp and body were not differentiated since some imagery have relatively lower resolution than others. For example, in the high resolution aerial photographs (0.5m resolution), most of the scarps and accumulation zones can be separately distinguished but (e.g.) not readily recognizeable in ALOS (10m resolution). Since there is wide range of pixels sizes among the satellite imageries

The landslide types were identified based on the following characteristics:

1. Slide – with more or less defined scarp and body;
2. Flow – more or less defined scarp and develops into a lobular form;
3. Fall – without defined body but with more or less defined source;
4. Avalanche – an addition in the checklist; it is identified as a massive flow similar to the motion of fragmented materials, and is associated with rock avalanche since it cannot be classified among any of the other types in terms of materials.

Subtypes were characterized as:

1. Translational – smooth planar slip surface;
2. Rotational – abrupt changes in concave or convex slope morphology; or
3. Complex – combination of more than one translational and rotational subtype.

Materials were differentiated as follows:

1. Rock – hard, firm mass that is intact and had been in its original location before the movement;
2. Debris – approximately contain more coarse materials than fine materials;
3. Earth – approximately contains fine materials that coarse materials;
4. Soil – an aggregation of debris and earth; only used if debris and earth could not be distinguished.

The criteria for the materials were interpreted using ground based field photographs taken from a fieldwork conducted on 2009-2010.

Although the photo check list is simple enough, other extra criteria was implemented such as uncertainty (table 4-3). The criteria for certainty was only used for the landslides induced by the 1958 earthquake event since the Corona image that was used for the interpretation does not have the color (e.g., the ALOS image) and high pixel resolution (e.g., 0.5 m pixel resolution for the aerial photograph).

Uncertainty	Criteria	Characteristic
Certain	Slope	Extremely steep to steep
	Tone	Very light gray to white
	Shape	More or less distinct head, scarp, body, and deposits; irregular body to lobate
	Size	Distinguishable size on a 1:10,000 scale
More or less certain	Slope	Moderate slope
	Tone	Very light gray to dim gray
	Shape	More or less distinguishable head, scarp, body, and deposits; irregular body to lobate
	Size	Distinguishable on a 1:15,000 scale
Uncertain	Slope	Gently sloping
	Tone	Very light gray to off-white
	Shape	Near to almost regular polygon
	Size	Too small to be distinguished; too big for its "shape"

Table 4-3. Uncertainty as added criteria used for mapping the earth

4.6. Landslide inventories

Four different inventories were produced for the Beichuan study area. The two for the Italian area were already available. The following are the lists of the inventories for Beichuan:

1. Paleo-landslides; this included inactive landslides that were formed under climatic and geomorphoogical conditions different from the present.
2. 1958 EIL ; this included landslides that were triggered by the 1958 M=6.2 earthquake in Beichuan.
3. Before 2008 landslides; this inventory includes landslides that occurred between the 1958 event and before the 2008 earthquake event.
4. 2008 EIL. This includes the landslides triggered by the 2008 Mw=7.9 earthquake in Beichuan

The following are the inventories from Italy:

1. 1997 Umbria-Marche earthquake event; includes the landslides that were triggered by a main shock (Mw=5.8) on 1997 in Umbria-Marche, Central Italy
2. 2009 L'Aquila Abruzzo earthquake event. This is the inventory for the earthquake triggered landslides in L'Aquila, Abruzzo, Central Italy.

4.6.1. Paleo-landslides

Paleo-landslide or also known as Relict landslides are inactive landslides which developed under climactic or geomorphological conditions considerably different from those at the present (WP/WLI, 1993). In

principle, paleo-landslide is used for describing the state of activity of a landslide. However, it can be inferred from the 2008 Wenchuan earthquake that this kind of event can trigger occurrences of very big landslide such as the Tanjiashan landslide dam (~20 million m³). The Corona image, CARTOSAT 1997 images were used in a stereoscopic manner to determine the paleo-landslides. Diagnostic features such as the presence of scarp, very big size, and the more or less presence of a displacement plane were utilized to identify the paleo-landslides. This criteria may not be sufficient in identifying a real paleo-landslide since, e.g., tectonic boundaries such as a shear zone may also show the mentioned diagnostic features. The type, subtype and materials for the paleo-landslide inventory are not distinguished. Six paleo-landslides are identified (figure 4-5). The smallest identified landslide has an area of 0.7 km2 while the largest is 5.4 km2.

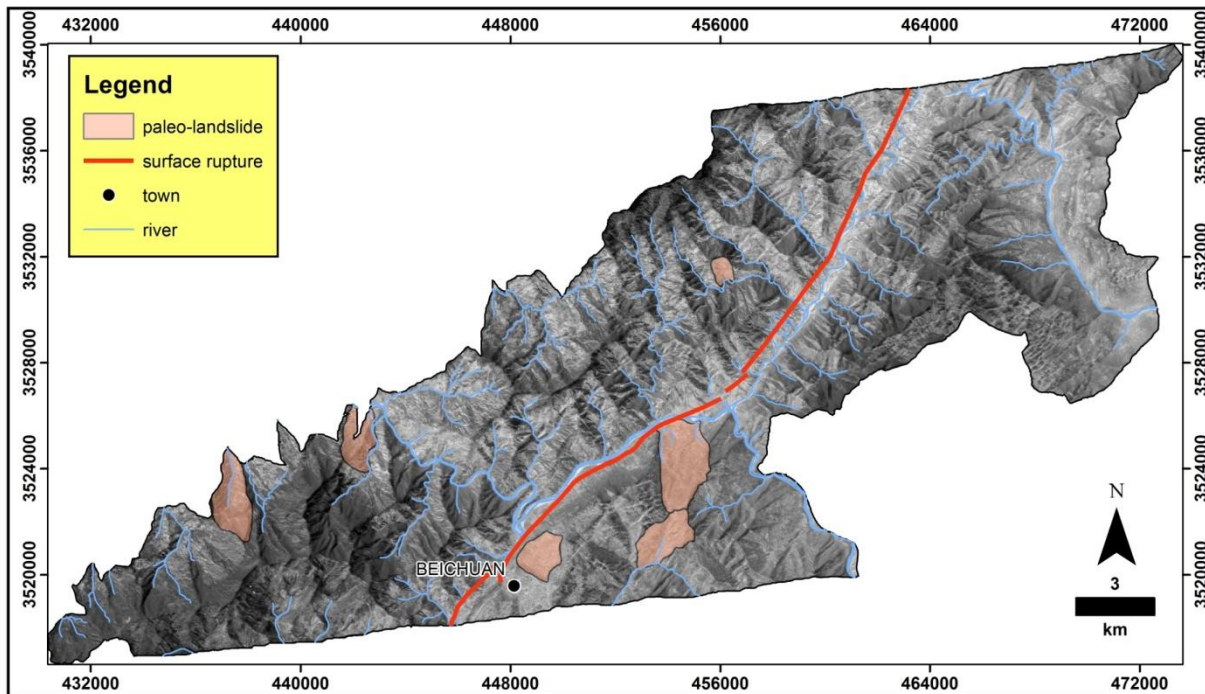| Paleo-landslides – summary statistics	
Total number of mapped landslides	6
Total area affected by landslides	16.9 km2
Percent of area affected by landslides	3.30%
Smallest mapped landslide	0.7 km2
Largest mapped landslide	5.4 km2
Mean size of landslides	2.8 km2

Table 4-4. Paleo-landslides summary statistics .

Figure 4-5. Extensive paleo-landslides located in Beichuan, China.

4.6.2. Landslides triggered by the 1958 earthquake event

The Corona image was used to map the EIL. The 15 m DEM derived from the contour lines was used to create a stereoscopic vision and anaglyph (figure 4-6a-b) at different scales. The image as such is not ideal for interpretation since the quality is less than the recent images. Contrast enhancements were utilized to enhance tonal variations and reveal unvegetated or barren features. The occurrence of rockfalls is very few that and it just may have been triggered by other phenomenon and not by, e.g., an earthquake. This uncertainty factor was categorized into three: certain, more or less certain, and uncertain. A framework is set to eliminate the bias of classifying the uncertainty of the landslide and is given in table 4-3. A few examples are given in figure 4-8.
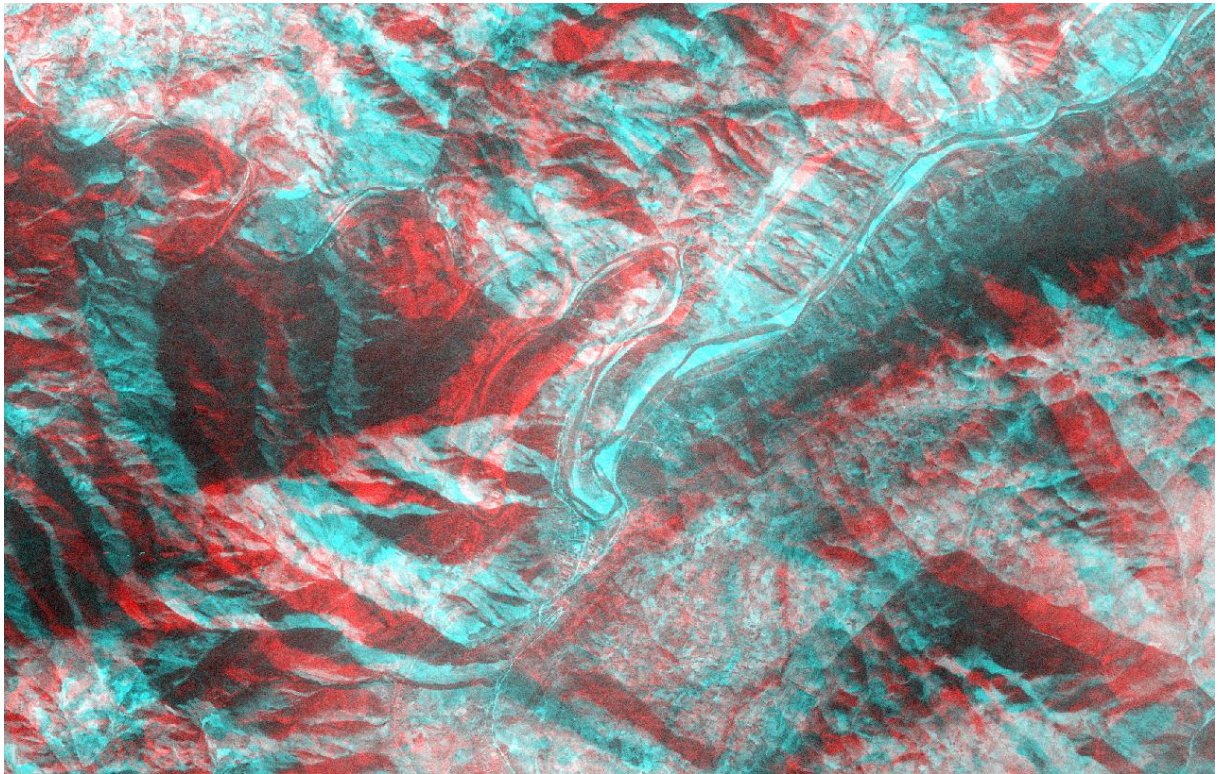
(a)
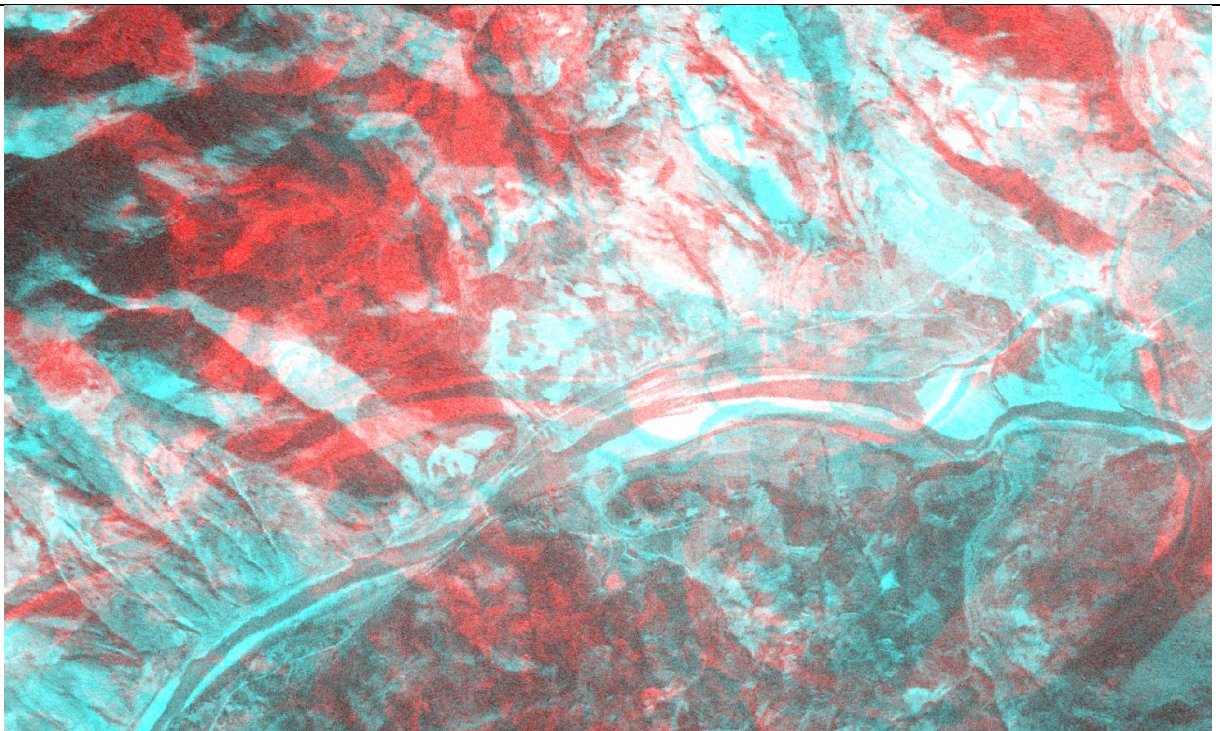
(b)

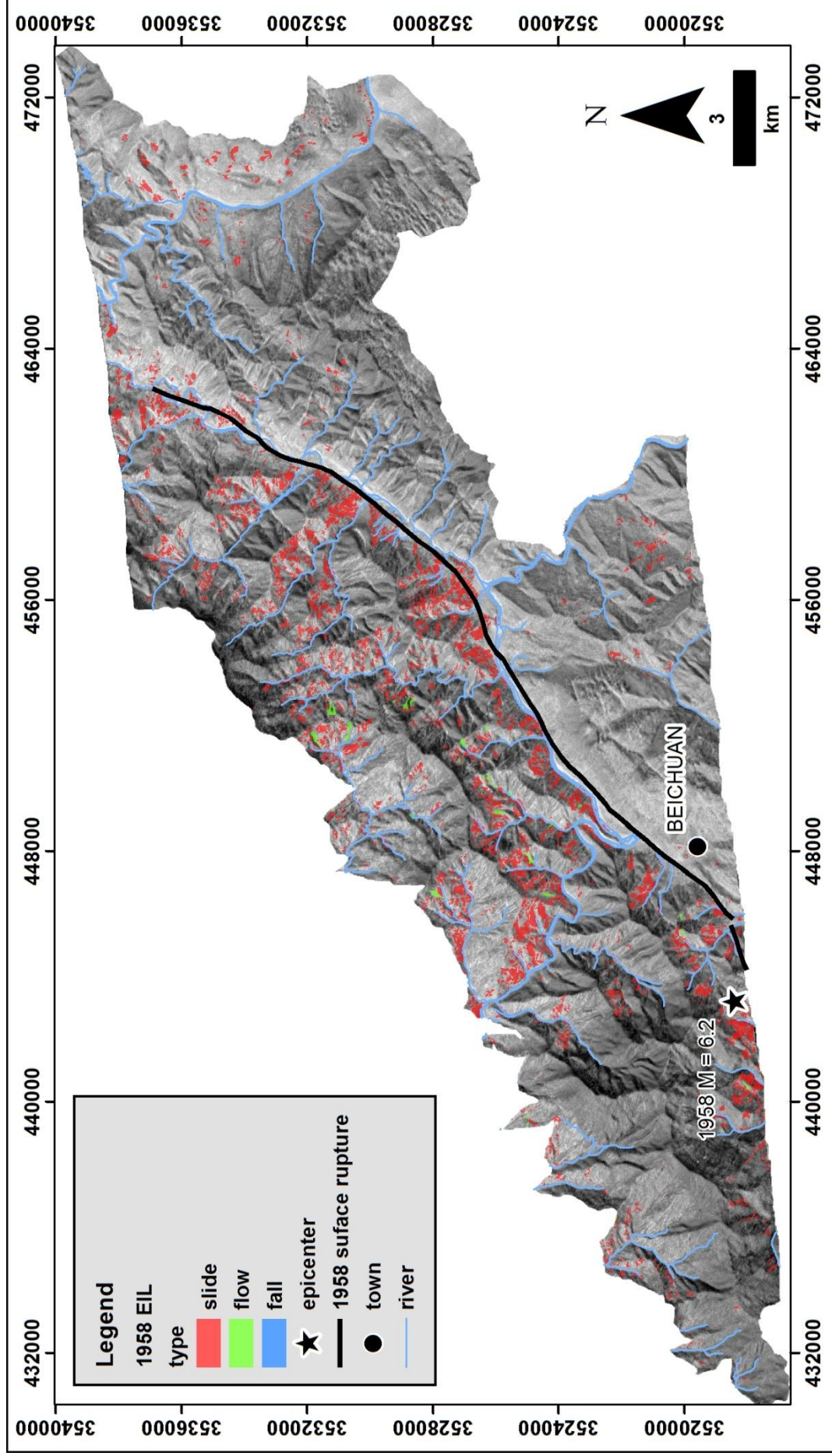Figure 4-6a-b. Corona image anaglyph at (a) 1:25,000 and (b) 1:10,000.

Figure 4-7. Landslide inventory for the 1958 earthquake event in Beichuan, China.
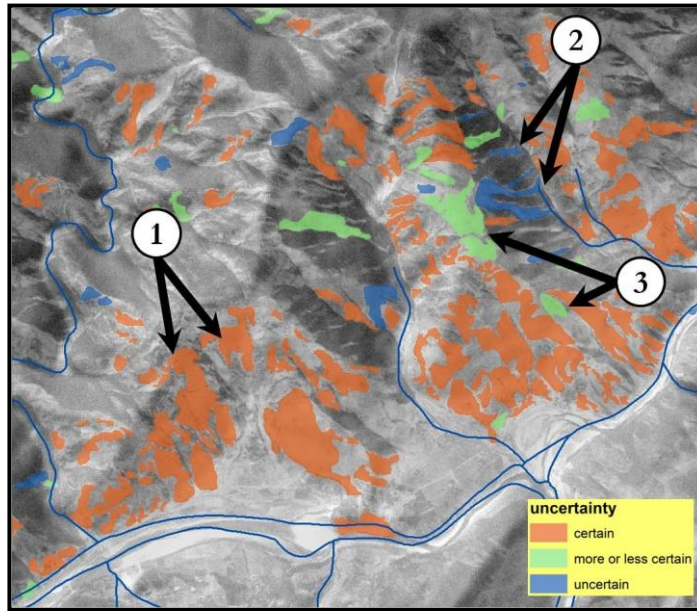
Figure 4-8. Uncertainties in the landslide inventory for the 1958 earthquake. 1 – certain landslides characterized by sloping morphology and a more or less lobate shape; 2 – more or less certain slides distinguished by moderate slopes but with darker tone; 3 – uncertain slides indicated by a bareland but on a very gentle slope and unusual form.

4.6.3.   Landslides present before 2008 earthquake event

Inspection of occurrence of landslides before the 2008 earthquake event is necessary to determine which landslides were present and might have just been reactivated. To do this, an inventory before the2008 earthquake should be secured. This was done by mapping the landslides from all the available data prior to 2008 and these satellite images were the ALOS (2007) and the CARTOSAT (2007). The 15 m DEM was used to create stereoscopic view and anaglyph images. The criteria given in table 4-1 are used in classifying landslides. The materials were not identified since a field check is not possible and no available reports were found to have studied these landslides. Only those that were certain were mapped in this inventory. The summary statistics is given in table 4-6. Of the 140 slides, 50 were reactivated from the 1958 EIL.

Before 2008 earthquake event – summary statistics	
Total number of mapped landslides	140
Total area affected by landslides	388209.7 m²
Percent of area affected by landslides	0.08%
Smallest mapped landslide	127.7 m²
Largest mapped landslide	16,876.2 m²
Mean size of landslides	2,775.1 m²

Table 4-5. Summary statistics of the landslide inventory representing the situation before the 2008 earthquake event

4.6.4.   Landslide triggered by the 2008 earthquake event

A comprehensive landslide inventory was made using high resolution (0.5m) aerial photographs, SPOT (5m), and ALOS (10m) for the situation after the May 2008 earthquake. The inventory lists the type, subtype, and materials of the landslide because of the availability of high resolution images (figure 4-9). It has to be noted that there was an intense rainfall event in Beichuan on September 22-24, 2008. Therefore, a cross check is also necessary since there are also images taken on and after September 2008. Landslide were not interpreted from imageries after the rainfall event since the landslides are triggered/reactivated now by the rainfall and not by the earthquake. However, this was still cross-checked with other images listed in table 4-1 with dates taken from 2008 onwards just to have an overview of the persistence of

landslides. It was found out that even two years after the event, some big landslides from the 2008 EIL still persisted. Fifty seven (57) slides were reactivated during the earthquake from the before 2008 earthquake event inventory. A summary statistics is given in table 4-7 and table 4-9.

After 2008 earthquake event – summary statistics	
Total number of mapped landslides	2172
Total area affected by landslides	16.9 km2
Percent of area affected by landslides	3.30%
Smallest mapped landslide	23.9 m²
Largest mapped landslide	1,311,400.4 m²
Mean size of landslides	17,176.4 m²

Table 4-6. Summary statistics of the landslides triggered by the May 2008 Earthquake in Beichuan.

According to type		According to subtype		According to materials	
Slide	1940	Translational	2122	Rock	382
Fall	179	Rotational	5	Debris	1773
Flow	46	Complex	45	Earth	17
Avalanche	7				
total	2172		2172		2172

Table 4-7. Count of 2008 EIL according to type, subtype, and materials.

Landslide name	count
translational debris slide	1641
translational rockslide	241
translational rock fall	119
translational debris fall	54
translational debris flow	35
complex debris slide	33
translational earth slide	17
translational rockflow	8
translational rock avalanche	6
complex rock slide	5
complex debris fall	4
rotational debris slide	3
rotational debris flow	2
translational earth fall	1
complex rock fall	1
complex rock avalanche	1
complex debris flow	1
Total	**2,172**

Table 4-8. Count of different landslides according to the combined subtype-material-type configuration. The translational desbris slide accounts for the most number of occurrence in Beichuan.
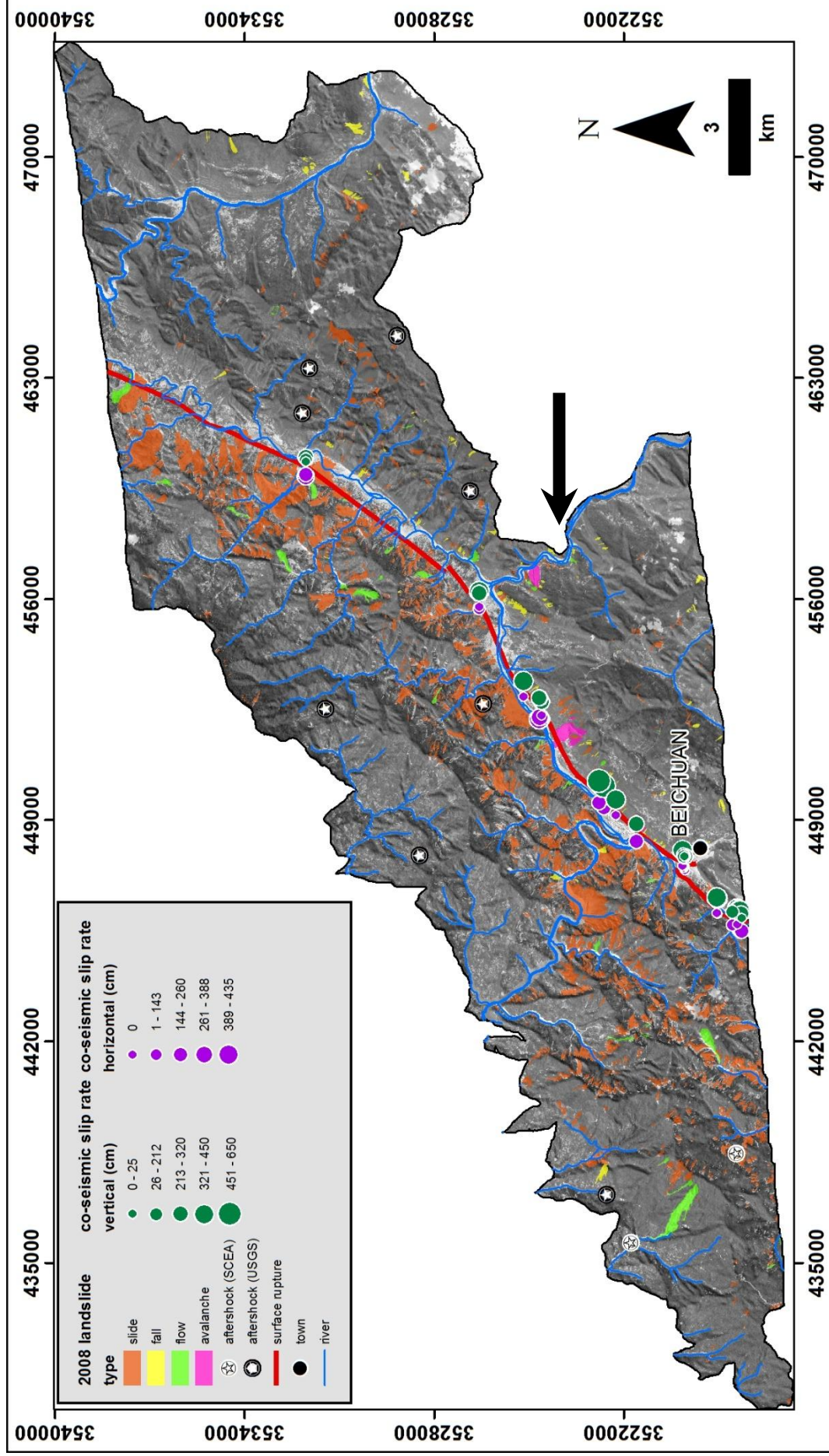
Figure 4-9. 2008 EIL types and the associated surface rupture, co-seismic slip, and aftershock.

4.6.5. Landslide inventories of the 1997 Umbria-Marche earthquake event

The landslide inventory for this event is taken from the database of the Consiglio Nazionale delle Ricerche – Instituto di Ricerca per la Protezione Idreogeologica (CNR-IRPI) in Perugia, Italy. The inventory is produced from an amalgamation of image interpretation of aerial photographs, field work, and other inventories both published and done by government and research centers in Italy (Esposito et al., 2000; Antonini et al., 2002). The inventory, however, is represented as points and not like the previous inventories that were interpreted as polygons (figure 4-10).
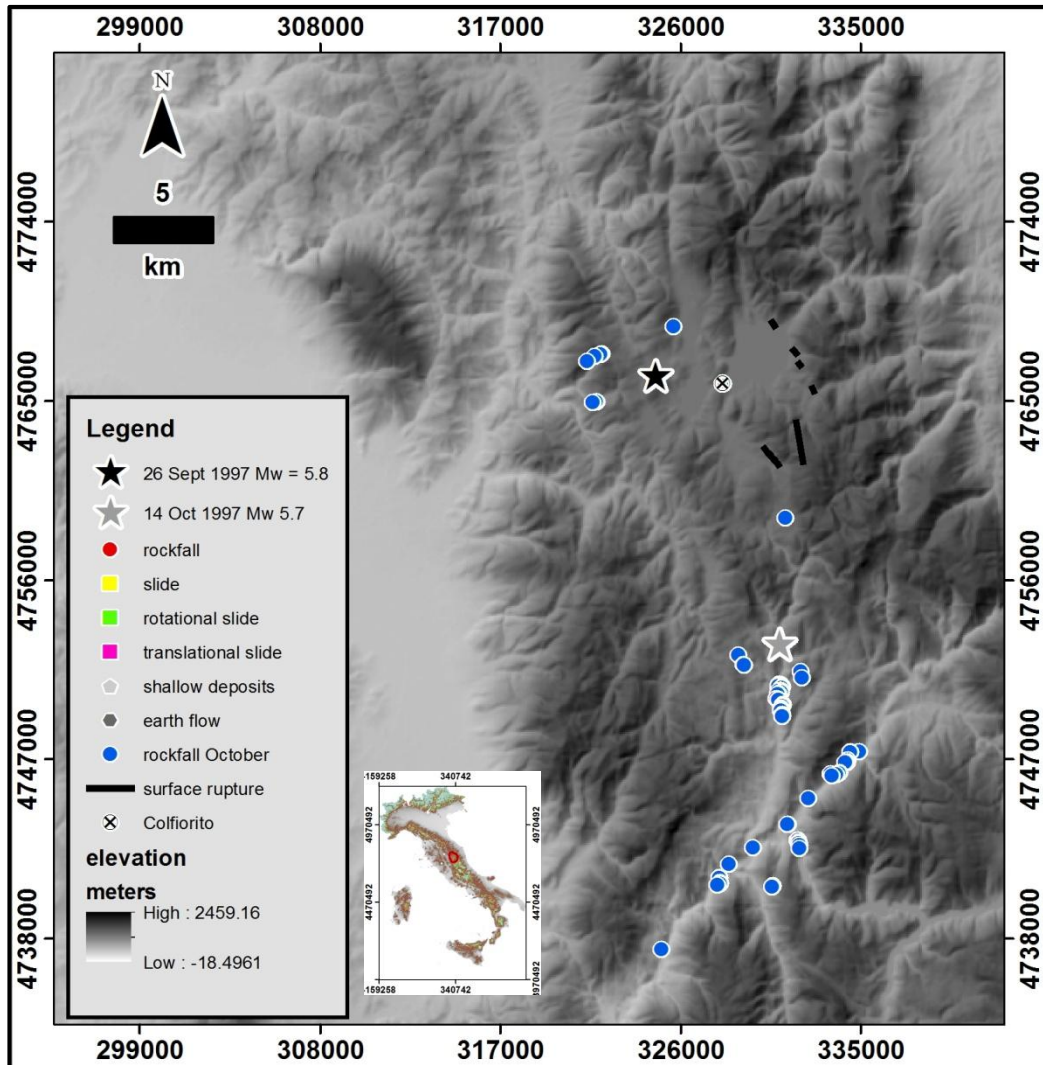
Figure 4-10. Landslide inventory for the 1997 Umbria-Marche earthquake. Inset shows location of Umbria-Marche in Italy.

September event		October event	
Landslide type	Count	Landslide type	Count
Rockfalls	99	Rockfalls	79
Slide	19		
Rotational slides	15		
Translational slides	11		
Shallow deposits	6		
Earthflows	4		
Total count	**233**		**79**

Table 4-9. Summary inventory of the Umbria-Marche EIL inventory.

4.6.6. Landslide inventory of the 2009 L'Aquila Abruzzo earthquake event

The landslide inventory for the 2009 L'Aquila Abruzzo is also taken from the database of CNR-IRPI. The dataset includes 99 identified rockfall source areas. Similar to the Umbria-Marche inventory, landslides are mapped as points and not as polygons. The rockfall source areas are used in this study among the dataset. Distribution is illustrated in figure 4-11.
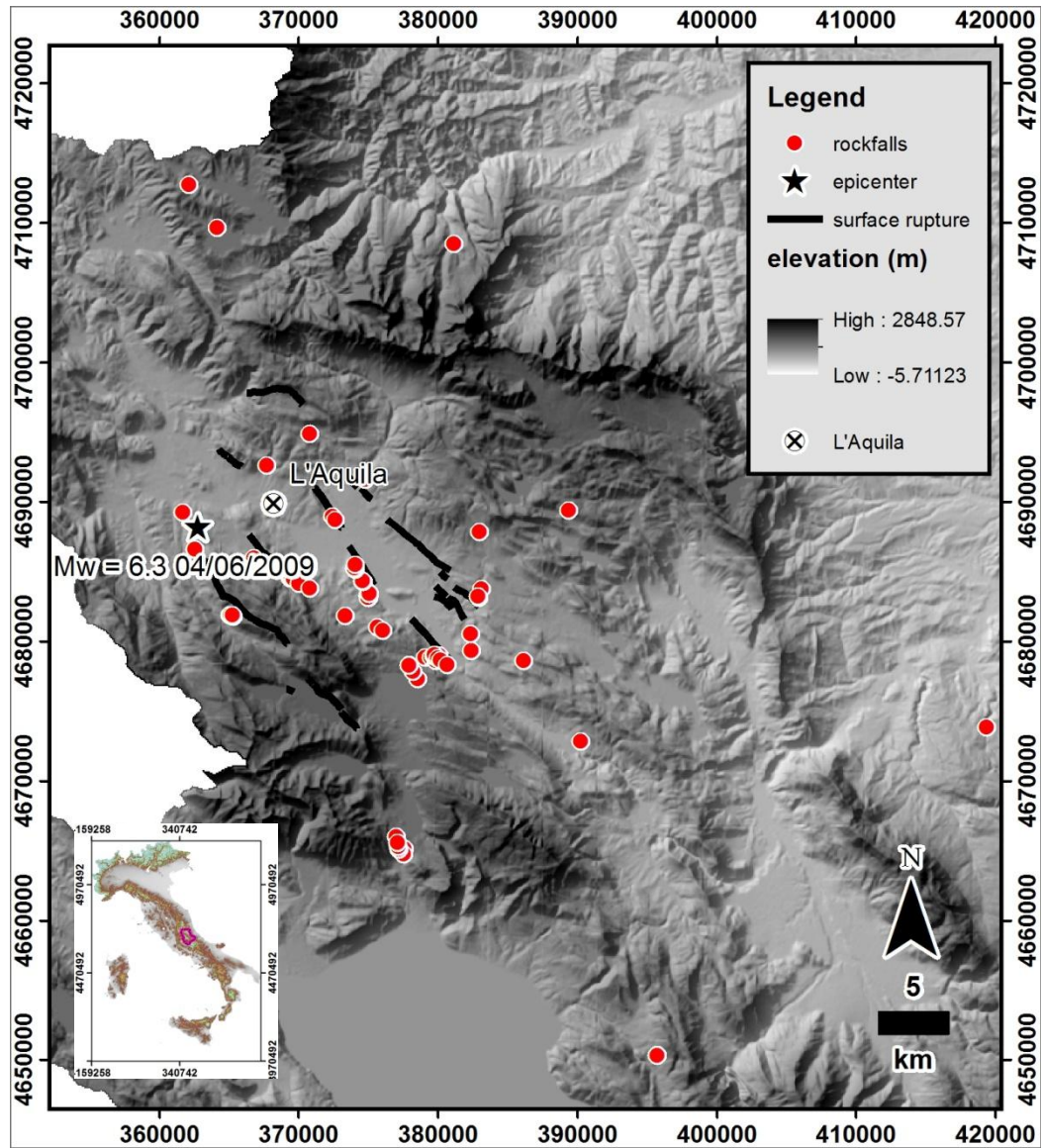

Figure 4-11. Landslide inventory for the 2009 earthquake in L'Aquile, Abruzzo in Central Italy. Inset shows location of L'Aquila in Italy.

5. SPATIAL DISTRIBUTION ANALYSIS

This chapter discusses the comparison of the distribution patterns of the different landslide inventories. These comparisons are separated in such a way that the paleo-landslides, 1958 EIL, pre-2008 landslides, and 2008 EIL inventories were compared in the Beichuan study and the L'Aquila EIL and Umbria-Marche EIL were compared in the Central Italy (figure 5-1). The analyses included frequencies of the typology between the inventories, the landslide densities, and the size probability. The typology comparative analysis does not include the paleo-landslide for the following reasons: (1) for this inventory the landslide types are not identified and (2) the approximate date of occurrence of the landslides is unknown. The size probability, however, was not done for the paleo-landslide and the pre-2008 landslides. The paleo-landslides are statistically too few to produce reliable results while the landslides triggering event for the pre-2008 inventory is uncertain. Moreover, since the main objective of this thesis is to compare EILs, then the size probability calculation is most suitable for the 1958 EIL and the 2008 EIL. The Central Italy inventories were also not calculated since EIL were represented as points and not as polygons.
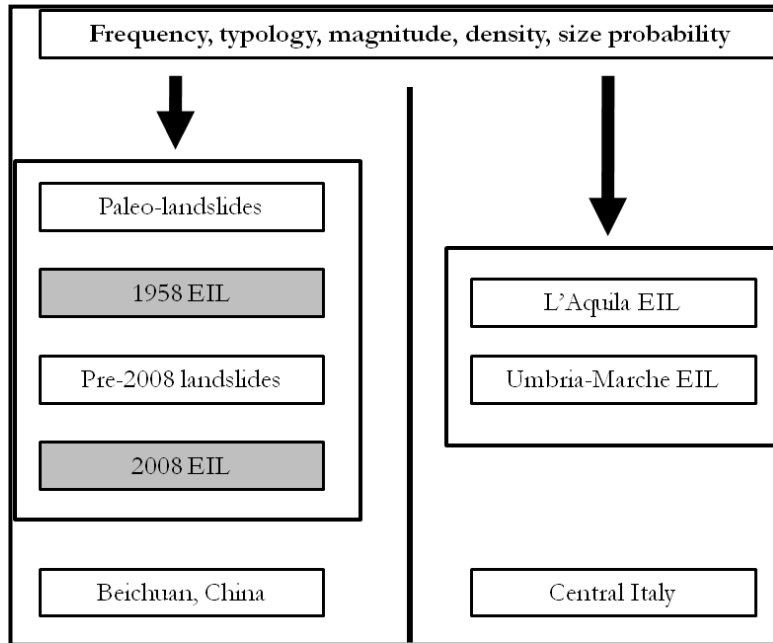

Figure 5-1. Approach to the landslide inventory comparison where two EIL inventories in Beichuan were compared as well as inventories prior to these. The same approach was done for the Central Italian area where only two inventories were compared. Frequency, typology, density, and size probability were used to compare the inventories.

5.1. Analyzing the areas occupied by landslides in 1958 and 2008

	Total area (km²)	Total number of landslides
1958 EIL	18(certain) to 25 (total)	2,210 (certain) - 3,154 (total)
2008 EIL (in the study area)	37 km	2,172
2008 EIL (in the entire Wenchuan area)	711,7807,37 (Dai et al., 2011)	48,007 (Dai et al., 2011) 60,107 (Gorum et al., (2010)

Table 5-1. EIL area and its corresponding number of occurrences for the 1958 EIL, 2008 EIL and the inventories of Gorum et al. (2010) and Dai et al. (2011) for the whole Wenchuan area.

The 1958 EIL and 2008 EIL area summary is presented in table 5-1. As such the total area covered for the 1958 EIL is lower than the 2008 EIL in the study area event when the number of landslides is bigger. This may have risen from the fact that the 1958 EIL inventory was made 10 years after the event. Therefore the landslides mapped may not be the actual landslides that were triggered by the 1958 earthquake. One possibility that may have produced the mapped landslides is the occurrence of a heavy rainfall. Within the 10 years interval between the earthquake and the Corona image, heavy storm and typhoons may have reactivated and created new. Earthquake induced landslides total area for each event and their corresponding number of landslides. Other possibility would be that it was in the rainy season when the Corona image was taken. This may although be less probable since during the month of December, the climate is relatively dry in Beichuan as reported in a 21 year (1971-2000) monthly precipitation record by Tang et al. (2009). The quality of the image is also a factor in recognizing the landslide. The quality is not ideal for mapping landslide; therefore confusion arises as whether a bare spot in the image is just due to removal of vegetation, a bright solar reflection, a clear area for cultivation, or a real landslide. Moreover, the study area, in the case of the 2008 EIL, is just a portion of a bigger landslide event. The difference in total area of the Wenchuan earthquake EIL of Dai et al. (2011) relates how big is the magnitude of difference on the study area and the whole landslides inventory. The 1958 event, although less strong than the 2008 event, produced more landslides by as much as 982 in the study area. However, if compared with the whole EIL count of the 2008 event such as the inventory accounted by Gorum et al., (2010) with more than 60,000 EIL occurrences, then the number of the 1958 EIL is just 5% of the 2008 event (figure 5-2).
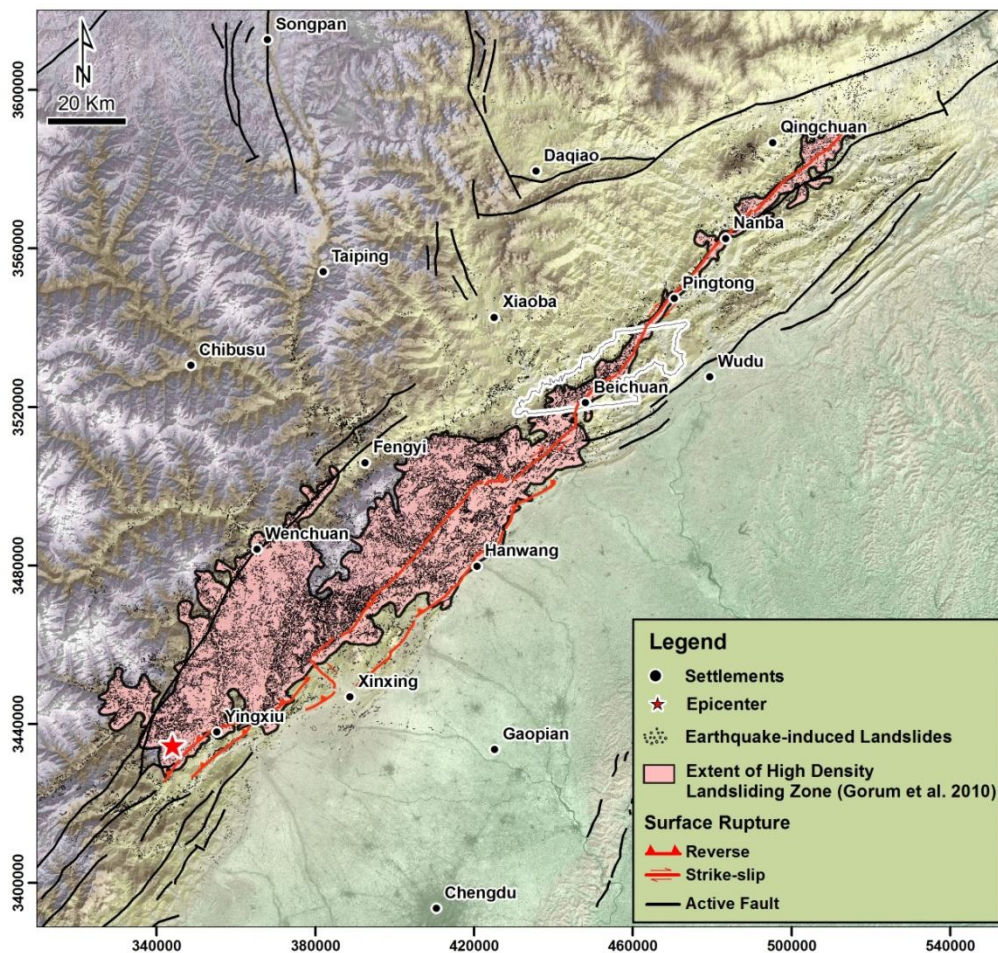

Figure 5-2. Extent of the study area (yellow outline) compared to a complete inventory of Gorum et al. (2010)

In Central Italy, the 1997 Umbria-Marche earthquake event, which is weaker than the 2009 L'Aquila, produced larger number of landslide occurrences (figure 5-3 and table 5-3). This may be attributed to other stong shock experienced in the area, such as a reported Mw = 5.7 (Esposito, et la., 1998). When compared to the 1958 event in Beichuan with only 0.1 Mw difference to the 2009 L'Aquile event, there is huge difference in the number of landslides (~97% relative difference).

	1997 Umbria-Marche	2009 L'Aquila
Magnitude (Mw)	5.8	6.3
Count of all landslides	233	99

Table 5-2. Count of landslide occurrences and their corresponding earthquake magnitude.
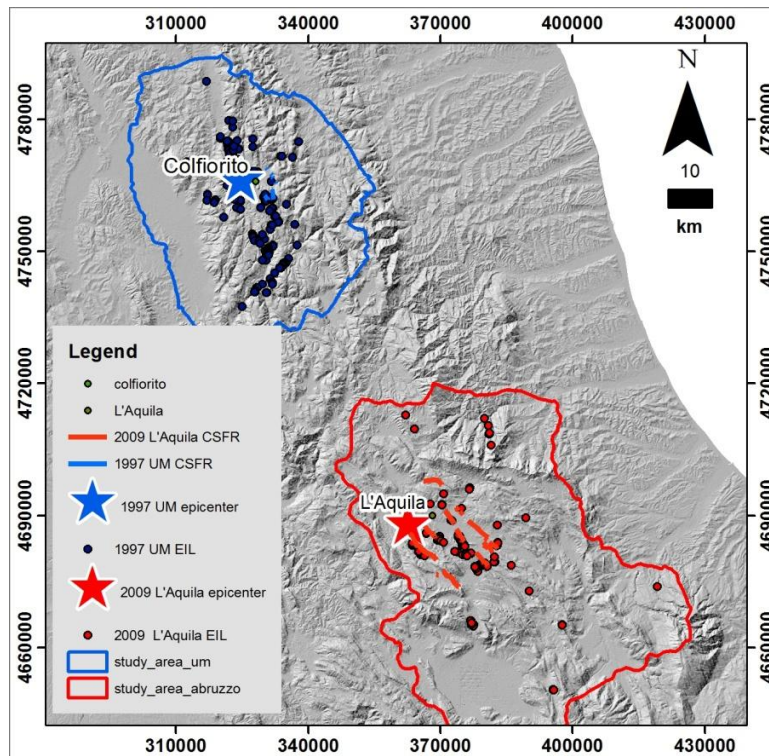

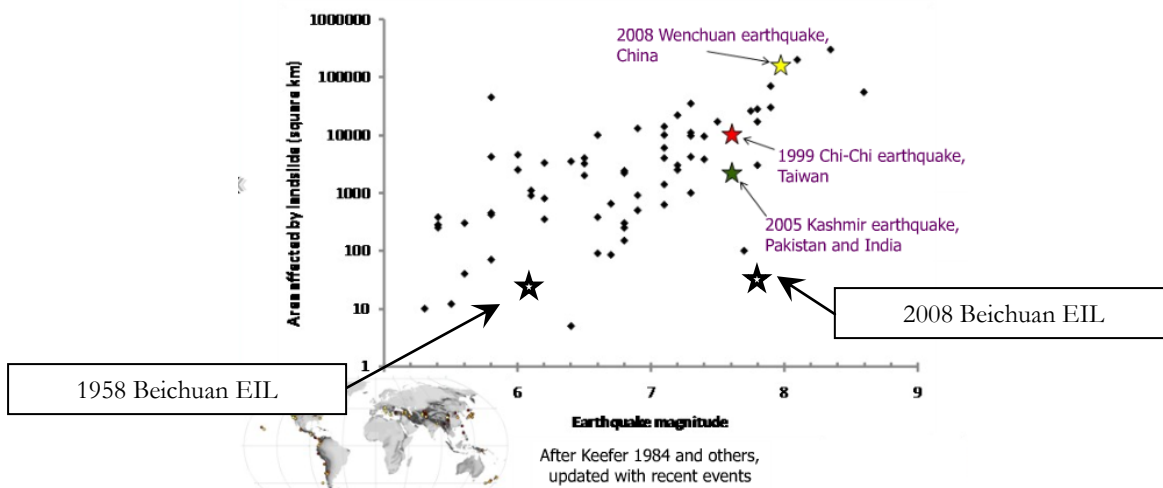
Figure 5-3. The two earthquake event in Central Italy.

Figure 5-4. The 1958 EIL and the 2008 EIL plotted on worldwide database of EIL area and earthquake magnitude (figure modified from Petley, (2009).

As a conclusion, an earthquake with a lesser magnitude produces less landslide area coverage. This is in agreement with the global database (figure 5-4) when the earthquake magnitude is plotted against the total coverage such as in the case of the 1958 EIL. To ensure good comparison, the whole landslides scenario should also be considered, otherwise, comparisons will be filled with inaccuracies.

5.2. Lanslide density analysis

5.2.1. Area density

Landslide density maps quantify the spatial extent of the EIL. These maps have many different purposes and among these are: (1) to show the general picture of the EIL distribution, (2) to illustrate a first degree overview of landslide abundance (Wright et al., 1974), and as a (3) weak proxy for landslide susceptibility. Advantages of these purposes are direct interpretation of landslide occurrences and good insight in the occurrence of landslides in the study area without leaving any unclassified areas. Moreover, since the density maps are independent of the extent of study area, comparisons are easily handled for different areas or different times (Guzzetti, 1999; Guzzetti, 2006).

Landslide density is usually calculated by the ratio of the landslide area to a mapping unit (e.g., slope unite, catchment basin, grid, etc.) and is given by the following equation:

$$D_{ls} = \frac{A_{ls}}{A_{mu}}, 0 \leq D_{ls} \leq 1 \qquad \text{(Eq.1)}$$

Where, D_{ls} is the landslide density, A_{ls} is the area of landslide within the mapping unit, and A_{mu} is the area of the mapping unit. (Guzzetti, 2006).

Although Eq. 1 provides the density within a certain mapping unit, it does not describe the density per unit area. This can be overcome by calculating the percentage of landslide within the whole study area with an artificial kernel moving systematically across the whole area. The kernel can be a circle, an annulus, a rectangle, an irregular pattern, or a wedge. Functions such as filtering, weighting techniques, and limiting distances are added to the kernel to achieve a smoother, consistent, and a more appropriate outcome (Guzzetti, 2006).

For this study, each event EIL inventory is transformed into a raster file. The pixel size of the raster is determined by the smallest area of landslides in any of the inventories. For example, in the 2008 EIL inventory, the smallest landslide size is ~25m². Therefore, to account for this size, the minimum pixel size chosen is 5 m. Then a counting circle with an area of 1km² (radius = 564.3 m) is moved throughout the area. The result is then normalized to the highest density value of the individual inventory, and finally, classified into 10 equal intervals. The area density maps for the 1958 EIL and 2008 EIL are shown in figure 5-6a and figure 5-6b. The area density is not calculated for the Central Italy since EIL are represented as points and not as polygons.

As seen in figure 5-6a and figure 5-6b, the density zones are concentrated near the CSFR. The density for the 1958 EIL is highest in the upper-left-half of the area (figure 5-5a). The footwall (right half) part is almost nil. High density zones of about 60% to 90%, indicated by green contours traversed the CSFR and is partly bent towards northwest at the top (figure 5-5a). For the 2008 EIL, the density approximately concentrates at the CSFR part of the area (figure 5-5b) where the high density zones also accumulate (60% to 90%). The lower part of the hanging wall and the footwall (left-half and right-half part has very) have minor densities.
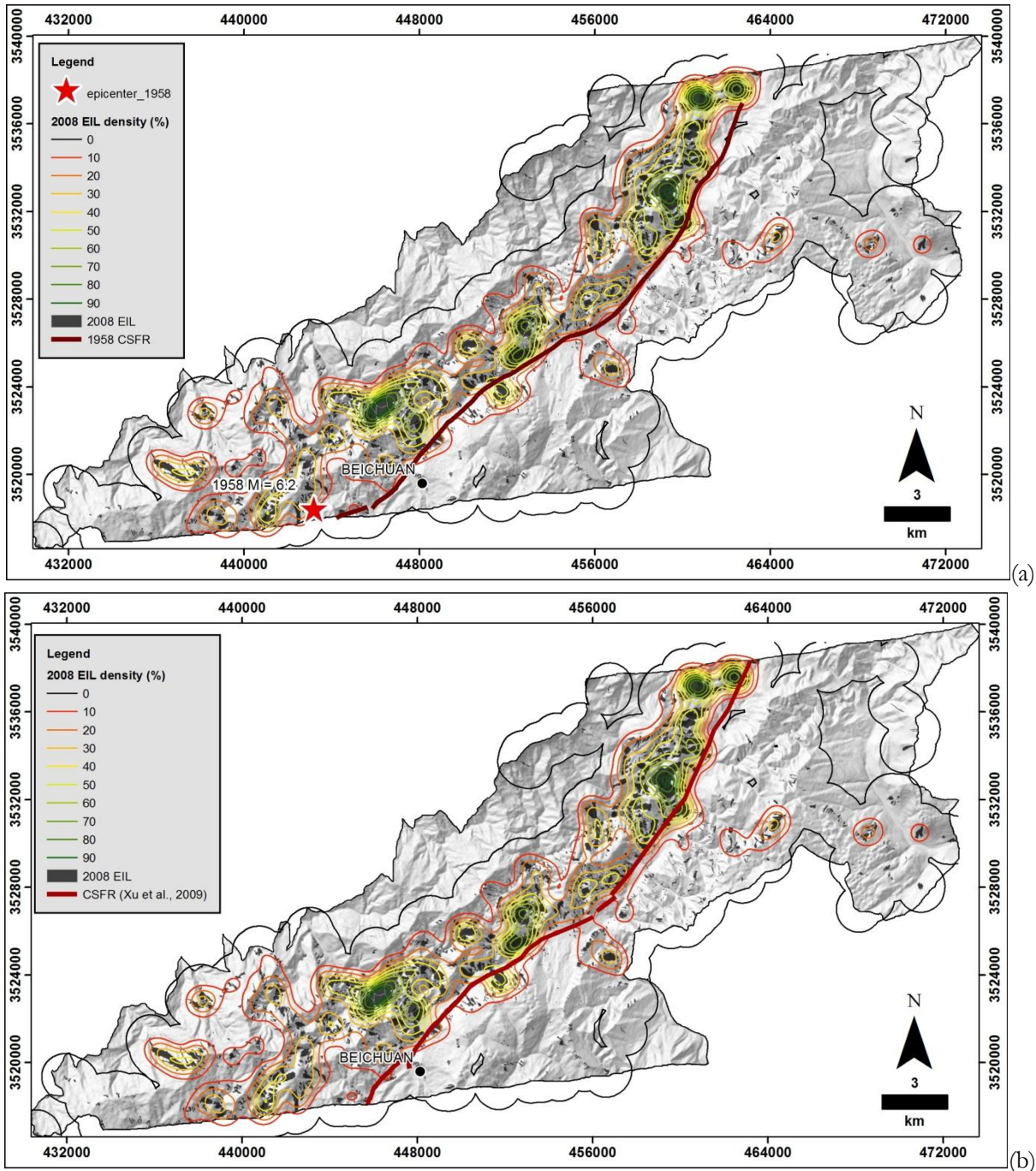
Figure 5-5a-b. Landslide density contour plots of: (a1958 EIL and (b) 2008 EIL

5.2.2. Number density

It should be noted that the landslides triggered by the 2008 earthquake (2008 EIL) in the study area are part of a bigger distribution with the epicenter located in Wenchuan, China. Consequently, there is a need at first to show the relation of the 2008 EIL to the whole scenario of the Wenchuan EIL before any quantification proceeds. To deal with this, an EIL inventory was taken from a previous work by Gorum et al. (2011) (will be termed 2008-EILT). However, the 2008-EILT inventory only accounts for the source area of each landslide. These sources areas were mapped as a point. The 2008 Beichuan EIL (which will be termed BEIL to avoid confusion) inventory was mapped as polygons. To have a better comparison with the 2008-EILT, the source areas of individual were considered.

The density of the source points of 2008-EILT and the BEIL were calculated. Then number density was calculated using a weighting kernel (refer to annex A.1 for the full explanation) (Huber, 2003). A search area of 1 km² was used. The density of the source points of 1958 EIL, and 2008 EILT just in the study area were calculated via the same manner. Results are presented in table 5-3.

	Average density (no. of landlisdes/km²)	Maximum density (no. of landlisdes/km²)
1958 EIL	3	57
2008 EIL	2	44
2008 EIL (Gorum et al.) For Beichuan area	1	67
2008 EIL (Gorum et al.) For entire area	2	41

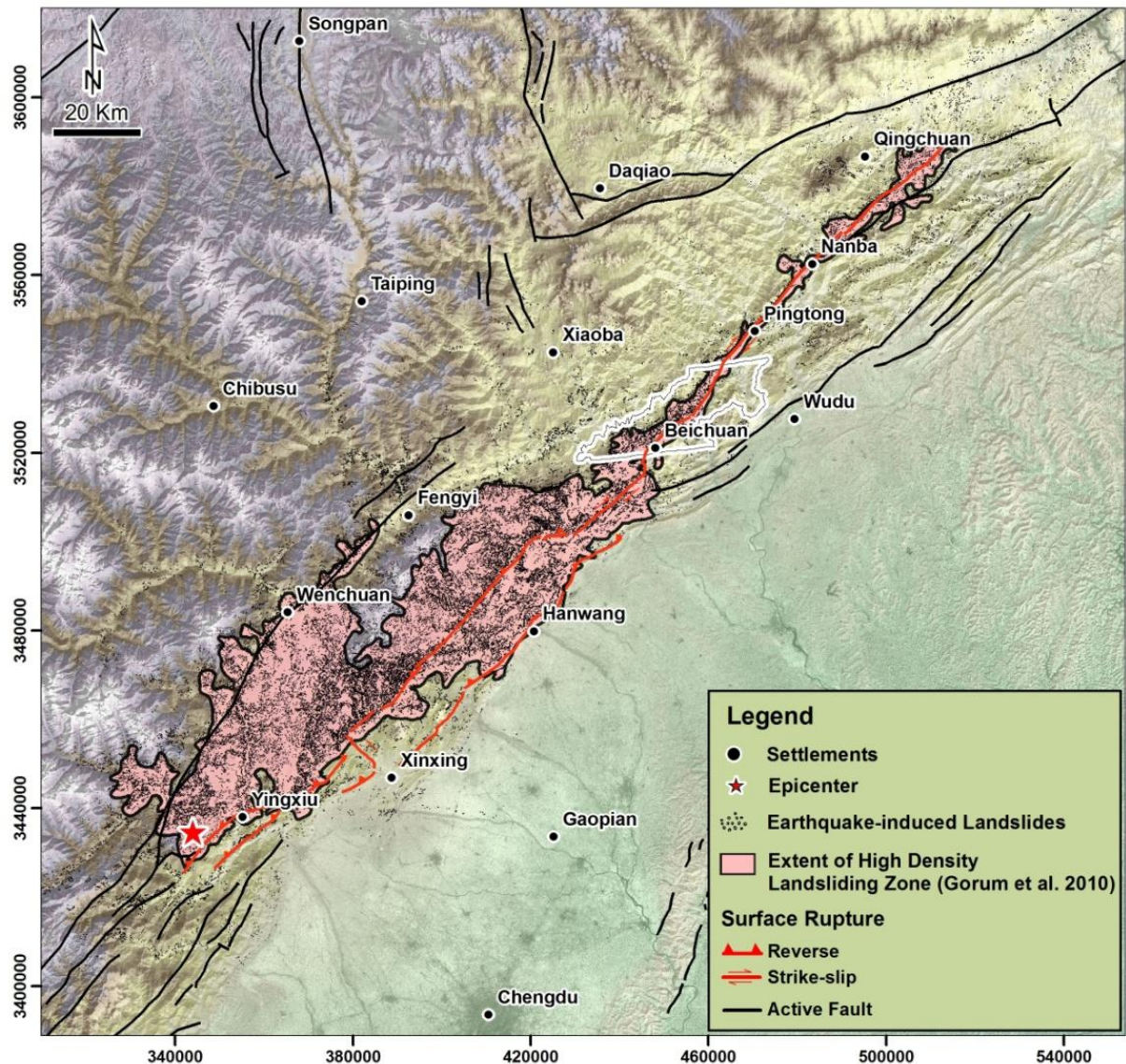Table 5-3. Landslide number densities compared for the 1958 and 2008 events

Figure 5-6. Comparative view of the density extent from the inventory done by Gorum et al. (2010) in black outline, to the study area of 2008 EIL in Beichuan inventory (light gray outline) done in this thesis. The black outline represents the 8 landslide/km².

Although the values quantify the number of landslide per square kilometer, it should be stated that the density value is dependent on the search area of the kernel. A bigger kernel size yields lower density values as the number is generalized for a bigger area. Furthermore, the inputs considered are source area points of individual landslide occurrence and not polygons. Obviously, a point does not represent the spatial extent of the landslides but only the representation of a landslide location.

5.2.3. Central Italy landslide density

The same sequence of calculations presented in section 5.2.2 were also done for the Central Italy EILs. These calculation sequences would fit the analysis of landslide density analysis for Central Italy since all landslides were mapped as point sources. The following table summarizes the number density statistics in Central Italy (table 5-4):

Landslide event	Mean (landslides/km2)	Standard deviation (landslide/km2)	Maximum (landslide/km2)
1997 Umbria-Marche	0.2	0.79	18
2009 L'Aquila	0.03	0.4	20

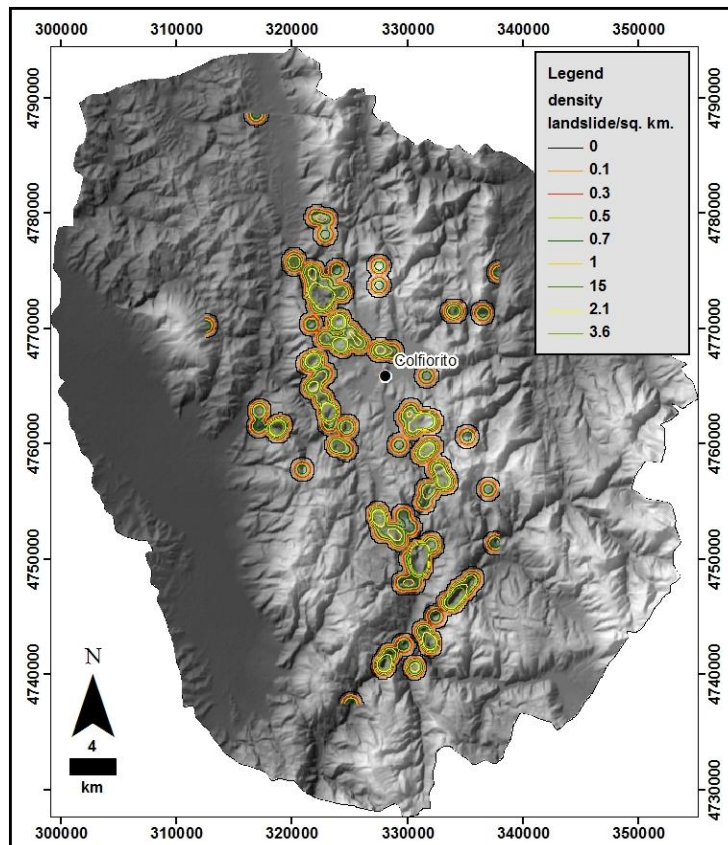Table 5-4. Landslide densities summary for the landslide inventories in Central Italy.

In the

Figure 5-7. Landslide density contour plot of all the landslides in Umbria-Marche.
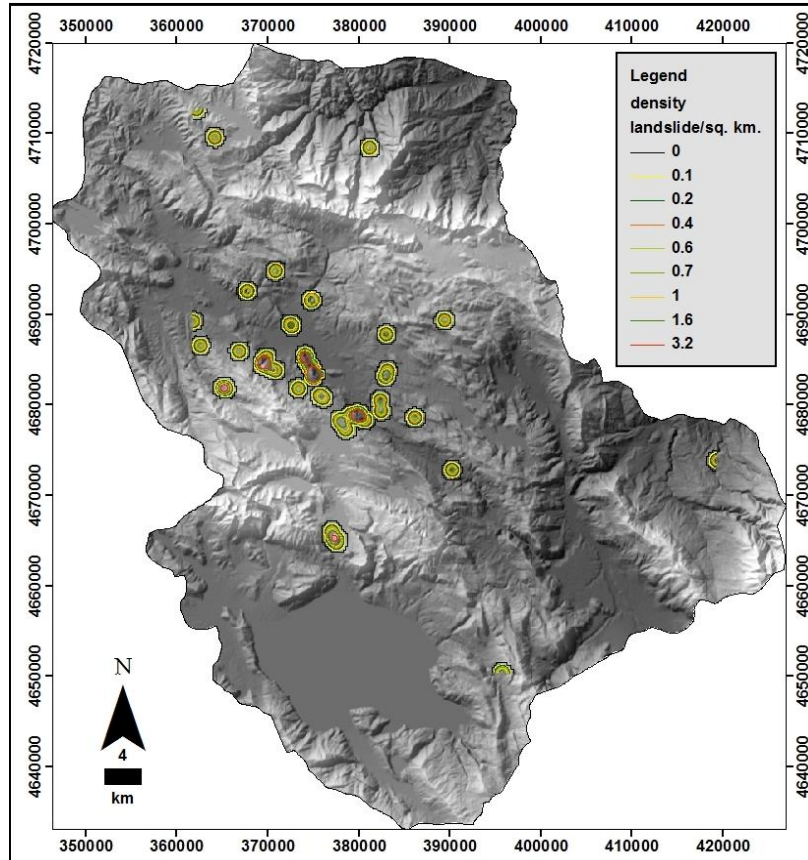
Figure 5-8. Landslide density contour plot of the L'Aquila EIL.

5.3.   Analysis of landslide types

It can be recalled from the inventories in chapter 3 that the largest number of landslide occurrences is mapped for the 1958 EIL(3154), followed by 2008 EIL (2172), pre-2008 landslide (140), and the paleo-landslides (6). The distribution and occurrences of landslides are illustrated in a small portion of the study area near the Beichuan town (figures 5-2a to figure 5-2d). The paleo-landslides, although very few, are very large in size (figure 5-2a) relative to any of the inventories. The 1958 EIL as seen in figure 5-2b are mostly on the left part of the 1958 surface rupture. The pre-2008 landslides are very few and have minor sizes (figure 5-2c). The 2008 EIL landslides occurred mostly on the left side of the 2008 surface rupture (figure 5-2d).

Furthermore, it can be observed from figure 5-3 that the landslide type "slide" has the greatest number of occurrences in all of the inventories followed by "fall" then "flow" types. The "avalanche" type had the fewest, with only seven counts. For the 1958 EIL, the majority of the landslide type is "slide". It accounted for about 98% of all the landslide types. The flow and fall combined (41 counts) is very minor compared to the "slide" type (3113) and accounted for about 2% of all the landslides. It does not have any "avalanche" type compared with the 2008 EIL. It has the greatest occurrence of landslides among the inventories – 982 landslides more than the 2008 EIL and 3014 landslide more than the pre-2008 (figure 5-3).
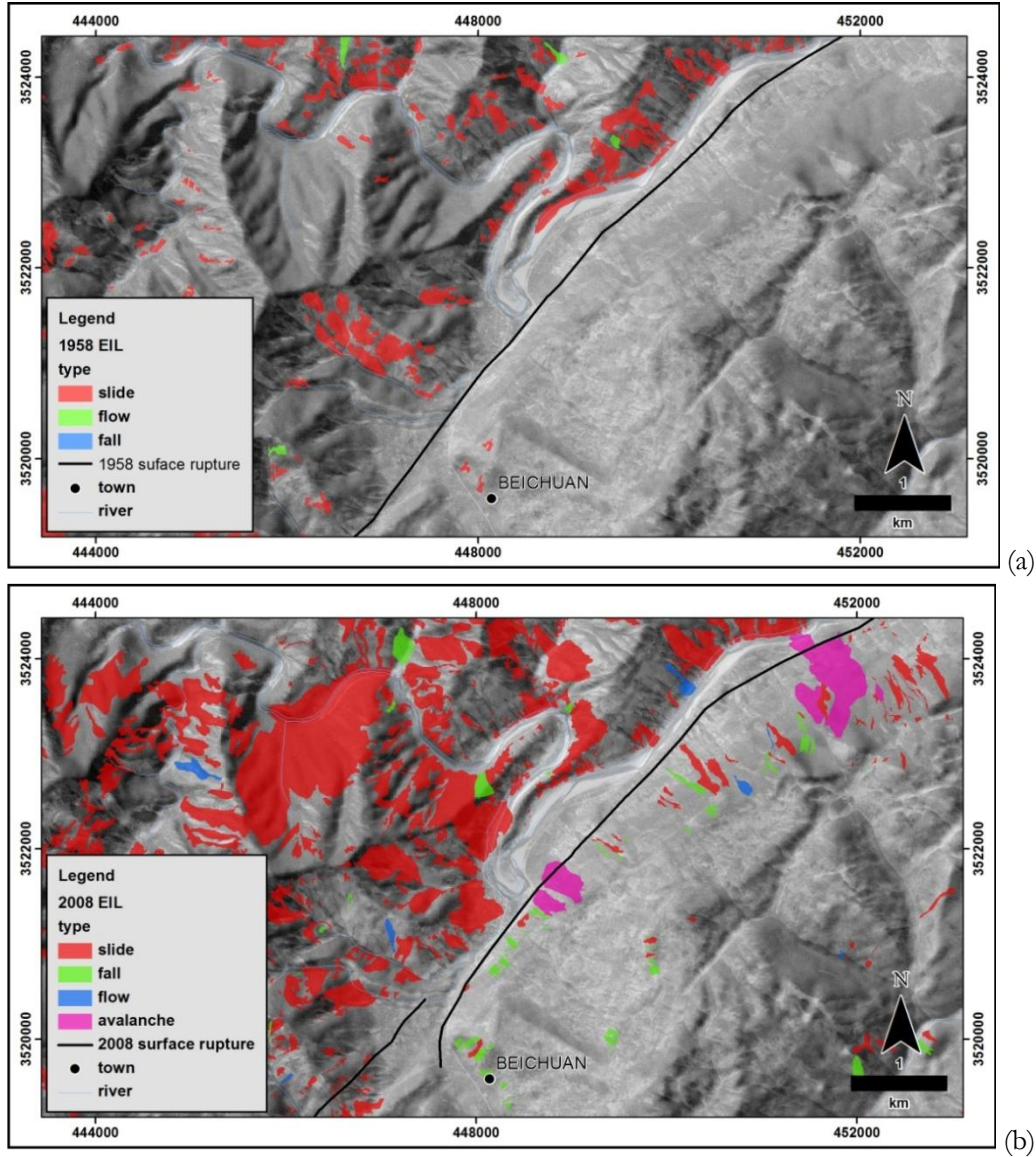
Figure 5-9a-b. Landslide comparison of the EIL inventory of for the 1958 event (a) and the 2008 event (b).
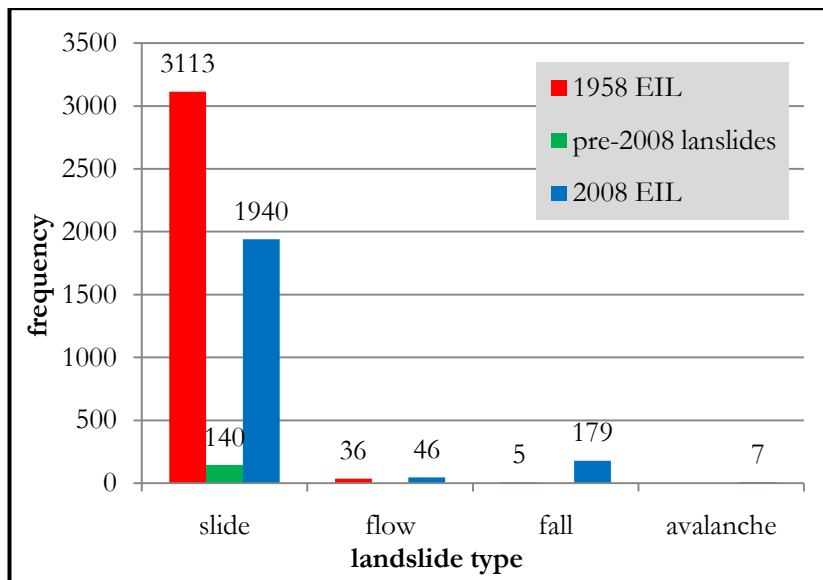

Figure 5-10. Landslide type and count for 1958 EIL, pre-2008 landslide, and 2008 EIL.

The pre-2008 landslides consist of only the type "slide" (140). It is very minor compared to the other occurrences

5.4. Analysis of reactivated areas

The number of spatial overlaps between the landslides triggered by the earthquake events in 1958 and 2008 in Beichuan, was calculated (table 5-2) to determine which landslides that were triggered by the 1958 event may have been reactivated by the earthquake in 2008 . This was calculated using the intersection operation in a GIS environment. Then the intersection was calculated between each landslide type. The results are presented in a cross table between the three landslide types of the 1958 EIL with the four landslide type of the 2008 EIL (table 5-2).

From table 5-2, it can be interpreted which landslide type of the 1958 EIL were reactivated in 2008. The 1958 EIL slide has the greatest co-occurrence (1114) to all the 2008 EIL. Similarly, the 2008 slide has the greatest co-occurrence (1067) with all of the 1958 EIL.

5.4.1. Degree of matching of the 1958 EIL and 2008 EIL

Although section 5.2.1. determined how many of the landslide from the 1958 earthquake were reactivated in the earthquake of 2008 were, it does not quantify how much of the area for each landslide type for 1958 EIL matches with the 2008 EIL or the other way around. This can be solved using a degree of matching or mismatching. A degree of mismatch can be calculated as proposed by Carrara et al. (1992). This method was originally used to quantify the comparison between two geomorphologic landslide inventory maps done by different individual(s) over the same area but is nonetheless a robust method for comparing two landslide inventories. To quantify a degree of mismatch between two inventory maps, E, an equation (Guzzetti, 2006) is given as:

$$E = \frac{(A'_{LT} \cup A''_{LT}) - (A'_{LT} \cap A''_{LT})}{(A'_{LT} \cup A''_{LT})} , 0 \leq E \leq 1 \qquad \text{(Eq. 1)}$$

Where A'_{LT} is the total landslide area in the first inventory map and A''_{LT} is the total landslide area in the second inventory map.. Since the values are normalized to $(A'_{LT} \cup A''_{LT})$, the range of E is from 0 to 1. Therefore, a degree of matching, M, can also be calculated:

$$M = 1 - E, 0 \leq M \leq 1 \qquad \text{(Eq. 2)}$$

Therefore, if M approaches the value of 1 then E approaches the value of 0 and vice-versa. This implies that if $E = 0$ this implies that there is a perfect match between the two inventories ($E = 1$). The opposite operation is also true, when there is a complete mismatch between the two inventories, $E = 1$, then the degree of matching (M) is 0. However, it is almost impossible to have a perfect match ($M = 1$) between two inventories as this would imply that the occurrence of a previous landslide is perfectly similar to another landslide event.

The percentage of the area covered by the 1958 EIL in the study area is 5.8% while 8.6% for the 2008 event. The total area common to both the 1958 EIL and the 2008 EIL is 3.4 km², which is 0.8% of the whole study area (figure 5-4b). The total area containing both event is 59.1 km² and accounts for 13.7% of

the study area (figure 5-4b). The degree of matching, M, between the two landslides is 0.05 (or 5%) while the mismatch is 0.95 (or 95%). The landslides that were reactivated is 700 during the 2008 event.
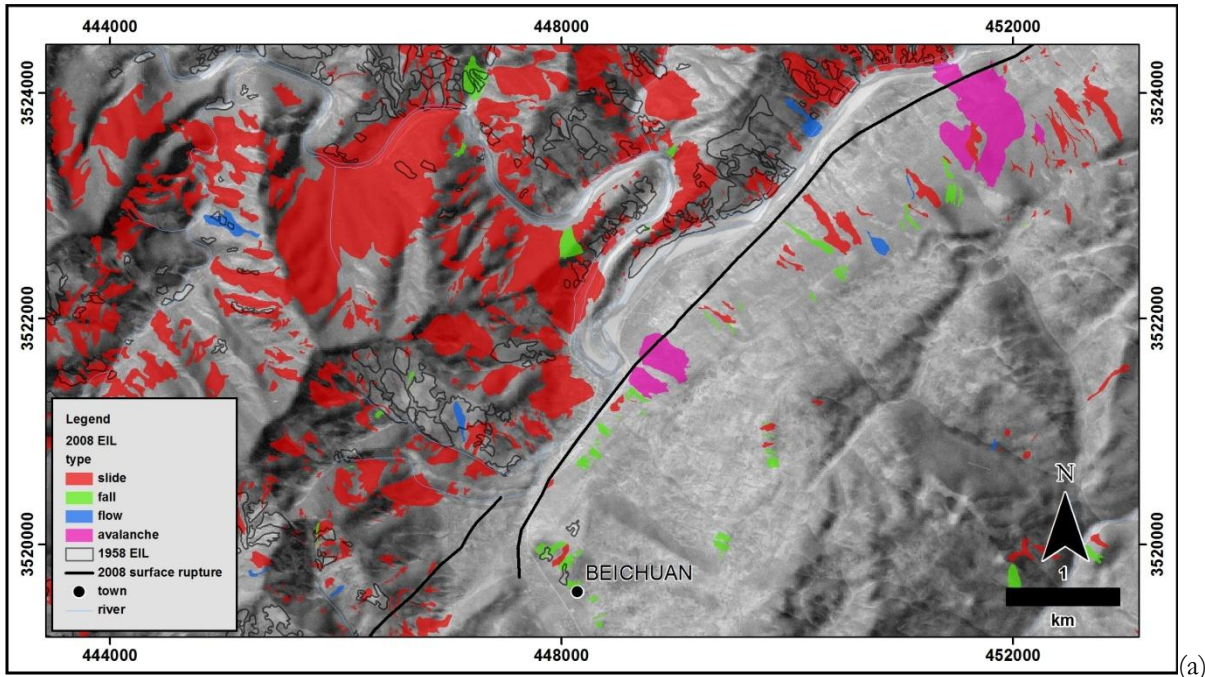
Figure 5-11a. Earthquake induced landslide spatial overlap. a – 1958 EIL (black outline) traced on top of the 2008 EIL.

5.5.   Landslide typology comparison in Central Italy

The type of landslide for the individual inventory and its respective frequency in Central Italy is illustrated in figure 5-2 below.
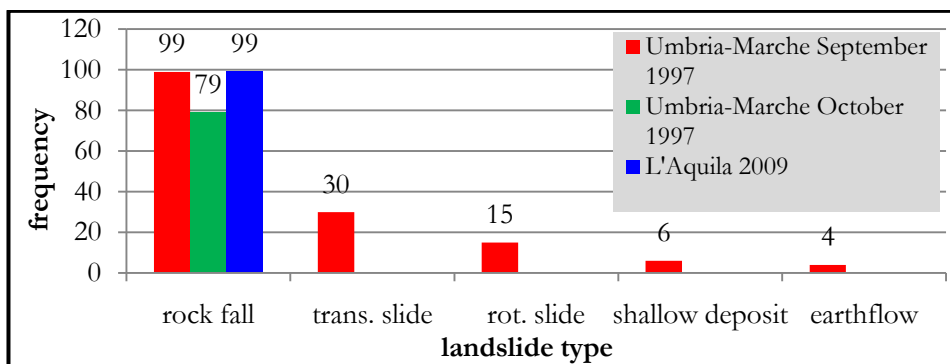
Figure 5-12. Landslide type and count for Umbria-Marche September 1997, Umbria-Marche October 1997, and L'Aquila 2009 EIL.

The EIL type that occurred the most is the rock fall for all the event.

5.6. Size frequency analysis

In section 5.2., the frequency of the EIL as a function of landslide type was discussed. However, there is a need to characterize and inspect the variability of the size or area of landslide occurrences. However, due to certain factors such as landslide freshness, quality of the available imagery, scale of maps, and the complexity of the terrain in terms of geology and morphology, the uncertainties that arose from the expert-based interpretation and the degree of completeness and reliability of the landslide inventory is affected (Malamud et al., 2004a). Other instances are landslides digitized in the GIS interface where the interpreter may not accurately delineate the boundary of the landslide. This can also be a function of the quality of the image. It may be hard for the interpreter to delineate small landslides on low resolution satellite imagery. It may also be the case when the images are taken at some time after a landslide triggering event, such as earthquake, occurred. The interpreter may miss out landslides that are cleared out by vegetation growth, precipitations, fluvial processes, anthropogenic processes, and other natural processes that erase traces of landslide occurrences. Therefore, it is important to assess the sizes of landslides through credible methods of calculating size-frequency distributions.

5.6.1. General size statistics and histogram distribution patterns

Min. : 104	Min. : 24
Mean : 79845	Mean : 17176
Max. : 373379	Max. : 1311400
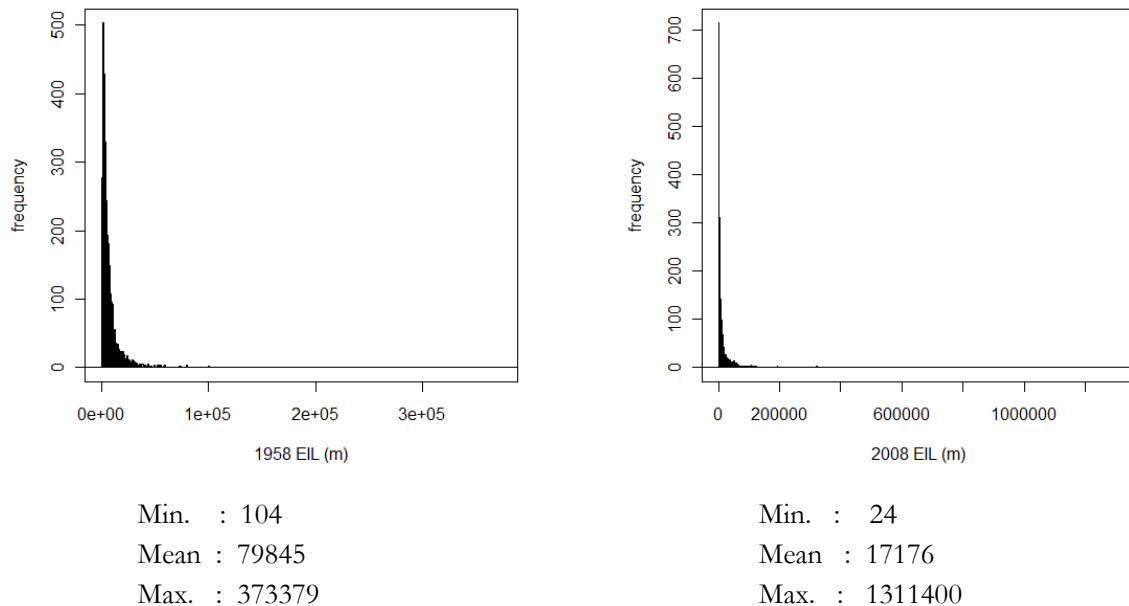
The 1958 EIL (figure 5-10b), is heavily skewed to the left and the histogram bins are not anymore recognizable on the left side of the histograms. This is due to the wide range of values spanning from scales of tens to millions of square meter. The paleo-landslides have the greatest range (=4,670,704 m²) of landslide area. The 2008 EIL slides have the widest range of values among all the EIL types (=1,311,376 m²). For the 1958 EIL, the slides also have the widest range of values (=373,275.60 m2).

5.6.2. Size-frequency statistics of EIL

The landslide area distribution can be statistically calculated through a cumulative or non-cumulative manner (Guzzetti, 2006). One way of representing non-cumulative distributions is through histograms. Before creating the histogram, a proper bin width and the bin endpoints must first be secured (Guzzetti, 2006). There are several was to accomplish this and one way is to transformed the area into logarithmic values to come up with a histogram having a log-normal distribution scale in the x-axis (figure 5-11).

Added procedures should be handled when plotting values in x- and y-axis with logarithmic values such that the number of landslides in each logarithmic bin is normalized by the width of the bin. This now represents the frequency density. To obtain the probability density, the frequency density in the logarithmic bin is normalized by the total number of landslides. However, the representation via histogram bin width selection poses a problem since the histogram depends on assigning bin width and the end points of the bin. If the data distribution is not smooth, it may give errors specially when there is a lack of data. Therefore, to have a better estimate, a Gaussian kernel density (figure 5-12a-d) and a maximum likelihood estimate is approached.

5.6.3. Probability distribution functions

The frequency density and the probability density for the areas are now calculated for the 1958 EIL and the 2008 EIL inventories. For this section, three probability distributions functions are fitted: double pareto (Stark and Hovius, 2001), double pareto-simplified, and the truncated inverse Gamma distribution (Malamud et al, 2004a).
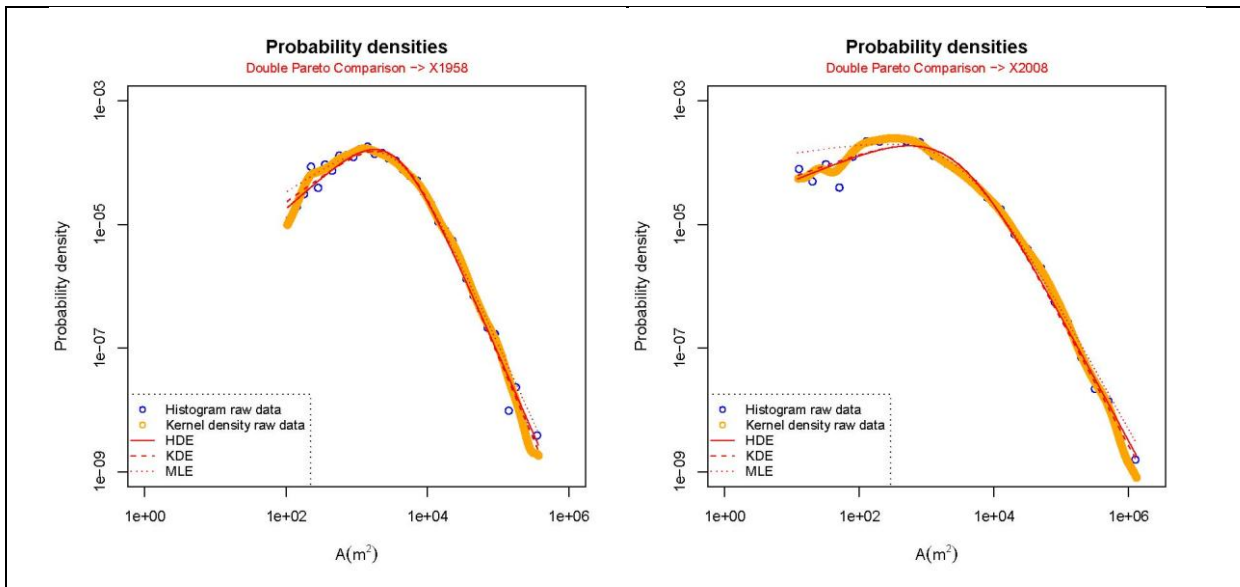

Figure 5-13. Probability densities estimated by a truncated inverse gamma distribution using histogram density (a and b), kernel density (c and d), and maximum likelihood estimations (e and f).

6. SPATIAL ASSOCIATION ANALYSIS

Various literatures have determined spatial distributions of Wenchuan EIL that were related to geologic, geomorphologic, topographic, and seismic parameters (e.g., Yin et al., 2009; Yun-Jie et al., 2009; Dai et al., 2011). However, none of the mentioned literature quantified the spatial associations with the different parameters. This chapter attempts to quantify spatial associations of landslide occurrences with different parameters or so-called causal factors: elevation, surface rupture, slope, slope aspect, lithology. Three methods were applied in quantifying spatial associations: yule's coefficient of association (YCA), distance distribution analysis (DDA), and a distance to ridge relation (DTR) method. The YCA (Yule, 1912) was used in quantifying spatial associations with discrete objects: slope aspects and the lithology. This method is a bivariate statistical method that determines correlation by giving with values ranging from -1 to +1. A negative value denotes negative association, 0 value implies independence or lack of association, and positive values denotes positive association. The DDA (Berman 1977; Berman, 1986) was used for the continuous objects: elevation, slope, and the distance from the surface rupture. This analysis relates the cumulative relative frequencies of distance from a feature to all locations or the probability density distribution (PDD1)of all locations and the cumulative relative frequencies of distances to the landslide locations or the probability density distribution of landslide to the feature (PDD2) (Carranza, 2002; Ghosh and Carranza, 2010). A PDD1 tracing the same PDD2 implies random distribution of landslide with respect to the feature, a positive difference of PDD2 to PDD1 (PDD2-PDD1 >0) implies a positive spatial association, and a negative difference of (PDD2 to PDD1 < 0). The positive spatial association represents the "likelihood of landslide occurrence higher than what would be expected due to chance". This can also be applied to slope and elevation since both are continuous features and a probability density distribution to every slope (or elevation) and a probability density distribution to the EIL can be calculated. The larger the PDD2-PDD1 difference means stronger positive association, which can be interpreted that a factor has a strong control to the EIL. The distance distribution analysis is plotted on an x-y graph where the x-axis represents the PDD1 (seen on the graphs as to every location in dashed line) and PDD2 (seen as a light gray solid line) of distance, elevation, and slope against the y-axis that is the cumulative relative frequency. The difference between the PDD1 and PDD2 is also plotted (dark gray solid line). The modified version of a DTR (Meunier et al., 2008) was used for quantifying the relationship of the source points to the ridge. In this method, only the distance of the source points to the ridge axis and the stream is measured instead of measuring the extreme ends of the individual landslides area to the ridge axis and stream. This would determine whether the landslide source points are closer, thus more spatially associated with the ridge rather than the stream. This would then test the theory that EIL are closer to the ridge axis than streams as proposed by Meunier et al. (2008).

6.1. Surface rupture factor

6.1.1. Estimating the 1958 earthquake surface rupture

Two pre-requisites are needed to estimate the surface rupture caused by the 1958 earthquake: length and spatial location. The length was estimated using the empirical relations presented by Wells and Coppersmith (1994). Using the relation they found, the surface rupture was estimated to have a length of 27 km. The spatial location is estimated to be within a 500 meter band from of the 2008 co-seismic surface rupture constrained by active fault maps of Densmore et al. (2008), the crustal shortening and cross-sections of the Longmenshan mountain range of Hubbard and Shaw (2009), the segmentation of Longmenshan fault and surface rupture by Liu-Zeng et al., 2009, and a three dimensional model of co-seismic fault, fold, and thrust belt caused by the Wenchuan earthquake by Li et al., 2010. A comparison of active fault and surface rupture is presented in annex 6.1. The 2008 surface rupture delineated by Xu et al. (2009) was used as the surface rupture for the 2008 EIL.

6.1.2.   Distance from surface rupture to hanging wall and footwall 1958 EIL
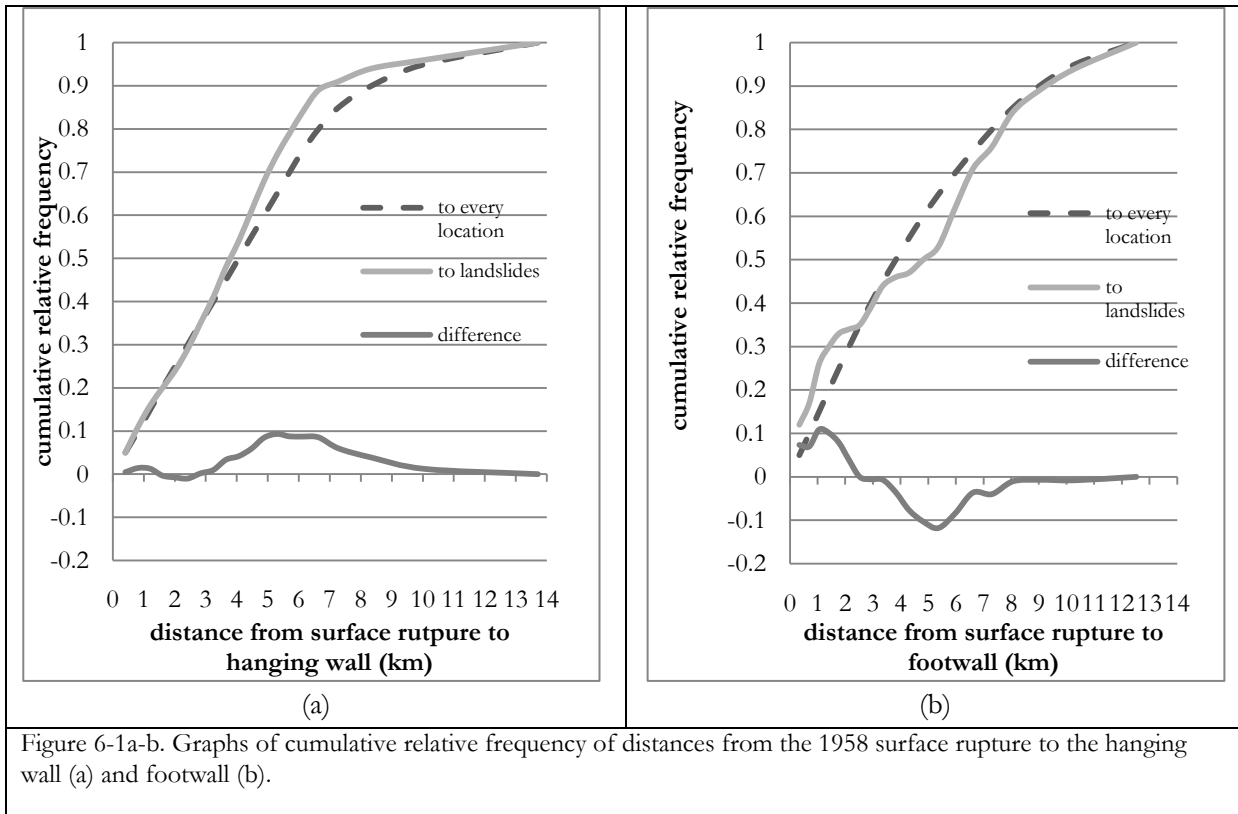

Figure 6-1a-b. Graphs of cumulative relative frequency of distances from the 1958 surface rupture to the hanging wall (a) and footwall (b).

It can be observed that the occurrences of landslides are positively associated to the hanging wall rather than the footwall. The optimum distance to the hanging wall (~5 km) is farther than the optimal distance to the footwall (~1km). This implies that majority of the landslides are associated with the hanging wall rather than the footwall (figure 6-1a-b) for the 1958 EIL.

6.1.3.   Distance from surface rupture to the hanging wall and footwall of 2008 EIL

Landslide occurrences are both positively associated either to the hanging wall (HW) or the footwall (FW). The optimum distance to the HW (~3.4 km) is farther than the optimal distance to the FW (~2 km) (figure 6-2a-b). This implies that majority of the landslides are associated with the HW rather than the FW. The 2008 EIL are more widely distributed than the 1958 EIL. The 2008 EIL are more distributed towards the HW and the FWas compared to the 1958 EIL that is more distributed towards that hanging wall than the FW. However, it should be noted that: (1) only the source points are considered and not the area and (2) this not the entire distribution of the 2008 EIL. If the landslide areas are considered, more landslide areas the HW part would definitely be covered by more landslides as observed in table 6-1 and figure 6-3. The study area only considered a tiny portion of the whole 2008 EIL event as pointed out in Chapter 5. The surface rupture used here is only part of a bigger co-seismic rupture (~200km). The study area is just a narrow zone from the surface rupture. This affects the precision of the analysis, since smaller distance coverage is just considered on the HW and the FW. Furthermore, the rupture dynamics of the 1958 may have been different from the 2008. The 2008 rupture dynamics have been thoroughly studied in different literatures while there are no accounts of detailed scientific measurements, observations, and reports about the 1958 event. However, it is suffice to say within this analysis that the distribution of landslides from is different for the 1958 event and the 2008

event with respect to their surface ruptures. A good test would be to calculate the landslide occurrences along the surface rupture and observe how the EIL behaves along the surface rupture. But this is beyond the objective of this research.
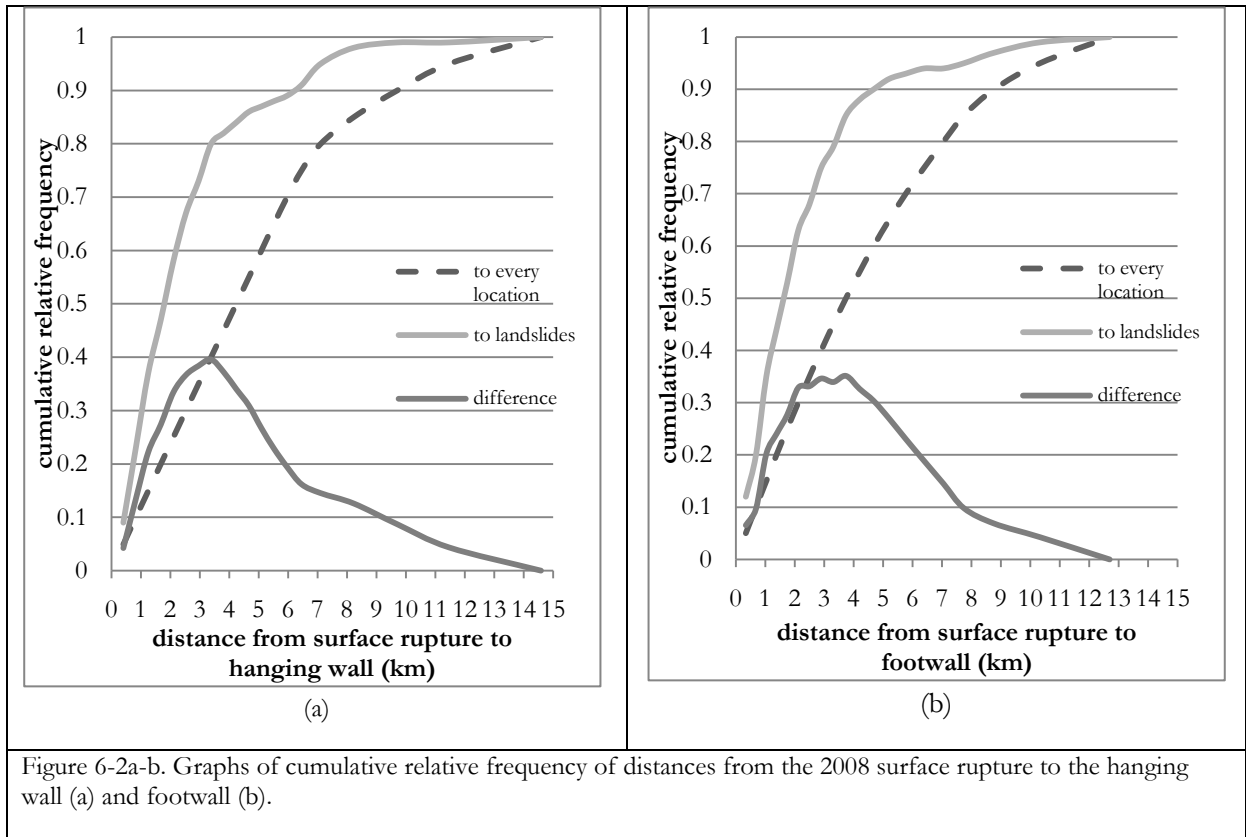

Figure 6-2a-b. Graphs of cumulative relative frequency of distances from the 2008 surface rupture to the hanging wall (a) and footwall (b).
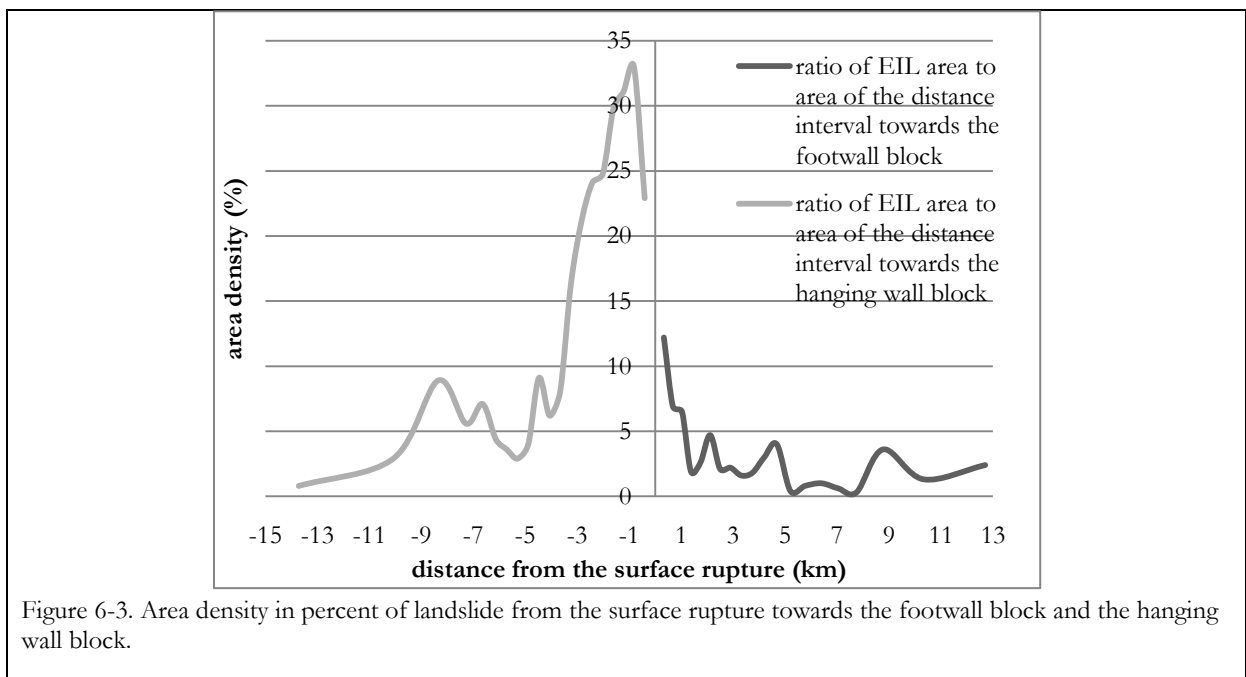

Figure 6-3. Area density in percent of landslide from the surface rupture towards the footwall block and the hanging wall block.

	Area coverage (km²)
1958 hanging wall	22

1958 footwall	4
2008 hanging wall	33
2008 footwall	7

Table 6-1. EIL coverage by the 1958 EIL and 2008 EIL in their respective hanging wall and foot wall block.

6.1.4. Distance from surface rupture in Central Italy
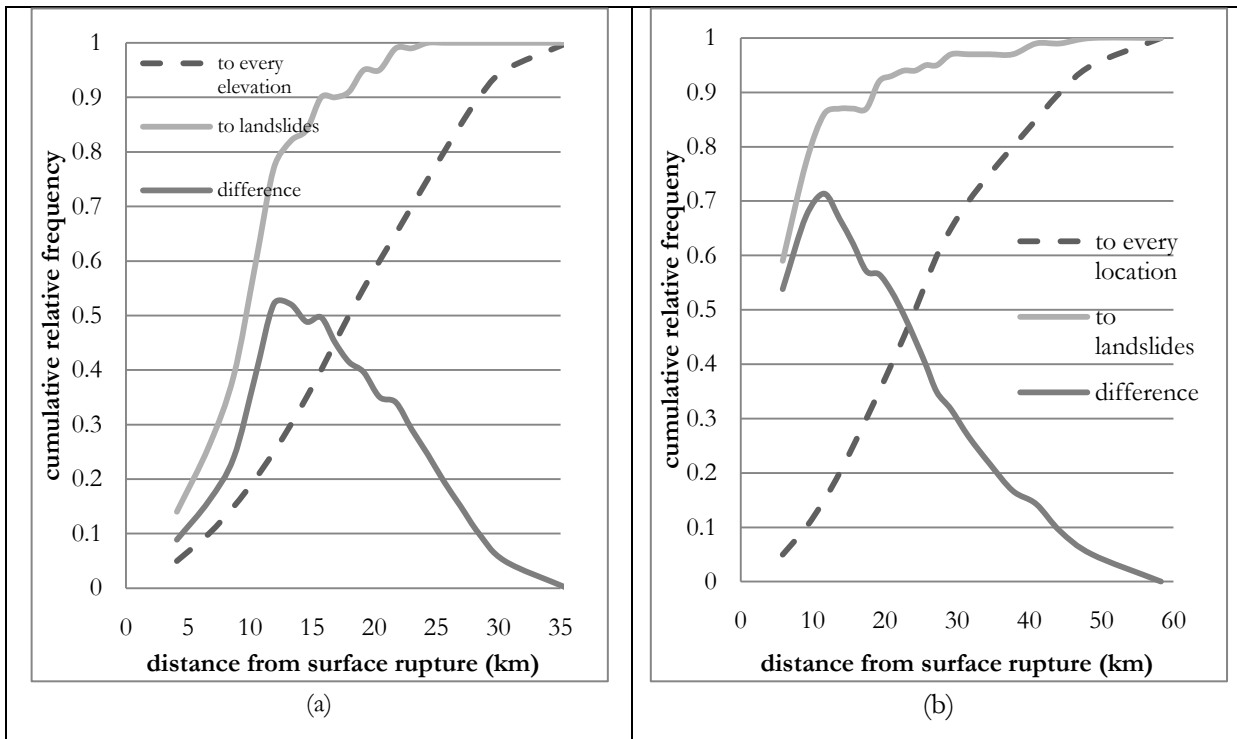
Figure 6-4a-b. Graph of cumulative relative frequency of distances from the 1997 co-seismic surface rupture to landslide occurrences in Umbria-Marche (a) and the 2009 co-seismic surface rupture in L'Aquila (b).

Both events have the optimum distance to EIL at about ~10km in which beyond this distance, the surface ruptures doesn't have any effect to the occurrences of EIL (figure 6-4a-b). The rupture process is more or less the same (high angle normal fault) even though the earthquake happened on different location.

6.2. Topographic factors

6.2.1. Elevation in Beichuan China

Although elevation does not really explain the spatial association of EIL, it gives, however, an insight to the general association of the EIL. In this case, the elevation is generally in positive relation for the 1958 EIL and 2008 EIL but at halfway of the elevation, the association turns negative. The elevation value associated with the 2008 EIL is higher than in the 1958 EIL, i.e., ~1 km for the 1958 EIL and ~1.3 km for the 2008 EIL (figure 6-5a-b). SATO et al 2007
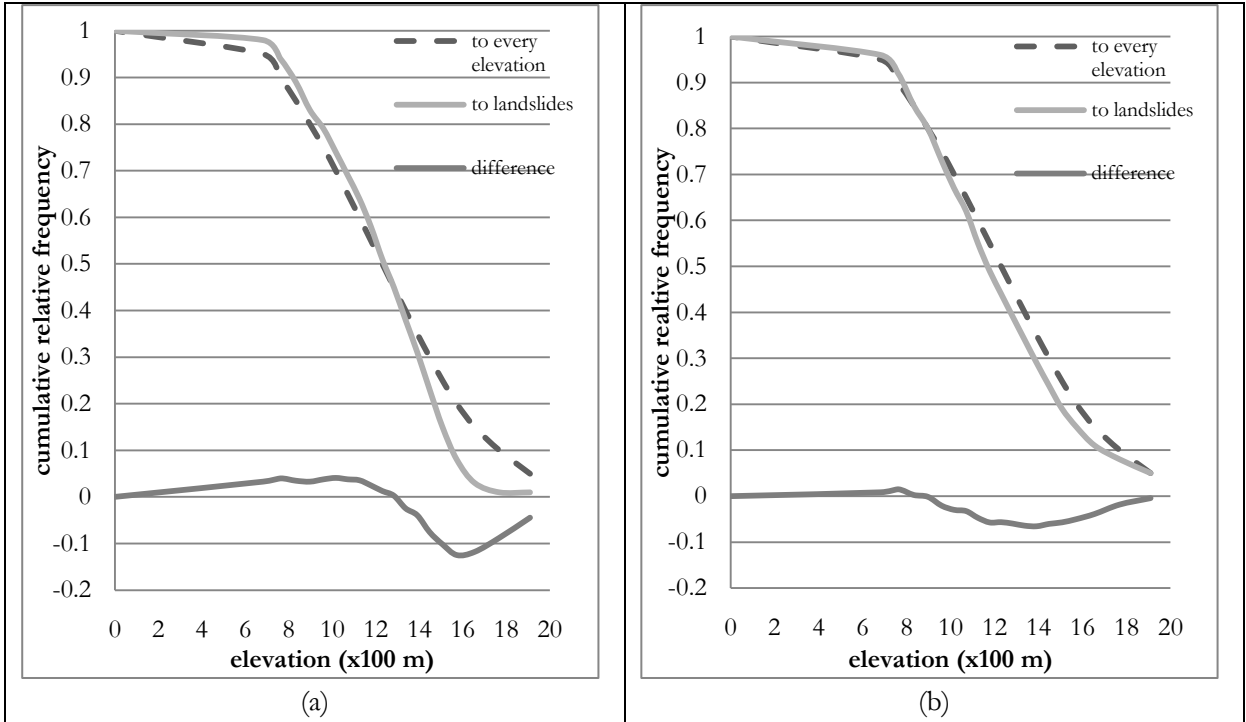
Figure 6-5a-b. Graphs of cumulative relative frequency of the 1958 EIL (a) and 2008 EIL (b) from the elevation.

6.2.2. Elevation in Central Italy

Figure 6-6a-b. Graphs of cumulative relative frequency of the 1997 Umbria-Marche EIL (a) and 2009 L'Aquila EIL (b) from the elevation.

The curve of the cumulative frequency distribution for elevation of the EIL has more positive association in Umbria-Marche EIL than in L'Aquila EIL. The optimal elevation is around 400 m for Umbria-Marche EIL while around 600 m for the L'Aquila (figure 6-6a-b).

6.2.3.   Slope in Beichuan China

Figure 6-7a-b. Graphs of cumulative relative frequency of the 1958 EIL (a) and 2008 EIL (b) to the slope.

The slope is generally positively associated with the the 1958 EIL and the 2008 EIL. The optimal slope for the 1958 EIL (~25 degrees) is lower than the optimal slope for the 2008 EIL (~40 degrees).
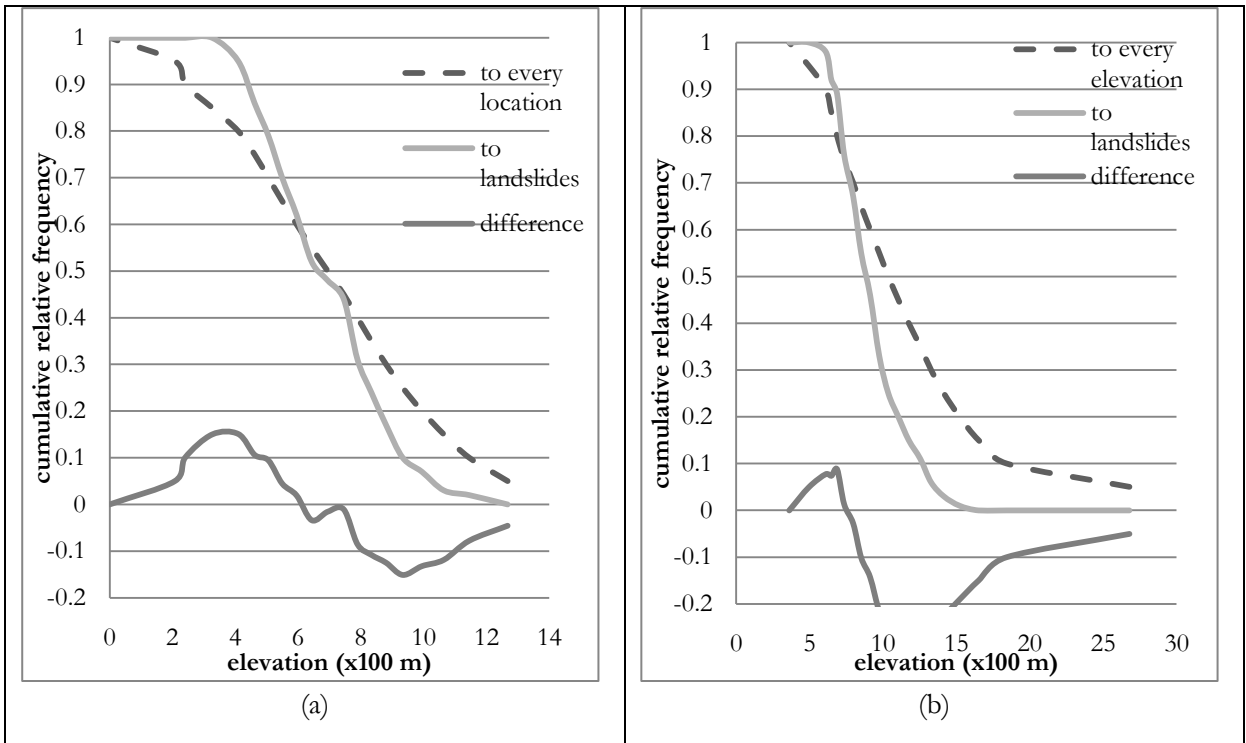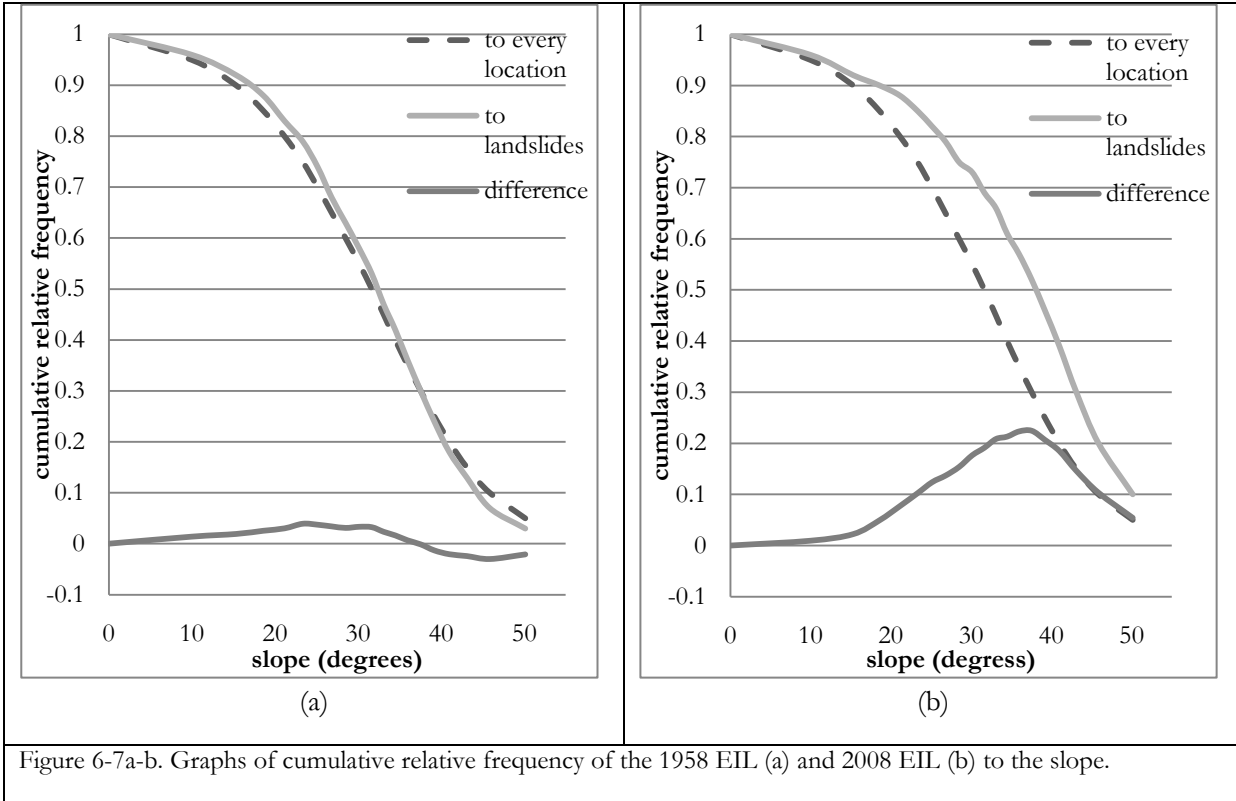
6.2.4.   Slope in Central Italy
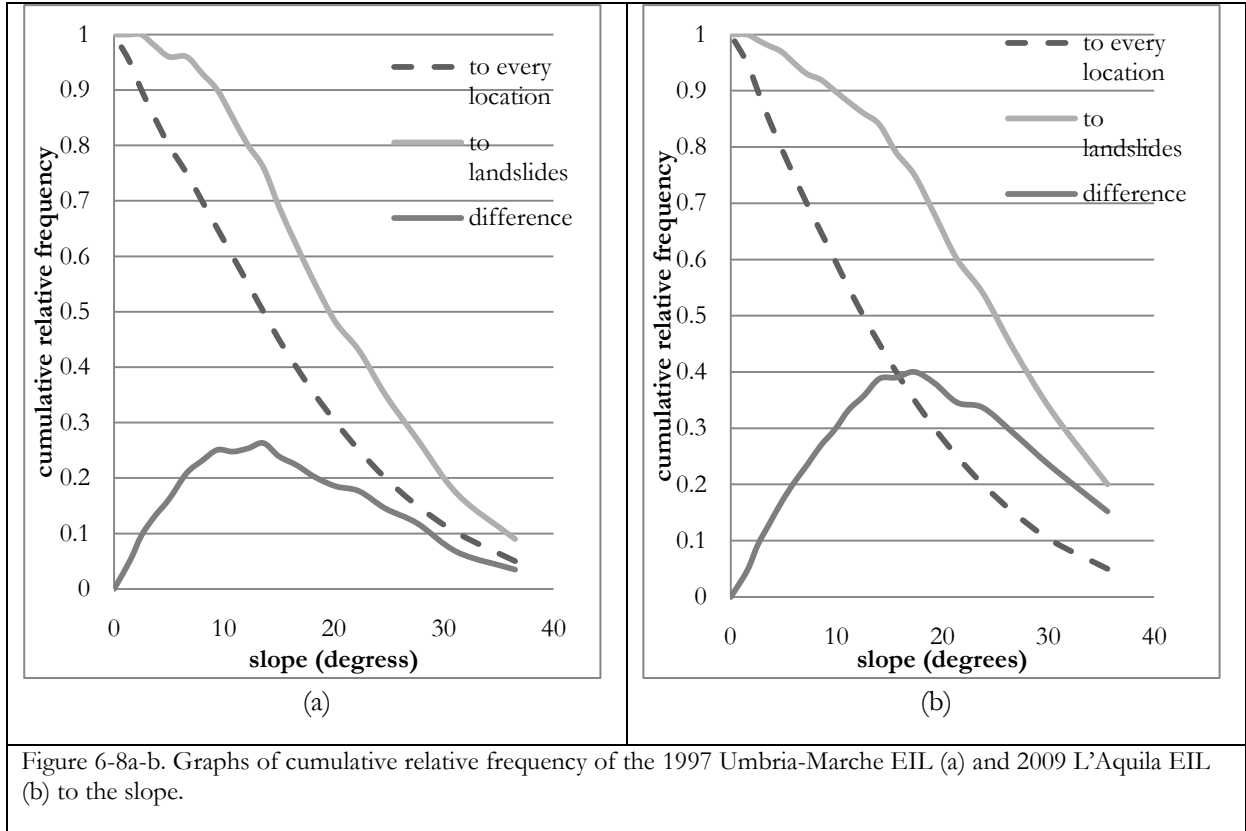
Figure 6-8a-b. Graphs of cumulative relative frequency of the 1997 Umbria-Marche EIL (a) and 2009 L'Aquila EIL (b) to the slope.

The slope both in the Umbria-Marche and L'Aquila is consistently positively associated with the EIL occurrences. The 1997 Umbria-Marche EIL has lower optimal slope (~13 degrees) compared with the L'Aquila EIL (~20 degrees).

6.2.5.   Aspect

	Beichuan, China		Central Italy	
Slope aspect	1958 EIL	2008 EIL	1997 Umbria –Marche	2009 L'Aquila
NNE	-0.2704	-0.0125	-0.2664	**0.082**
NE	-0.261	**0.0047**	-0.0665	**0.1807**
ENE	-0.1434	**0.0275**	-0.0548	**0.1607**
ESE	-0.0404	**0.0155**	-0.022	**0.2308**
SE	**0.0908**	**0.0473**	**0.0981**	-0.2902
SSE	**0.1954**	**0.0988**	**0.0684**	-0.5136
SSW	**0.2095**	**0.0691**	**0.125**	-0.4111
SW	**0.1862**	**0.0097**	**0.1187**	-0.1043
WSW	**0.1105**	-0.0395	**0.0715**	0.1276
WNW	-0.0326	-0.0724	**0.0187**	-0.2819
NW	-0.2431	-0.0961	-0.1179	-0.2595
NNW	-0.2822	-0.0655	-0.3109	-0.2599

Table 6-2. Yule's coefficient values for the EIL occurrences in Beichuan China and Central Italy.

The slope aspect EIL distribution associated with the 1958 EIL changed from SE-WSW to NE-SW in the 2008 EIL. The slope aspect associated with Umbria-Marche ranges from SE-WNW while NNE-ESE in L'Aquila.

6.3.   Morphologic

6.3.1.   Distance to ridge of source points

(a)   (b)
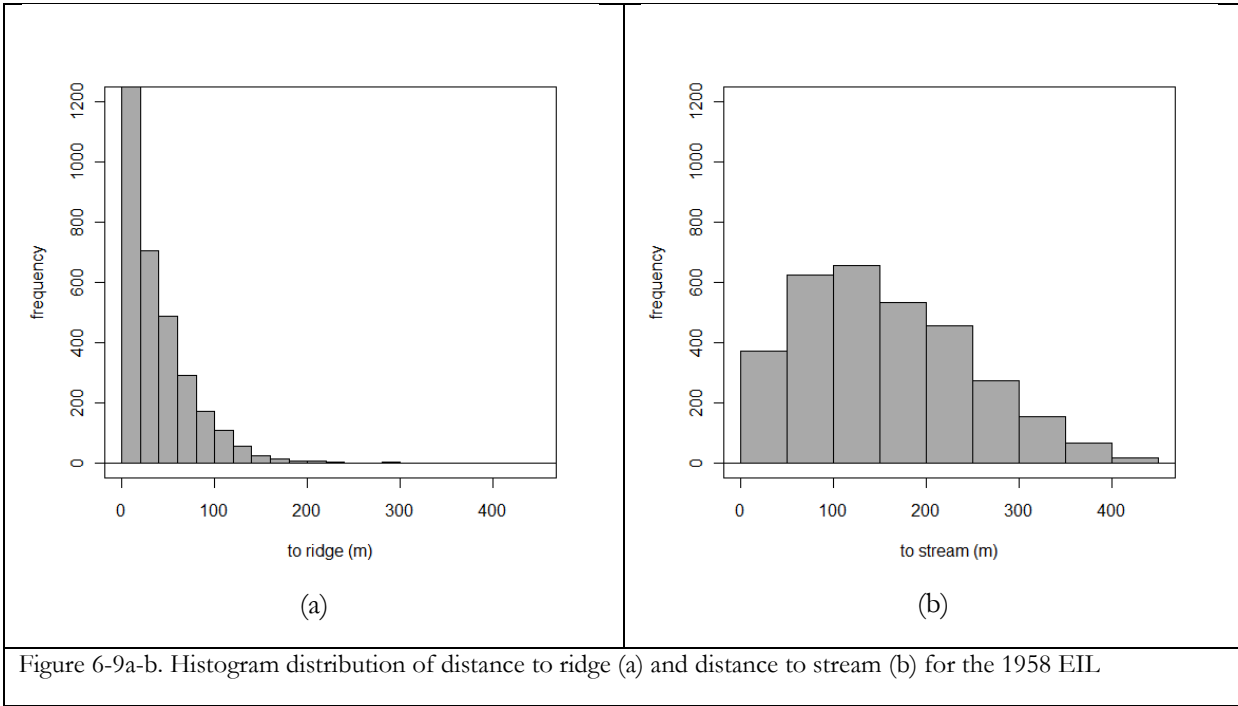
Figure 6-9a-b. Histogram distribution of distance to ridge (a) and distance to stream (b) for the 1958 EIL

(a)   (b)

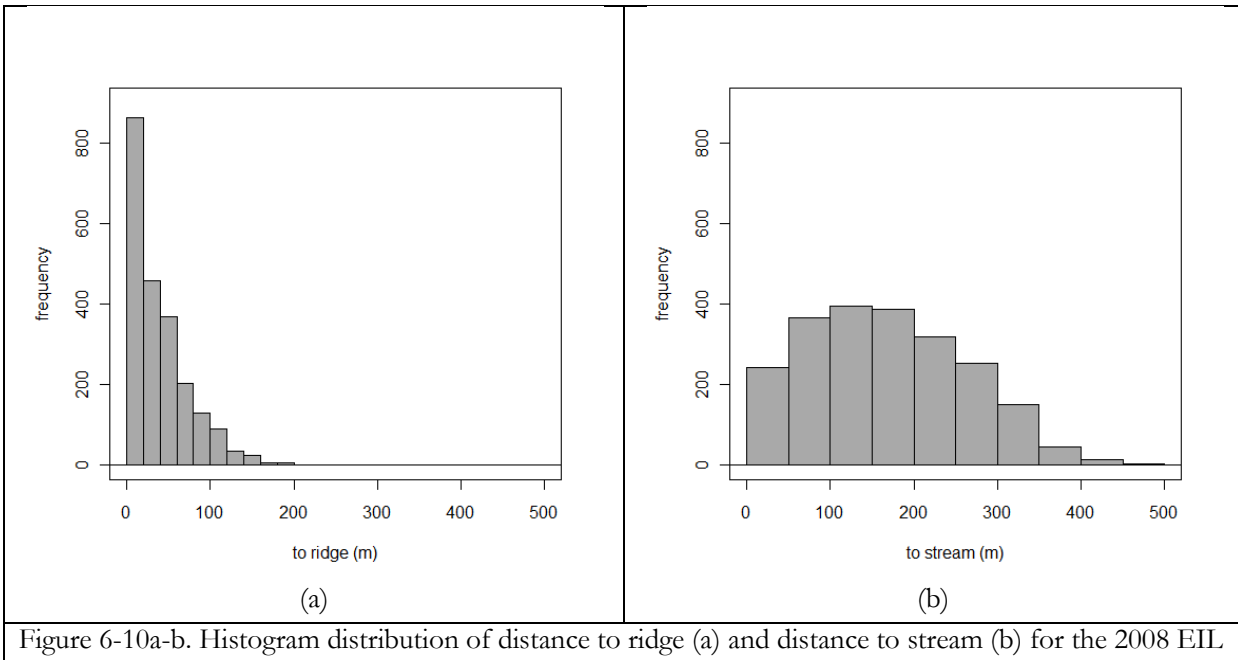Figure 6-10a-b. Histogram distribution of distance to ridge (a) and distance to stream (b) for the 2008 EIL

From figure 6-9a-b and figure 6-10a-b, it can be observed that majority of the source points are nearer to the ridge than to the stream. A big percentage for both 1958 EIL and 2008 EIL occurs very near to the ridge crest. This entails that most EIL are spatially associated to the ridge more than to the stream.

6.4. Lithology

6.4.1. Beichuan, China

Lithology	Units	1958 EIL	2008 EIL
Quaternary Alluvium	Alluvial gravel and clay	-0.0526	**0.2199**
Feixianguan	Shale, mudstone and siltstone	-1	-1
Lower(longmenshan)	limestone	-1	-0.1196
Upper(longmenshan)	limestone and shale	-0.3748	0.0645
Longmenshan region	Limestone	-0.7766	-0.135
Ganxi Group	Sandstone, mudstone and shale	-0.157	-0.229
Pingyipu Group	Sandstone and siltstone	-0.3667	-0.0243
Guanwushan Group	Limestone, shale and sandstone	-0.265	-0.2785
Yangmaba Group	Limestone and sandstone	-0.3206	-0.188
Tangwangzhai Group	Limestone	-0.2956	-0.1282
Longmaxi	Phyllite, schist, slate with sandstone and limestone	**0.134**	-0.028
Maoxian Group	Phyllite,schist, slate with sandstone and limestone	**0.1072**	-0.2754
Ordovician	Limestone, muddy limestone intercalated with slate	**0.3175**	**0.2027**
Cambrian	Sandstone and siltstone intercalated with slate	**0.1647**	**0.342**

Table 6-3. Yule's coefficient of association of the 1958 EIL and the 2008 EIL.

The lithologies associated with the 1958 EIL are Longmaxi, Maoxian, Ordovician, and Cambrian rocks. The lihologies associated with the 2008 EIL are the Quaternary alluvium, Ordiovician, and Cambrian (table 6-3).

6.4.2. Central Italy

Lithology	Units	1997 Umbria-Marche
upper Miocene	sandstones and clays	-1
Paleogene- Upper Cretaceous	Limestones and pelagic limestones marl	0.2055
Jurassic	Limestones and sometimes neritic dolomites and from platform	**0.1884**
Cretaceous - Jurassic	Micritic limestones and pelagic micrite clay	**0.0226**
Jurassic	Limestones,limestones marl and marl, limestones flint, pelagic limestones	**0.0091**
Pleistocene- Pliocene	Lacustrine deposits and fluvial - lacustrine 's	-1
Pleistocene	Debris, flood terraces, fluvial - lacustrine 's and fluvioglacial's	-0.1669
Holocene	Debris, alluvial deposits and fluvial - lacustrine 's, current beaches	-1
Paleogene	Marls and calcareous marl of pelagic facies	-0.21
Middle-Lower Miocene	Marls, sometimes marls with chert of pelagic facies	**0.2313**
middle-lower Miocene	Sandstone units and arenaceous - marl	-0.6998
middle-lower Miocene	Clay units (turbidite)	-1

Table 6-4. Yule's coefficient of association between the Umbria-Marche EIL and the lithologies.

Lithology	Units	2009 L'Aquila
middle-lower Miocene	sandstones and conglomerates, sometimes turbidites conglomerates	-1
upper Miocene	sandstones and clays (subordinate limestones and evaporites	-0.408
Pleistocene	Clays	-1
Pliocene	Clays and marls, sometimes marls with Olistostrom	-1
Paleogene	Limestones and biodetric and neritic limestones and of platform	**0.5716**
Lower cretaceous	Limestones and biodetric and neritic limestones and of platform	-1
Cretaceous	Limestones and detritic marl limestones of escarpment	-0.4622
Paleogene- upper Jurassic	Limestones and detritic marl limestones of escarpment	-1
Jurassic	Limestones and marl limestones,with chert and escarpment debris	-0.0781
Jurassic	limestones and sometimes neritic and platform dolomites	-1
Cretaceous- Jurassic	Micritic limestones and clay micrites of platform	0.2314
Paleogene- upper Cretaceous	Neritic and platform limestones	-1
Cretaceous	Organogenic, biodetritic and platform limestones	-0.2094
middle lower Miocene	Organogenic limestones, calcarenite	**0.4103**
Jurassic	Limestones, marl limestones and marls, limestones flint, pelagic limestones	-1
Pleistocene	glacial deposits	-1
Pleistocene and Pliocene	Lacustrine deposits and fluvial - lacustrine 's	**0.047**
Pleistocene	Debris, flood terraces, fluvial - lacustrine 's and fluvioglacial's	-1
Holocene	Debris, alluvial deposits and fluvial - lacustrine 's, current beaches	-0.5818
Upper Triassic	Neritic and platform crystalline dolomites	-1
Jurassic	Neritic and platform dolomites	-0.3018
Upper Miocene	chalky sulphurous formation	-1
	Lakes and glacier	-1
Paleogene	Marl and detritic calcareous marl of escarpment facies	-0.3521
middle Miocene	Marls, sometimes detritic marls with chert of escarpment facies	-0.3172
middle - lower Miocene	Marls, sometimes detritic marls with chert of pelagic facies	-1
middle- lower Miocene	Sandstones and arenaceous - marl units	0.3009

Table 6-5. Yule's coefficient of association between the L'Aquila EIL and the lithologies.

It can be observed in table 6-4 that most of the landslides in Umbria-Marche are associated with the limestones of almost the same age (table 6-4). However, the lithology with the highest is not in the limestones. The L'Aquila EIL are also mostly associated with the limestone with the exception of the Pilocene-Pleictocene lake depoits.

7.   DISCUSSION AND CONCLUSIONS

Table 7.1 summarizes the characteristics of the four studied Earthquake Induced Landslide (EIL) inventories presented in the previous chapters: the 1958 and 2008 EILs from the Beichuan area in China, and the 1997 and 2009 EILs from Central Italy. All the study areas experienced earthquake with different magnitudes with the 2008 event in Wenchuan as the strongest among all cases (Mw = 7.9). All the individual earthquake events propagated in a unilateral manner. In Beichuan, although the 1958 event has a lower magnitude as compared to the 2008 event, the number of landslides interpreted from the Corona image were far greater in number, within the study area. However, it should be considered that the 2008 EIL inventory within the study arean is part of a much larger EIL scenario for the entire Wenchuan area, consisting of over 60,000 landslides which was mapped by Gorum et al. (2011) and Dai et al. (2011). Therefore, although the 1958 event has more landslides within the study area, the 2008 EIL has a much larger total area affected by landslides in the entire Wenchuan area as well as in the Beichuan study area. This follows the concept that higher magnitude earthquakes produce more landslides in a wider area and with a larger total area. This has been the advantage of mapping landslides as polygons and not as points since the count of landslides alone may be misleading. Furthermore, it should be reminded that the 1958 EILs were interpreted from an image 10 years after the event (a Corona image from1968). Other triggering mechanisms, such as intensive rainfall events, may have happened over that long time interval. Unfortunately there are no earlier images or meteorological data available to verify this. To account for the possible area variability, probability density functions using the double-pareto, double pareto-simplified, and the truncated inverse-Gamma functions were estimated through a histogram density function, kernel density function, and a maximum likelihood function for the 1958 EIL and the 2008 EIL. The calculation resulted into approximately the same t-value (~ 3000 m²), which is the most frequent size of landslides. The long tail end that accounts for the medium and large size landslides, and short tail end that accounts the small landslides, is a bit different. The long tail end is steeper for the 1958 EIL as opposed to the more gentle long tail slope of the 2008 EIL. This indicates then that the 2008 EIL has a higher proportion of larger landslides, and the 1958 EIL a higher proportion of smaller ones. Following that the area coverage of the 2008 EIL is greater than the 1958 EIL, the same can be said for the area density. The area density for the 2008 EIL is 3% more than the 1958 EIL. However, since the number of 1958 EIL landslides is greater than the 2008 EIL, it can be expected that the average number density of the 1958 EIL is greater.

In conclusion, the high number of small landslides that were mapped using a Corona image, obtained 10 years after the 1958 event is remarkable, and not according to the initial expectations. Small landslides caused by an earthquake are generally masked by vegetation regrowth within a few years. Therefore it is difficult to conclude whether the 1958 event actually caused more small landslides in the Beichuan area than the 2008 event, or whether an intensive rainfall event that happened between 1958 and the time of acquisition of the Corona image, is responsible for triggering the high number of small landslides. When comparing the earthquake induced landslide inventories from China and Italy, we can see that the number density for the Central Italy are is much less than for China. Although the 2009 L'Aquila earthquake had a comparable magnitude as the 1958 Beichuan earthquake (Mw 6.2 – 6.3) the number of landslides caused in the Chinese area are 30 times more. Although the average number density is zero in Central Italy (Table 7.1), it should be noted that density calculation is a function of the counting radius and the size of the counting kernel. The bigger the size, the more the density is generalized. Nonetheless, the density was calculated in number of landslides/km² to have a comparable unit for both study areas. The series of area manipulations and area density calculations that were done for the Beichuan study area could not be done in Central Italy since there the EIL were represented as points and not polygons.

Factors	Beichuan China		Central Italy	
	1958 EIL	**2008 EIL**	**1997 Umbria-Marche**	**2009 L'Aquila Abruzzo**
Magnitude (Mw)	6.2	7.9	5.8	6.3
Type of propagation	unilateral	unilateral	unilateral	unilateral
Number of landslides	3154	2172	233	99
Types	Mostly slides, minor flows, rarely falls	Mostly slides, minor falls, flows, and avalanches	Mostly rockfall, minor translational slide	rockfalls
Representation	Polygon based for the whole landslide, points for the source areas and accumulation zone	Polygon based for the whole landslide, points for the source areas and accumulation zone	Point based for all landslides	Point based for all landslides
Landslide area (m²)	2,5184,493	3,7307,044	NA	NA
Minimum size (m²)	104	24	NA	NA
Maximum size (m²)	373379.2066	1,311,400.394	NA	NA
Average size (m²)	7,985	17,176	NA	NA
Most frequent area (m²)	~3000	~3000	NA	NA
Area density (%)	6	9	NA	NA
AVG Nr density (nr/km²)	3	2	0	0
Maximum number density (landslide/km²)	57	45	18	20
Optimum distance to CSFR	4.8 km to hanging wall; 1 km to footwall	3.3 km to hanging wall; 2.9 km meters to footwall	12 km from CSFR	11.5 km from CSFR
Optimum elevation (m)	1000	1300	300	700
Optimum slope (°)	23	38	9	17
Associated slope aspect(s)	SE, SSE, SSW, SW, WSW	NE, ENE, ESES, SE, SSE, SSW, SW	SE, SSE, SSW, SW, WSW, WNW	NNE, NE, ENE, ESE
Nearer to ridge or stream	ridge	ridge	ridge	ridge
Associated lithology	Longmaxi (Phyllite, schist, slate with sandstone and limestone); Maoxian group (Phyllite,schist, slate with sandstone and limestone); Ordovician (Limestone, muddy limestone intercalated with slate); Cambrian (Sandstone and siltstone intercalated with slate)	Quaternary alluvium; Ordovician (Limestone, muddy limestone intercalated with slate); Cambrian (Sandstone and siltstone intercalated with slate)	Paleogene- Upper Cretaceous (Limestones and pelagic limestones marl); Jurassic (Limestones and sometimes neritic dolomites and from platform); Cretaceous – Jurassic (Micritic limestones and pelagic micrite clay) ; Jurassic(Limestones, limestones marl and marl, limestones flint, pelagic limestones)	Paleogene (Limestones and biodetric and neritic limestones and of platform); middle lower Miocene (Organogenic limestones, calcarenite); Pleistocene and Pliocene (Lacustrine deposits and fluvial)

Table 7-1. Summary result of the 1958 EIL, 2008 EIL in Beichuan China and the 1997 Umbria-Marche EIL and 2009 L'Aquila EIL in Central Italy. See text below for discussion.

In terms of the landslide type, both the 1958 EIL and 2008 EIL are dominantly slides as compared to the Central Italy which are mostly small rockfalls.

Several spatial association techniques were utilized to determine how causal factors are related to the occurrences of the landslides: the yule's coefficient of association or YCA (Yule, 1912) for discrete causal factors (slope aspect and lithology), the distance distribution analysis or DDA (Berman, 1997; Berman 1986) for continuous features (distance from CSFR, elevation, slope), and a modified approach of the distance to ridge or DTR (Meunier et al., 2008) calculation for testing whether the source areas were nearer to ridges than streams. Many publications report criteria of good spatial evidence of causal factor to landslide occurrences based on positive spatial correlation but only few have quantified the degree to which the causal factors are spatially associated with the EIL occurrences. For example, Dai et al. (2011) reported variations of EIL density as a function of lithology and argued that the Cambrian sandstone and siltstone intercalated with slate is the most susceptible lithological unit for slope failure. However, this inference is only limited to those with high density correlation but it may have happened that other lithological units are also spatially associated with the landslides. The YCA and DDA methods account for this limitation. It was found out in Beichuan that the landslides of the 1958 EIL are much more associated to the hanging wall than the footwall of the active fault. This can be explained by the hanging wall effect where the peak ground acceleration is propagated more on the hanging wall rather than the footwall (Oglesby, 1998; Oglesby et al., 2000; Oglesby and Day, 2001; Oglesby and Archuleta, 2003) and that the hanging wall experiences near-field ground motion than the footwall (Oglesby, 1998; Oglesby et al., 2000). The effective distance to the hanging wall is also greater than to the footwall in the case of the 2008 EIL. To further support this claim, the area density was calculated (Figure 6-3) on the hanging wall and the footwall for the 2008 EIL. The area density is much greater in the hanging wall than in the footwall.

To have better understanding between an earthquake event and its associated landslides, it is very important to collect a good dataset such as a detailed inventory of EIL by interpreting multiple high resolution images. The availability of a sufficiently high resolution image that is also cloudfree and can be used in a stereo-image interpretation, as soon as possible after the earthquake event, is therefore essential. A comparison of the EIL inventory with other existing EIL inventories, if present, is also essential to maximize the accuracy of the analysis. Then, if the integrity of the inventory is secured, the EIL can be related to the causal factors, i.e., the geo-enviromental factors and the seismic factors. One way of this kind of relationship analysis is through spatial associations that this will determines which among the causal factors are spatially associated to the EIL, i.e., negative or positive association.

It can be concluded that, although earthquakes of different magnitudes may happen in the same area, they may create quite different landslide inventories, which are not clearly related to the same geo-environmental factors. Earthquakes that happen in different geo-environmental settings, such as Central Italy and the Sichuan mountains in China, may also produce EILs with entirely different characteristics. Different earthquakers may not have the same effect on the geo-environment such as in the maximum spatial relation to slope, slope aspect, and lithology.

This study has shown that as far as the two study areas and four EILs that were studied are concerned, it is not possible to draw general conclusions that can be used for designed an improved method for earthquake induced landslide susceptibility assessment.

LIST OF REFERENCES

References

Chen, G., Ji, F., Zhou, R., Xu, J., Zhou, B., Li, X., Ye, Y., 2007. Primary research of activity segmentation of Longmen Shan fault zone since Late-Quaternary. Seismol. Geol. 29 (3), 657-673 (in Chinese with English abstract).

Chen, J., Shao, G., Lu, Z., Hudnut, K., Jiu, J., Hayes, G., and Zeng, Y., 2008. Rupture history of 2008 May 12 Mw8.0 Wen-chuan earthquake: Evidence of slip interaction: Eos (Transactions, American Geophysical Union), v. 89, Fall meeting supplement, abs. S23E-02.

Chigira, M., Wu, X., Inokuchi, T., Wang, G., 2010. Landslides induced by the 2008 Wenchuan earthquake, Sichuan, China, Geomorphology (2010), doi:10.1016/j.geomorph.2010.01.003

China Earthquake Administration (CEA)., 2008. Magnitude of the 12 May 2008 Wenchuan Earthquake and aftershocks. http://www.cea.gov.cn/manage/ html/8a8587881632fa5c0116674a018300cf/_content/09_02/02/1233562387132.html (February 2010).

Densmore, A.L., Ellis, M.A., Li, Y., Zhou, R., Hancock, G.S., Richardson, N., 2007. Active tectonics of the Beichuan and Pengguan fault at the eastern margin of the Tibetan Plateau. Tectonics 26, TC 4005, doi:10.1029/2006 TC001987.

Gorum, T., Fan, X., van Westen C.J., Huang, R.Q., Xu, Q., Tang, C., Wang, G., 2010. Distribution Pattern of Earthquake-induced Landslides Triggered by the 12 May 2008 Wenchuan Earthquake. Geomorphology (Accepted).

Keefer, D.K., 2000. Statistical analysis of an earthquake-induced landslide distribution the 1989 Loma Prieta, California event. Engineering Geology 58, 231–249.

Hao, K.X., Si, H., Fujiwara, H. and Ozawa, T., 2009. Coseismic surface-ruptures and crustal deformations of the 2008 Wenchuan earthquake Mw 7.9, China, Geophysical Research Letters, 36, doi:10.1029/2009GL037971

Ji, C., Hayes, G., 2008. Preliminary Result of the May 12, 2008 Mw 7.9 Eastern Sichuan, China Earthquake. http://earthquake.usgs.gov/eqcenter/ eqinthenews/2008/us2008ryan/finite_fault.php (March 2010).

Lee, S.,Talib,J.A., 2005. Probabilistic landslide susceptibility and factor effect analysis. EnvironmentalGeology47, 982–990.

Li, Y., Allen, P.A, Densmore, A.L. and Xu., Q, 2003. Evolution of the Longmen Shan Foreland Basin (western Sichuan, China) during the Late Triassic Indosinian Orogeny, Basin Research. 15, 117-138.

Lin, A., Ren, Z. and Jia, D. 2009a. Co-seismic ground-shortening structures produced by the 2008 Mw 7.9 Wenchuan earthquake, China, Tectonophysics, doi:10.1016/j.tecto.2009.10.027.

Lin, A., Ren, Z., Jia, D. and Wu, X., 2009b. Co-seismic thrusting rupture and slip distribution produced by the 2008 Mw 7.9 Wenchuan earthquake, China. Tectonophysics, doi:10.1016/j.tecto.2009.02.014.

Nishimura, N., and Yagi, Y., 2008. Rupture process for May 12, 2008 Sichuan earthquake: (preliminary result): http://www.geol.tsukuba.ac.jp/~nisimura/ 20080512/ (March 2010).

Ran, Y.K., Shi, X., Wang, H., Chen, L.C., Chen, J., Liu, R.C. and Gong, H., 2009. The maximum coseismic vertical surface displacement and surface deformation pattern accompanying the Ms 8.0 Wenchuan earthquake. Chinese Science Bulletin doi: 10.1007/s11434-009-0453-3.

Richards, J.A. and Jia, X., 2006. Remote sensing digital image analysis: An Introduction. Springer-Verlag, Berlin Heidelberg, 431 pp.

Shen, Z., Sun, J., Zhang, P., Wan, Y., Wang, M., Bürgmann, R., Zeng, Y., Gan, W., Liao, H., Wang, Q., 2009. Slip maxima at fault junctions and rupturing of barriers during the 2008 Wenchuan earthquake, Nature Geoscience, 2, pp718-724, DOI: 10.1028/NGEO636.

Shi Y.T, Gao Y., Zhao C.P., 2009. Study of seismic anisotropy on Wenchuan earthquake sequence (in Chinese). Chinese Journal of Geophysics, 52, 398−407.

U.S. Geological Survey, 2008. Magnitude 7.9 - Eastern Sichuan, China, 2008 May 12 06:28:01 UTC. http://earthquake.usgs.gov/earthquakes/eqinthenews/ 2008/us2008ryan/ (March 2010).

Wang, W., Sun, W. and Jiang, Z., 2009. Comparison of fault models of the 2008 Wenchuan earthquake (Ms 8.0) and spatial distribution of co-seismic deformations. Tectonophysics, doi:10.1016/j.tecto.2009.08.035.

Wang, W.M., Zhao, L.F., et al., 2008. Rupture process of the Ms8.0 Wenchuan earthquake of Sichuan, China. Chinese Journal of Geophysics. 51 (5), 1403-1410 (in Chinese).

Wang, H.B., Sassa, K., Xu, W.Y., 2007. Analysis of a spatial distribution of landslides triggered by the 2004 Chuetsu earthquakes of Niigata Prefecture, Japan. Natural Hazards 41 (1), 43-60.

Wu, Z. Dong, S., Patrick, J.B., Zhang, Z. and Liao, H., 2009. Dextral-slip thrust faulting and seismic events of the Ms 8.0 Wenchuan earthquake, Longmenshan Mountains, Eastern Margin of the Tibetan Plateau. Acta Geologica Sinica 83 (4), 685-693.

Xu, X., Wen, X., Yu, G., Chen, G., Klinger, Y., Hubbard, J., Shaw, J., 2009. Coseismic reverse- and oblique-slip surface faulting generated by the 2008 Mw 7.9 Wenchuan earthquake, China. Geology 37, 515-518.

Yarai, H., Nishimura, T., Tobita, M., Amagai, T., Suzuki, A., Suito, H., Ozawa, S., Imakiire, T., Masaharu, H., 2008. A fault model of the 2008 Wenchuan earthquake estimated from SAR measurements. 7th ASC meeting, X2-040.

Zeng, J.L., Zhang, Z., Wen, L., Tapponnier, P., Sun, J., Xing, X., Hu, G., Xu, Q., Zeng, L., Ding, L., Ji, C., Hudnut, K.W., Van der Woerd, J., 2009. Co-seismic ruptures of the 12 May 2008, Ms 8.0 Wenchuan

earthquake, Sichuan: East-west crustal shortening on oblique, parallel thrusts along the eastern edge of Tibet. Earth and Planetary Science Letters 286, 355-370.

Zhang, P., et al., 2008a. China Crustal Observation Network Project, Co-seismic displacements of the 2008 Wenchuan earthquake (Ms8.0) observed by GPS. Science China 38 (10), 1195–1206.

Zhang, Y., et al., 2008b. Spatial–temporal rupture process of the 2008 Wenchuan earthquake. Science China 38 (10), 1186–1194.

Zhao, C.P., Chen, Z.L., Zhou, L.Q., Li, Z.X. and Kang, Y., 2010. Rupture process of the Wenchuan M8.0 earthquake of Sichuan, China: the segmentation feature. Chinese Science Bulletin 55 (3), 284-292.

Ji, C., Hayes, G., 2008. Preliminary Result of the May 12, 2008 Mw 7.9 Eastern Sichuan, China Earthquake. http://earthquake.usgs.gov/eqcenter /eqinthenews/2008/us2008ryan/finite_fault.php.

Wang, W., Sun, W. and Jiang, Z., 2009. Comparison of fault models of the 2008 Wenchuan earthquake (Ms 8.0) and spatial distribution of co-seismic deformations. Tectonophysics, doi:10.1016/j.tecto.2009.08.035

Zhao, C.P., Chen, Z.L., Zhou, L.Q., Li, Z.X. and Kang, Y., 2010. Rupture process of the Wenchuan M8.0 earthquake of Sichuan, China: the segmentation feature. Chinese Science Bulletin 55 (3): 284-292.

Shi Y.T, Gao Y., Zhao C.P., 2009. Study of seismic anisotropy on Wenchuan earthquake sequence (in Chinese). Chinese Journal of Geophysics, 52: 398−407.

ANNEX

A.1. Kernel density function

A distance weight function is calculated around each point to create densities at different location. This weight function, $K(s,t)$ with a vector displacement (s,t) to any point relative to the location (x,y) is where the density is calculated. Therefore, a density estimate will be a function of a value, $f(x+s,y+t)$ located at $(x+s,y+t)$, and the contributing weight $K(s,t)$, will have a $f(x+s,y+t) \cdot K(s,t)$ factor to the estimate at (x,y). This implies that the density at (x,y) is the sum of all $f(x+s,y+t) \cdot K(s,t)$. Furthermore, since the density is calculated for a certain area, the integral of $K(s,t)$ over all possible (s,t) must be 1 (Huber, 2003).

Since the source area points are somehow close to each other, a regular circular kernel with the following expression would be inappropriate:

$$K(s,t) = \frac{1}{\pi r^2} \qquad \text{(Eq. A-1)}$$

Where $K(s,t)$ is the kernel within a circular area for values (s,t), else, zero outside this kernel.
To account for weights, quartic approximation to a Gaussian kernel is used:

$$K(s,t) = \frac{1}{2\pi C^2} \, e^{\frac{-(s^2+t^2)}{2C^2}} \qquad \text{(Eq.A-2)}$$

Where $K(s,t)$ is the kernel, point (s,t) and C as the effective range. In polar coordinates, $K(s,t)$ is equivalent to:

$$K(s,t) = \frac{1}{2\pi C^2} \, e^{\frac{r^2}{2C^2}} \qquad \text{(Eq. A-3)}$$

The quartic approximation deals with an effective range of (3C), which implies that anything beyond the (3C) does not contribute to the kernel. The only symmetric quartic polynomial equal to 1 at r=0, to 0 at r=3, and with derivative 0 at r=3 is (Huber, 2003):

$$q(r) = \left[1 - \left(\frac{r}{3}\right)^2\right]^2 \qquad \text{(Eq.A-4)}$$

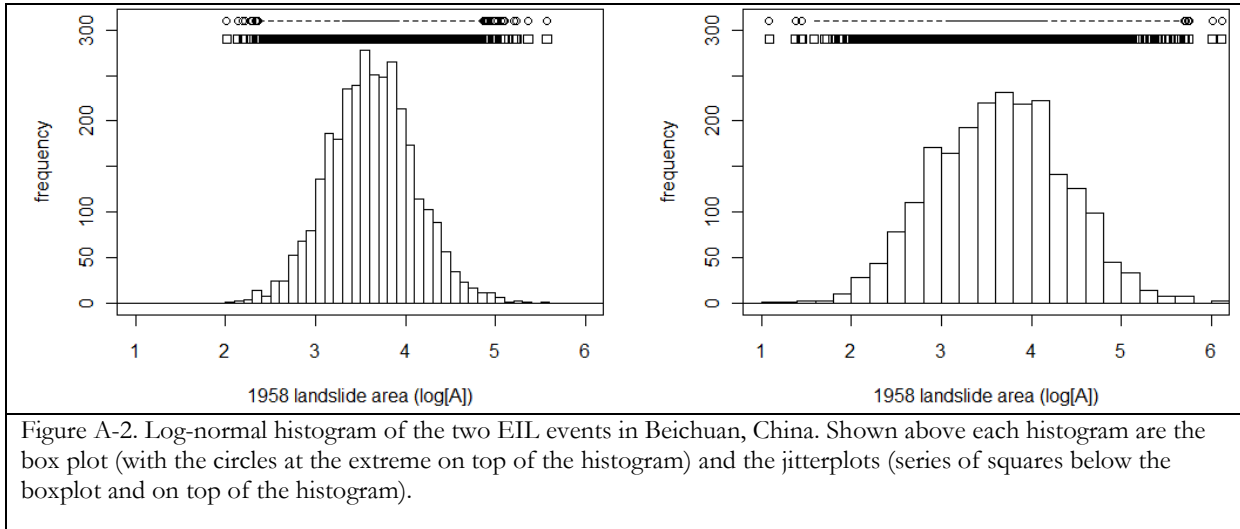Therefore, a final Gaussian kernel density function of:

$$K(r,\theta) = \left[1 - \left(\frac{r}{3C}\right)^2\right]^2 \qquad \text{(Eq. A-5)}$$
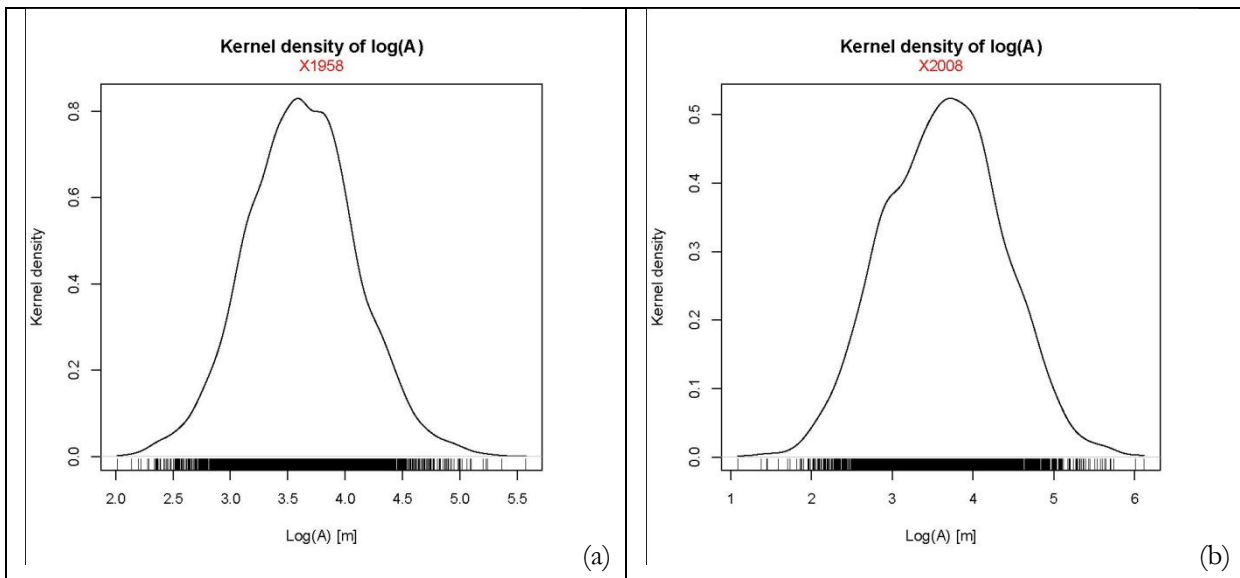
A.2. Bin size selection

The relation between size and landslide type is discussed in this part. Some of these values were already reported in Chapter 4. The size histograms were calculated for each inventory (figure 5-10a-j) to have a first approximation on the distribution of the landslide areas. Additionally, the histograms were also calculated for the 1958 EIL types and the 2008 EIL types. The Freedman-Diaconis rule (Freedman and Diaconis, 1981) rather than the Sturges rule was used to compute for a consistent number of bins since most of the data were more than 200. The Freedman-Diaconis rule is mathematically expressed as:

$$bin\ size = 2 \cdot IQR(x)n^{-\frac{1}{3}} \qquad \text{(Eq.A-6)}$$

Where IQR is the interquartile range and n is the number of observations in the sample (x). The bin width is in turn calculated by dividing the maximum value to the bin size. The minimum (Min), mean, and maximum (Max) values for each histogram were also calculated located below each plot.

Figure A-2. Log-normal histogram of the two EIL events in Beichuan, China. Shown above each histogram are the box plot (with the circles at the extreme on top of the histogram) and the jitterplots (series of squares below the boxplot and on top of the histogram).
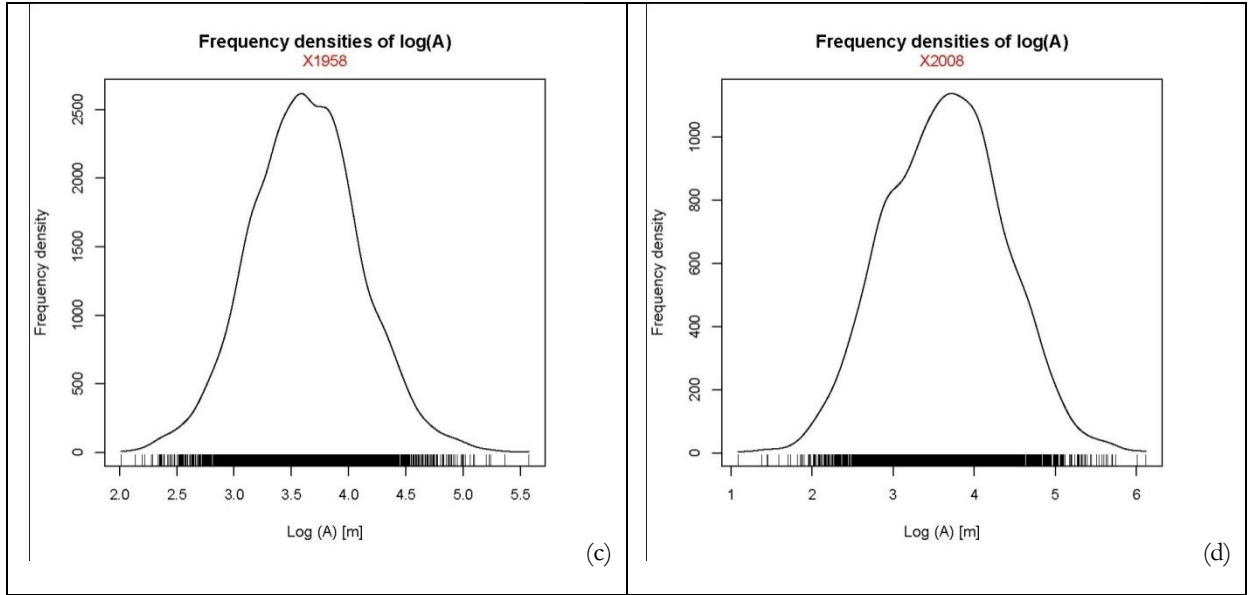
A.3. Kernel density fits

Figure A-1a-d. kernel density functions of 1958 EIL (a) and 2008 EIL (b) used to estimate the frequency density plot of the 1958 EIL (c) and 2008 EIL (d).

A.3. Size probability estimation

The five parameter double pareto distribution (Stark and Hovius, 2001) is given by:

$$p(x) = \eta \left[\frac{\left[1+\left(\frac{m}{t}\right)^{-\alpha}\right]^{\frac{\beta}{\alpha}}}{\left[1+\left(\frac{x}{t}\right)^{-\alpha}\right]^{1+\frac{\beta}{\alpha}}} \right] \cdot \left(\frac{x}{t}\right)^{-\alpha-1} \qquad \text{(Eq. A-7)}$$

Where $(x) = p(A_l; \alpha, \beta, c, m, t)$, $\eta = \frac{\beta}{t(1-\delta)}$, and $\delta = y(c) = \left[\frac{\left[1+\left(\frac{m}{t}\right)^{-\alpha}\right]^{\frac{\beta}{\alpha}}}{\left[1+\left(\frac{x}{t}\right)^{-\alpha}\right]} \right]$

The five parameters are:

α – slope of the power law tail for large landslide areas

β – slope of the power law for small landslides

c – cutoff values for small landslides

m – cutoff values for large landslides

t – maximum value of the probability distribution; below this value is the rollover, i.e., the optimum number of landslide occurrence with a certain area A_l.

The double pareto simplified is in the same mathematical expression as the double pareto without the c and m parameters.

The truncated inverse-gamma distribution (Malamud et al., 2004) is given by:

$$p(A_l; \alpha, t, s) = \frac{1}{t\Gamma(\alpha)} \left[\frac{t}{A_l - s}\right]^{\alpha+1} exp\left[-\frac{t}{A_l - s}\right] \qquad \text{(Eq. A-8)}$$

Where $\Gamma(\alpha)$ is the gamma function of α. The parameters are:

α –primarily controls power law decay for medium and large values

t – primarily controls the location of the maximum probability distribution

s – primarily controls exponential rollover for small values.